Fiducial Marker-Based Motion Capture System for Biomechanics and Lower Limb Prosthesis Alignment

By

Raju Gupta

A Thesis submitted to the Graduate Faculty of
Auburn University
In partial fulfillment of the
requirements of the Degree of
Master of Science

Auburn, Alabama
August 3, 2019

Keywords: Prosthetic alignment, Aruco markers, motion capture, fiducial marker, marker tracking

Approved by

Michael Zabala, Chair, Assistant Professor in Dept. of Mechanical Engineering
Mark Schall, Assistant Professor in Dept. of Industrial & Systems Engineering
Dan Marghitu, Professor in Dept. of Mechanical Engineering

ABSTRACT

Lower limb loss is a disability that is currently estimated to affect more than one million Americans. Development of lower limb prostheses has allowed the amputee to regain their mobility to some extent and reengage in society, work, sports, military service, and other activities. However, correct alignment of the prosthetic limb is even more critical as it may lead to discomfort, pain and serious diseases such as osteoarthritis, osteopenia, and osteoporosis. Currently, prosthetic alignment is carried out mostly by eye-balling or with one of the static alignment devices available in the market. Additionally, lower limb prosthetic alignment is an iterative and time-consuming procedure that can be emotionally difficult and frustrating for the patient as it requires multiple appointments, fitting trials, and alignment events. Thus, the goal of this thesis is to make developments towards a portable system that can deliver real-time alignment data to the prosthetist resulting in a more expedient prosthetic alignment process. This will allow the prosthetist to focus more on patient care and less on constant adjustment.

In this study, a cost effective, self-contained, and portable system for prosthetic alignment was developed utilizing a low-cost fiducial marker tracking system, which also included determination of the landmarks to be tracked. The identified landmarks were then used to develop algorithms to calculate the joint angle kinematics for each lower limb prosthetic joint. The system also includes a webpage application with the ability to digitally provide biomechanical (static and dynamic) alignment data to the prosthetists. A pilot validation study utilizing conventional motion capture system as gold standard was conducted in order to validate the fiducial marker system for use in human motion capture and prostheses alignment. The study yielded a RMSE of 3.3±0.91˚

for flexion/extension angle of the prosthetic limb with average difference in maximum flexion and extension angles between the systems of 0.035±0.9˚ and 1.96±0.04˚, respectively.

The second goal of the thesis study was to develop a component-based coordinate system for lower limb prosthesis. The technique presented in this study provides a method of creating a component-specific coordinate system for a standard transtibial prosthesis. The developed coordinate system was used for the purpose of calculating objective measures of alignment while the prosthesis was being worn during both static and dynamic activities. The development method is based on the selection of anatomically relevant points tracked on the residual limb and the prosthesis along with Euler angle decomposition techniques. No such method has been developed previously for a transtibial prosthesis.

The third goal of the study included validation of the augmented reality marker-based tracking system for utilization in general motion capture, specifically for prosthetic alignment. The proposed study was validated on five physically fit participants of varying age using a traditional retroreflective marker-based motion capture system. This study design tested the effect on position and orientation of fiducial markers of 3 different marker sizes placed on the thigh of participants walking at 3 different speeds walking from 0 to 3.5 m away from the action camera. The results indicated an increase in RMSE for the position and orientation of the fiducial marker with an increase in speed and decrease in fiducial marker size. The results were comparable to the previous studies performed at static condition of fiducial markers for utilization in augmented reality. Thus, the results obtained in this study suggest that the fiducial marker system can be used for general motion capture and lower limb prosthesis alignment.

ACKNOWLEDGEMENTS

I want to thank my academic advisor, Dr. Michael Zabala for providing me this opportunity to be involved in this project. He is a great advisor that anyone can have. He has been very supportive throughout my master's study. I have learned a lot about field of biomechanics, prosthetic alignment, kinematics and kinetics analysis, and the broad application of motion capture in the field of biomechanics. Beside academics, I have also learned time management, how to design and conduct research, work with timeline and most important to have positive attitude while working under his supervision. Further, he has been very supportive about every event that came through my life during this period. I had to take a leave for a full semester and summer because of my US Army training and he completely supported it in a very positive way which really increased respect for him as my advisor. I could not have finished my masters in this timeline without his full support.

I also want to thank Dr. Howard Chen, my unofficial second advisor as I call him. He has been a great support and help throughout my research this semester. He is another reason I have been able to finish my thesis by this semester. It would have been almost impossible without his unconditional help and advices regarding research design, coding, result interpretation, answering all my questions, and teaching how to use and write programs to track Aruco markers in Robotic Operating System (ROS). He always made himself available whenever I needed his advice and help.

I would also like to thank Dr. William Murrah, Dr. Mark Schall, and Dr. Sean Gallagher for helping me with statistical analysis. I also want to thank Dr. Dan Marghitu and Dr. Mark Schall for accepting my request to be on my thesis committee member. Further, I would like to thank all of

my friends and AUBE lab mates who volunteered to be the subject for my study. I would also like to thank my ABE Lab mates Jordan, Scott, Morgan, Taylor, Jake, Kyle, Sean, Reed and Mohammad Badawy for being there and supporting me mentally and giving me hope and making me laugh during the whole time I was a part of AUBE Lab. Last but not the least, I would like to thank my parents and my brothers and sisters who were so supportive and didn't bother me much while I was busy with my thesis and were so understanding when I didn't call them for more than a week sometimes.

TABLE OF CONTENTS

ABSTRACT ii

ACKNOWLEDGEMENTS iv

LIST OF TABLES viii

LIST OF FIGURES ix

CHAPTER 1 INTRODUCTION 1

1.1 INTRODUCTION 1

CHAPTER 2 VARIOUS MOTION CAPTURE METHODS USED IN THE FIELD OF BIOMECHANICS 4

2.1 BACKGROUND 4

2.1.1 OPTICAL MOTION CAPTURE SYSTEM 5

2.1.2 FIDUCIAL MARKER-BASED TRACKING SYSTEM 7

2.3 GAP IN LITERATURE: NEED FOR VALIDATION OF FIDUCIAL MARKER SYSTEM FOR HUMAN MOTION TRACKING 12

CHAPTER 3 SYSTEM FOR PROSTHETIC ALIGNMENT UTILIZING REAL-TIME KINEMATICS (SPAURK) SYSTEM 14

3.1 INTRODUCTION 14

3.2 METHOD OF PROSTHETICALIGNMENT USING SPAURK SYSTEM 15

3.3 SPAURK SYSTEM SPECIFICATION AND INNOVATIONS 16

3.3 VALIDATION OF THE SPAURK SYSTEM FOR APPLICATION IN PROSTHETIC ALIGNMENT 19

3.3.1 METHODS 19

3.3.2 RESULTS 21

3.3.3 DISCUSSION 22

3.4 ACKNOWLEDGEMENTS 23

CHAPTER 4 A COMPONENT-BASED COORDINATE SYSTEM FOR STANDARD TRANSTIBIAL PROSTHESES 24

4.1 ABSTRACT 24

4.2 INTRODUCTION 25

4.3 COORDINATE SYSTEM FOR TRANSTIBIAL PROSTHESIS 27

4.3.1 FEMUR/THIGH 28

4.3.2 TIBIAL SOCKET 30

4.3.3 PYLON 32

4.3.4 FOOT/FOOT SHELL 34
4.4 EXAMPLE CASE 36
4.5 DISCUSSION 39
4.6 CONCLUSION 42
4.7 CONFLICT OF INTEREST STATEMENT 43
4.8 ACKNOWLEDGMENTS 43
CHAPTER – 5 ACCURACY OF A FIDUCIAL MARKER-BASED TRACKING SYSTEM FOR HUMAN MOTION CAPTURE SYSTEM 44
5.1 ABSTRACT 44
5.2 INTRODUCTION 45
5.3 METHODS 48
5.3.1 Participants 48
5.3.2 Experimental Procedure 48
5.3.3 Instrumentation 50
5.3.4 Image Processing 50
5.3.5 Fiducial System Accuracy 51
5.3.6 Statistical Analysis 52
5.4 Results 52
5.4.1 RMSE in the Position 52
5.4.2 RMSE of Orientation 57
5.5 Discussion 60
5.6 Conclusion 62
CHAPTER – 6 CONCLUSIONS, STUDY LIMITATIONS, AND FUTURE WORKS 64
REFERENCES 66
APPENDIX A (IRB) 70
APPENDIX B (Prosthesis alignment Algorithm) 72
APPENDIX C (Populating data for alignment) 80
APPENDIX D (Alignment Algorithm) 84
APPENDIX E (Test Protocol) 90
APPENDIX F (FiducialSystem Installment and Operational Guide) 94
APPENDIX G (Statistics) 100
APPENDIX H (ROS files) 105

LIST OF TABLES

TABLE 1: MAXIMUM FLEXION AND EXTENSION ANGLES OBTAINED FROM BOTH SYSTEM AND THEIR DIFFERENCES ALONG WITH RMSE FROM EACH TRIALS..... 22
TABLE 2: STATIC ALIGNMENT VALUES OF THE TRANSTIBIAL PROSTHESIS DURING QUIET STANCE. *INTERNAL ROTATION OF THE FOOT MEASURED WITH RESPECT TO THE SOCKET..... 37
TABLE 3: MANOVA RESULT FOR MAIN EFFECT AND INTERACTION EFFECT ON POSITION RMSE. **STATISTICALLY-SIGNIFICANT ($p<0.01$)..... 53
TABLE 4: MANOVA RESULT FOR MAIN EFFECT AND INTERACTION EFFECT ON ORIENTATION RMSE. **STATISTICALLY-SIGNIFICANT ($p<0.01$) 58
TABLE 5: MARGINAL MEAN RMSE TABLE FOR POTION OF FIDUCIAL MARKER WITH STANDARD DEVIATION (SD) FOR ALL THE TESTING CONDITIONS 100
TABLE 6: MARGINAL MEAN RMSE TABLE FOR ORIENTATION OF FIDUCIAL MARKER WITH STANDARD DEVIATION (SD) FOR ALL THE TESTING CONDITIONS 101
TABLE 7: RESULT STATISTICAL ANALYSIS OF BETWEEN SUBJECT EFFECTS FOR RMSE OF POSITION OF FIDUCIAL MARKER. *STATISTICALLY SIGNIFICANT AT $p<0.05$, **STATISTICALLY-SIGNIFICANT AT $p<0.01$ 102
TABLE 8: RESULT STATISTICAL ANALYSIS OF BETWEEN SUBJECT EFFECTS FOR RMSE OF ORIENTATION OF FIDUCIAL MARKER. *STATISTICALLY SIGNIFICANT AT $p<0.05$, **STATISTICALLY-SIGNIFICANT AT $p<0.01$ 102
TABLE 9: UNIVARIATE ANALYSIS OF VARIANCE (UNIANOVA) MULTIPLE COMPARISON (TUKEY HSD) TEST RESULTS OF POSITION BETWEEN INDEPENDENT VARIABLES (IVS) WITH MEAN DIFFERENCES AND THEIR SIGNIFICANCE VALUES. *THE MEAN DIFFERENCE IS STATISTICALLY-SIGNIFICANT AT THE 0.05 LEVEL. **THE MEAN DIFFERENCE IS STATISTICALLY-SIGNIFICANT AT THE 0.01 LEVEL. 103
TABLE 10: VARIATE ANALYSIS OF VARIANCE (UNIANOVA) MULTIPLE COMPARISON (TUKEY HSD) TEST RESULTS OF ORIENTATION BETWEEN INDEPENDENT VARIABLES (IVS) WITH MEAN DIFFERENCES AND THEIR SIGNIFICANCE VALUES FOR ORIENTATION RMSE. *THE MEAN DIFFERENCE IS STATISTICALLY-SIGNIFICANT AT THE 0.05 LEVEL. **THE MEAN DIFFERENCE IS STATISTICALLY-SIGNIFICANT AT THE 0.01 LEVEL. 104

LIST OF FIGURES

FIGURE 1: EXAMPLES OF SOME OF FIDUCIAL MARKERS AVAILABLE CURRENTLY 8

FIGURE 2:SYSTEM FOR PROSTHETIC ALIGNMENT UTILIZING REAL-TIME KINEMATICS (SPAURK) SYSTEM: FROM LEFT TO RIGHT; (A) MARKER PLACEMENT, (B) CALIBRATION (C) WEB-BASED USER INTERFACE, (D) IDS UI3160 CAMERA 16

FIGURE 3: UPPER GRAPH SHOWING SOCKET TO FEMUR FLEXION/EXTENSION ANGLE FORM VICON AND SPAURK SYSTEM ALIGNED AND THE DIFFERENCE IN BETWEEN BOTH SYSTEM IN THE BOTTOM GRAPH 21

FIGURE 4: RELEVANT POINTS AND REFERENCE FRAMES FOR COMPONENT-BASED COORDINATE SYSTEM. PROSTHESIS DEPICTED IS NEUTRALLY ALIGNED. *WITH NEUTRAL ALIGNMENT, O_{TS} WILL BE COINCIDENT WITH O_P AND P_P, AND THE REFERENCE FRAMES OF THE TIBIAL SOCKET AND PYLON WILL BE ALIGNED 27

FIGURE 5: DASHED CIRCLE INDICATES LOCATION OF FEMORAL CONDYLE CONTOUR THAT IS OFTEN EVIDENT ON A TIBIAL SOCKET. 29

FIGURE 6: PROXIMAL TUBE CLAMP ADAPTER SCREW. 33

FIGURE 7: REFLECTIVE MARKER PLACEMENT 37

FIGURE 8: A. TIBIAL SOCKET ORIENTATION MEASURED FROM THE IPSILATERAL THIGH; B. PYLON ORIENTATION MEASURED FROM THE TIBIAL SOCKET; C. FOOT DORSIFLEXION AND INVERSION MEASURED FROM THE PYLON AND INTERNAL ROTATION MEASURED FROM THE TIBIAL SOCKET; D. FOOT TRANSLATION FROM THE DISTAL PYLON. NOTE: ALTHOUGH NO MOVEMENT IS POSSIBLE, MECHANICALLY, AT THE JOINT CONNECTING THE FOOT AND THE DISTAL PYLON, TRANSLATION IS NON-ZERO BECAUSE OF THE LOCATION OF THE ORIGIN OF THE FOOT COMBINED WITH DEFORMATION OF THE FOOT DURING GAIT. 38

FIGURE 9: PYLON TRANSLATION MEASURED FROM THE TIBIAL SOCKET. ZERO TRANSLATION, AS EXPECTED, SINCE THE PYLON AND TIBIAL SOCKET SHARE THE SAME ORIGIN FOR THIS PARTICULAR TRANSTIBIAL PROSTHESIS (TRANSLATION BETWEEN THESE TWO COMPONENTS IS NOT POSSIBLE, MECHANICALLY) 39

FIGURE 10: TEST SUBJECT MARKERED UP WITH 79 RETROREFLECTIVE MARKERS AND A FIDUCIAL MARKER OF SIZE 10X10, 11X11, AND 12X12 CM FROM LEFT TO RIGHT 49

FIGURE 11: HISTOGRAM OF RMS ERROR FOR THE POSITION OF FIDUCIAL MARKER FOR ALL 3 SIZE OF MARKERS, THREE WALKING SPEEDS AND IN ALL AXIS COLUMN1: RMSE IN X-AXIS FOR ALL 3 SIZES OF MARKER FROM TOP TO BOTTOM, COLUMN 2: RMSE IN Y-AXIS FOR ALL 3 SIZES OF MARKER FROM TOP TO BOTTOM, COLUMN 3: RMSE IN Z-AXIS FOR ALL 3 SIZES OF MARKER FROM TOP TO BOTTOM, AND COLUMN 4: RMSE IN MAGNITUDE OF POSITION (R) FOR ALL 3 SIZES OF MARKER FROM TOP TO BOTTOM 54

FIGURE 12: TIME SYNCHRONIZED POSITION DATA FROM BOTH SYSTEMS FOR THE 11X11 CM MARKER SIZE DURING SLOW SPEED. 55

FIGURE 13: TIME SYNCHRONIZED ALIGNED ORIENTATION DATA FROM BOTH SYSTEM FOR 11X11 CM MARKER SIZE AND SLOW SPEED TRIAL 55

FIGURE 14: RMSE OF ORIENTATION BETWEEN BOTH SYSTEM DATA IN X-AXIS, Y-AXIS, AND Z-AXIS FOR 11X11 CM MARKER SIZE AND SLOW SPEED TRIAL 56

FIGURE 15: RMSE OF POSITION IN X-AXIS, Y-AXIS, AND Z-AXIS FOR 11X11 CM MARKER SIZE DURING A SLOW SPEED TRIAL 56

FIGURE 16: HISTOGRAM OF RMSE FOR THE ORIENTATION OF FIDUCIAL MARKER FOR ALL 3 SIZE OF MARKERS, THREE WALKING SPEEDS AND IN ALL AXIS COLUMN1: RMSE IN X-AXIS FOR ALL 3 SIZES OF MARKER FROM TOP TO BOTTOM, COLUMN 2: RMSE IN Y-AXIS FOR ALL 3 SIZES OF MARKER FROM TOP TO BOTTOM, COLUMN 3: RMSE IN Z-AXIS FOR ALL 3 SIZES OF MARKER FROM TOP TO BOTTOM, AND COLUMN 4: RMSE IN MAGNITUDE OF POSITION (R) FOR ALL 3 SIZES OF MARKER FROM TOP TO BOTTOM 59

FIGURE 17: TIBIAL SOCKET ALIGNMENT. A. FLEXION. B. ABDUCTION. C. EXTERNAL ROTATION. 76

FIGURE 18: PYLON ALIGNMENT. A. FLEXION. B. ABDUCTION. C. ANTERIOR TRANSLATION. D. LATERAL TRANSLATION. 77

FIGURE 19: FOOT ALIGNMENT. A. DORSIFLEXION. B. INVERSION. C. EXTERNAL ROTATION. D. ANTERIOR TRANSLATION. E. LATERAL TRANSLATION. 79

CHAPTER 1
INTRODUCTION

1.1 INTRODUCTION

Lower limb loss is a permanent disability caused by traumatic accidents, cancer, congenital disorders, dysvascular disease, and diabetes[1–3]. In 2005, lower limb losses in the United States were estimated to affect more than one million people, of whom more than 600,000 were classified as major amputations (excluding toes)[1]. Unsurprisingly, the loss of the limb has shown a significant decrease in the measurable quality of life due in part to changes in employment status, occupation, lifestyle as well as impairments in physical function, discomfort and pain.[4,5]. The continuous advancement of the prosthetic limb devices has shown to improve measurable quality of life scores since it allows individuals with lower limb amputations to regain their ability to walk and pursue other activities that require mobility (e.g. work, sports, military service) [3].

Optimal fit and alignment of a lower limb prosthesis is essential for maximizing the quality of life of an individual following limb loss [2,5,6] since the use of the prosthesis alters gait biomechanics. Alterations of gait biomechanics can lead to secondary complications such as discomfort or pain in the lower limbs, osteoarthritis of knee and/or hip joint, back pain, embarrassing gait, postural changes, leg length discrepancy, general deconditioning as well as serious bone disease such as osteoarthritis, osteopenia and osteoporosis[2,6].

The prosthesis alignment is conducted in a three step process; bench alignment, static alignment and dynamic alignment [7]. Bench alignment starts with the fitting of socket and assembly of prosthetic components (socket, pylon and foot). In this process, a plumb-line is used to visually match a point on the socket and another point on the ankle bolt and/or the center of the heel of the shoes. For static alignment, the prosthesis is worn by the subject in the standing position

and the prosthesis is evaluated in term of its length, toe-out angle, and knee flexion angles at static condition. Modifications are then made by the prosthetist for any possible misalignment. Lastly, dynamic alignment is accessed based on the observation of the prosthetists and the feedback from the subject while navigating through different paths of motion on various surfaces and inclines. The static and dynamic alignment process is repeated until a comfortable fit is achieved. However, prosthetic alignment based on the observation and feedback from the patient can be unreliable and unrepeatable because of inconsistency and subjectivity [8].

Various devices have been developed for prosthetic alignment. These include the adjustable coupling [9] Computerized Prosthetic Alignment System by Orthocare Compass[10], the Intelligent Prosthetic Endoskeleton Component System by College Park[11], and Alignment Reader and Recorder Device (ARRD) [8]. However, the usability of these instruments in a clinical environment remains unclear [12].

The Auburn University Biomechanics Laboratory is currently developing the System for Prosthetic Alignment Utilizing Real-time Kinematics (SPAURK) for prosthetic alignment. SPAURK is intended to be a low-cost, self-contained, portable prosthetic alignment device that can be easily setup in clinical environments. It is designed to provide precise biomechanical alignment data to the prosthetists for both static and dynamic alignment. A critical component of the SPAURK system is the fiducial marker-based motion tracking capture system, a comparatively low-cost motion tracking technology that will enable the device to be both inexpensive and portable.

While fiducial markers have been used to track motion in various applications such as augmented reality [13], endoscopic ultra-sound guidance [13–17], and liver radiotherapy[18], little to no work has been done to examine the accuracy and repeatability of fiducial markers in

biomechanics and human motion tracking applications, which requires smaller markers to be tracked at farther distances and higher velocities compared to typical applications. The objective of this thesis is to i) provide an objective method for measuring alignment through the creation of a component-based coordinate system for standard transtibial prosthesis and ii) validate the fiducial marker system for human motion tracking.

CHAPTER 2
VARIOUS MOTION CAPTURE METHODS USED IN THE FIELD OF BIOMECHANICS

2.1 BACKGROUND

Motion Capture is a technology used to capture the movements in the digital environment [19]. A motion capture system includes all kinds of digital capture as well as storage technologies used to capture and store the motion of humans or any other objects. Geometrical properties of the objects or living beings are used to establish a virtual/digital replica through this technology for various purposes. The geometrical data is mapped to a 3D model so that the model performs the same actions as the object. The actions and the virtual locations used to map the 3D models are used in order to perform a different analysis depending on the purpose. This technology is widely used in the entertainment, video gaming, and film industry. However, it has recently gained popularity in the field of augmented reality, virtual reality, robotics, industrial design & ergonomics, and advanced medical Research & Development laboratories [19]. Moreover, motion capture systems have gained popularity in the field of biomechanics. It is used for application such as preventive interventions for musculoskeletal diseases, performance improvement, rehabilitation, clinical and sports applications [19–21].

Currently, motion capture systems are based on different technologies. Electromechanical Motion capture systems perform using potentiometers placed on the subject's body through connecting rods. Similarly, electromagnetic motion capture systems use electromagnetic sensors which transmit the data to the computer where the position and the orientation of the sensors are inferred. Another method uses flexible fiber optics sensors to measure joint rotation and are complemented with electromagnetic systems to measure position of head and torso. There are also motion capture systems that use ultrasound, inertial sensors (accelerometer and gyroscope), and

optical cameras to track motion. In depth knowledge on these systems can be found in the study done by Estévez-García et. al. and Zhou et. al[19,22]. This study will look into optical based motion capture systems. According to Estevez et. al., optical systems that use reflectors or markers placed at strategic points on the body are the most well-known and commonly used motion capture system to track the human motion.

2.1.1 OPTICAL MOTION CAPTURE SYSTEM

Optical motion capture systems are the most commonly used motion capture system in the field of biomechanics because of their high accuracy and complete freedom of movement [21]. This system makes use of image sensors to infer the position of an object. Data collection is done by capturing the three dimensional coordinates of subjects through optical cameras with capture speed of between 30 to 1000 frames per second [19]. A minimum of 2 cameras is required to capture motion of the subject in 3D space. The position and the distance between the cameras are very important in order to generate the motion capture data without error[23].

There are two types of optical motion capture systems: i) marker-less motion capture, ii) marker-based motion capture.

1. **Marker-less motion capture systems:** With a marker-less motion capture system, the subject does not need to wear specialized equipment to track their movement. Instead, the system identifies the human forms through different sources of input images and differentiate into pieces to keep track of their movements [19]. Some of the marker-less systems are: A visual hull system, which uses shape estimation method called shape-from-silhouette 3D reconstruction technique to estimate and construct the three dimensional geometric image of an object[24], DARI, marker-less motion capture system, which uses

eight high speed camera and a state-of–art computer-vision engine to acquire an accurate skeletal model and collect whole body data [25], and Kinect motion capture system which uses Kinect sensor integrated with software to capture the movement. The Kinect technology was initially used for the video game market but it is now widely used for the movie, sport therapy, robotics and other research industries [26,27]. Although marker-less motion captures systems add freedom for the subject as no markers need to be placed on the body, requires small duration of time for data capture and convenient for subjects, it does not provide an accurate data compared to retroreflective marker based motion capture system. They produces less accurate skeleton solves, have noisier data and inaccurate rotational measurements[28].

2. Traditional marker-based motion capture system

Marker-based motion capture systems are considered to be the gold standard for human motion capture and analysis [29]. Marker-based motion capture systems can be further divided into active and passive systems.

- **Active marker systems:** In the active marker system, each markers emit their own light. As each marker emits a different wavelength, the range of movements of the subject is increased. It is important that the marker should be integrated with all the cameras so that all the movement data can be captured in a single phase. Being a very precise system it has a very small viewing angle. It can perform real-time tracking of up to 8 human subjects at high speed of up to 960 frames per second [30].
- **Passive marker systems**: This system is a marker-based optical motion capture system. Here a small sphere covered with a reflective material acts as a marker. These markers are placed on the predetermined position of the subject. The cameras are installed in

orientation with the marker which capture the reflecting light from the reflective markers. The light reflected by the markers are seen by the infrared cameras configured to receive a specific threshold of light. In order to eliminate error during motion capture, the cameras are configured in such a way that they will accept only a specific threshold of light; which is being reflected from the markers.

In general, marker-based systems can be used to obtain accurate data at fast capture rates and can be applied to multiple shapes. However, this system is expensive, obtrusive, and requires significant time for marker placement, system setup, and post processing.

2.1.2 FIDUCIAL MARKER-BASED TRACKING SYSTEM

A fiducial marker tracking system is one of the marker-based optical tracking systems which consist of patterns that are mounted in the environment and automatically detected in digital camera images using an accompanying detection algorithm [31]. Fiducial marker systems are very inexpensive as they only uses printed markers and inexpensive digital cameras along with freely available open source codes. This system is used in the situation where object recognition or pose estimation is needed with high reliability, high speed, precision and robustness [32,33]. Currently, fiducial systems are mostly used for augmented reality (AR), virtual reality, robot navigation and video games [34–36]. However, very little or almost no work has been done exploring the fiducial's tracking potential in the field of biomechanics and motion capture of human subjects despite having similar tracking capability as of the other motion capture systems used for human motion tracking. Thus, there is a big gap of work to be done for utilization of fiducial marker for human motion capture.

2.1.2.1 FIDUCIAL MARKERS

Fiducial markers are a set of 2D planar markers with unique patterns created using computer vision algorithms with capability to provide special information about a product when recognized and detected in an image. Different types of fiducial maker systems have been proposed in literature. They differ from each other in terms of their shape, the method used for encoding the information and their computer vision algorithms. However, all of the marker systems use a simple geometric shape and each marker has its own unique id which is detected by the computer vision software. The most common shape used in fiducial marker systems are square and circular. Some of the available marker systems are: ARToolKit, ARToolKit Plus, Aruco, ARTag, SVMS, TRIP, Fourier Tag, Rune-Tag, PI tag, Intersense, Matrix, BinARyID, CyberCode, VisualCode, IGD, SCR, HQM, and ReacTIVision are (Figure 1) [32,37].

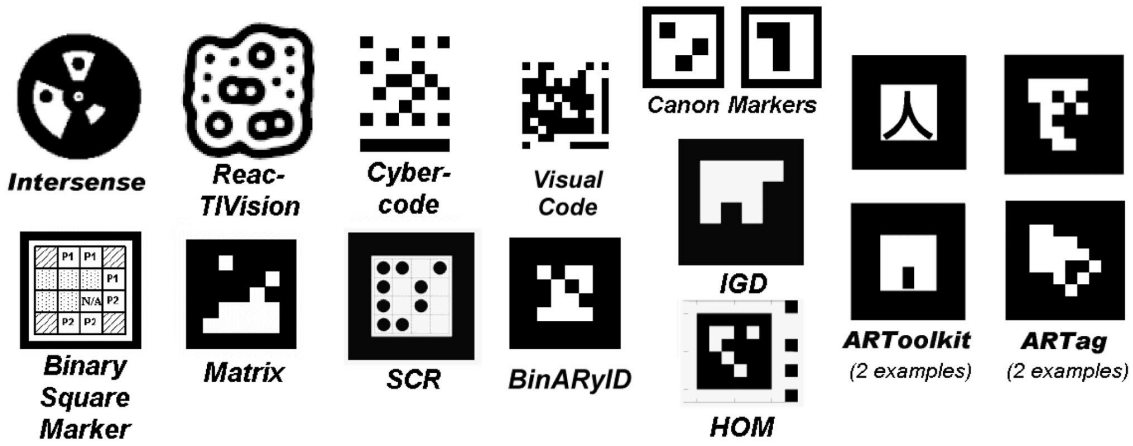

Figure 1: Examples of some of fiducial markers available currently

A study by Samarin et. al. found that out of all the different marker systems available, ARTag marker system is the most robust marker system in the context of false positive and inter-marker confusion rate, false negative rate, minimal marker size, and immunity to lighting condition because of its edge linking method [37,31]. ARTag is a square shaped marker system with a library of 2002 unique markers of either polarity (black on white background or white on black

background). Its library has its own algorithm based on edge detection method and designed to minimize falsely detect markers [37].

2.1.2.2 MARKER DETECTION AND POSE ESTIMATION

There are several algorithms developed in previous works for fiducial marker detection . The Aruco algorithm is commonly used to detect of ARTag markers [37]. The ARTag markers are automatically generated by Aruco through its dictionary. Detection occurs by extraction of binary code from the grids that make the fiducial markers. This process occurs in steps starting with image segmentation, contour extraction and filtering followed by marker code extraction to obtain the internal binary code, leading to marker identification and dictionary based error correction after binary code is extracted. After markers are identified, pose estimation is possible with respect to camera using Levenberg-Marquardt algorithm [37].

Aruco uses a digital coding system which consists of a six by six grid of bitonal cells in the interior of the marker. Quadrilateral contours which belongs to the outside border of a marker is first found by an edge-based method. Then edge pixels are thresholded and linked into segments, which are in turn grouped into “quads”. The four corners of the quad boundary are used to create a homography mapping to sample the interior. The edge based approach allows markers to be found under less controlled light conditions and this approach also provides the ability to detect markers in the presence of occlusion by heuristics of line segments that almost meet.

2.1.2.3 VALIDATION OF FIDUCIAL MARKER SYSTEM ACCURACY AND RELIABILITY

The robustness and usefulness of a fiducial marker system is characterized by eleven practical evaluation criteria:

1. The false positive rate
2. The intermarker confusion rate

3. The false negative rate
4. The minimal marker size
5. The vertex jitter characteristics
6. The marker library size
7. Immunity to lightning conditions
8. Immunity to occlusion
9. Perspective support
10. Immunity to photometric calibration
11. The speed performance

All the fiducial markers address all these criteria to be usable for tracking system. However, not all of them have been able to meet all of the criteria except for the ARTag. Accuracy of a tracking system is described by the accuracy of the corner detection process or looking at the result of the pose estimation. Some relevant parameters that limit the accuracy of the fiducial markers and also are the reasons for not letting the marker system to meet all the criteria are distance of the object, focal length and resolution of the camera, viewing angle, noise, illumination and distortion.

Several studies have been performed on the above-mentioned relevant parameters to find the limitations for fiducial tracking accuracy and reliability[32,33,36–39]. Since fiducial marker systems are mostly used in the field of Augmented Reality and Virtual reality, most of the studies for evaluating fiducial accuracy are assessed with ground truth data obtained through simulation [32,36,39–41]. However, fiducial marker systems have their own limitations. For example, the distance between the camera and the marker should be within 1-5 m, depending on the testing environment and camera specifications, to reduce capture error[15,16]. Furthermore, accuracy of

fiducial marker systems vary with respect to the environment due to the variability in lighting (indoor versus outdoor) [15,32].

Previous researchers have worked to validate the accuracy of the fiducial marker tracking system. Malbezin.et al. performed a study to track accuracy of one of the fiducial markers (ARToolKit) in the static condition. In their study, one 20 cm x 20 cm marker was placed on the ground with the camera placed at different distances from the marker to see the effect of distance on marker detection. This study reported that the error increases with increase in distance and error also varies in X and Y-axis[34]. Similarly, another study by Lopez-Cerone et. al.[36] conducted an accuracy analysis on the fiducial marker (AprilTag) in static condition and found that under 4 m the distance error keeps below 5 cm and further the marker is in front of the camera, bigger will be the error in 3D estimations. In their study, one to multiple markers were fixed on the wall and at different planes and the camera was placed at different distances to see the effect of multiple markers in the same frame, distances of markers form the camera, and orientation of markers on the accuracy of tracking the markers. A third study performed by Abawi et. al. defined an error function based on intervals which differs between high and low systematic error and standard deviation of estimated camera distance and viewing angle again in static condition of the marker[35,40]. Abawi et. al study used similar procedure as Malbezin et. al. to validate the accuracy. Further, Pentenrieder et. al.[40] created a large data base to be used as a look-up table for accuracy queries creating a new model based on simulation of ground truth data and as improvement of previous work by Abawi et. al.[35], Malbezine et. al.[34] and Zhang et. al.[41].

2.3 GAP IN LITERATURE: NEED FOR VALIDATION OF FIDUCIAL MARKER SYSTEM FOR HUMAN MOTION TRACKING

Fiducial marker systems have been widely used in the field of augmented reality (AR). Research has been conducted to validate the system's accuracy to be used in AR field and that too in reference to simulated ground truth data [34,35,40]. Ground truth data used in computer vision or fiducial marker tracking system are obtained through simulation tools designed with almost ideal parameters. In contrast, certain error can be expected from experimental data because of human error and instrumental error. However, no study was found that has used fiducial marker system to track human motion. Further, it has neither been validated against another existing retroreflective marker-based human motion tracking system.

Although fiducial marker systems are robust and accurate systems to be used in the field of AR, several new aspects comes into play while considering human motion such as human error, instrumental error, error caused by noise and occlusion, skin artifacts and joint center relative movements [39,40,42]. Additionally, human motion is often cyclical (e.g. gait) and the orientation may change continuously which might cause continuous occlusion of marker if the marker reaches its threshold orientation according to camera viewing angle. Thus, the error might be significantly different compared to error obtained in previous studies carried out for static placement of fiducial markers.

In the field of biomechanics, traditional retroreflective marker-based motion capture systems (such as the Vicon motion capture system) is most widely used for human motion tracking and gait analysis [43,44]. It is a robust and established system being widely used in the field of biomechanics and general motion capture. At the same time, a fiducial marker system has not been looked at to be used in the field of biomechanics, specifically human motion tracking. Thus, it

would be interesting to study the accuracy of fiducial marker system against an existing motion capture system in this field.

CHAPTER 3
SYSTEM FOR PROSTHETIC ALIGNMENT UTILIZING REAL-TIME KINEMATICS (SPAURK) SYSTEM

3.1 INTRODUCTION

The System for Prosthetic Alignment Utilizing Real-time Kinematics (SPAURK) is a low-cost, self-contained, portable prosthetic alignment device. It is capable of providing precise biomechanical (static and dynamic) alignment data to the prosthetists, digitally. This device is portable, requires small space and thus can be easily setup in clinical environments. Also, this device, being cost effective is easily affordable to a variety of clinics who cannot afford conventional expensive motion capture systems used for motion analysis. The SPAURK system can currently provide transtibial prosthetic alignment data both statically and dynamically utilizing fiducial marker-based motion tracking capture system, a comparatively low cost camera and novel prosthetic alignment and coordinate system algorithms.

In the SPAURK system, the pre-determined biomechanical locations are tracked and recorded by the fiducial marker-based tracking system. The recorded data is then processed in real time by the algorithm running in the background, which transmit the alignment data on a digitally displayed web-based user interface as shown in Figure 2. Setup and calibration requiring about 5-10 minutes. It is done before the biomechanical locations can be tracked. Based on the alignment data obtained, the prosthesis is adjusted by the prosthetists and the alignment data is stored separately for each individual subject for future alignment reference. Currently, the SPAURK system has been developed for lower limb transtibial alignment based on the algorithms developed. However, this device can be further expanded for transfemoral prosthetic alignment, sound limb tracking and both limbs tracking simultaneously.

3.2 METHOD OF PROSTHETICALIGNMENT USING SPAURK SYSTEM

The method for prosthetic alignment utilizing the SPAURK system follows the same conventional step method discussed in the Introduction. However, it utilizes the SPAURK system to obtain the alignment data instead of eye-balling, using goniometer, or using plumb line method. After the prosthetic leg is assembled and fitted to the subject, four fiducial markers are attached to the lateral side of the four components, namely: the foot, pylon, socket and intact femur of the subject (Figure 2). The camera (IDS UI3160 PC rev. 3.1) is placed on the lateral side of the subject at about 3 feet from the subject oriented in a way to be able to see the fiducial markers. A calibration wand is then used to obtain the coordinates of the ten biomechanical points on the 4 components of the subject and are assigned by tracking algorithms to the corresponding fiducial markers. After the calibration is complete, the subject is then subjected to a static standing position in order to record static data followed by adjustment made by prosthetists based on the standard reference static data for static alignment of the lower limb prostheses.

Further, the subject is asked to walk and possibly jog with a normal pace on a level plane and inclined surfaces accompanied with continuous tracking of prosthesis for each event through SPAURK system. The SPAURK system then processes the collected data utilizing the prosthetic alignment algorithms and prosthetic coordinate system algorithms. The system then provides the dynamic alignment data to the prosthetists on the digital display along with the recommended alignment measures. Using recommended alignment measures, the static and dynamic alignment is repeated until a satisfied and comfortable prosthetic alignment is achieved. The alignment data of the individual is then stored in the cloud storage database for future alignment visits of the subject, making the alignment procedure quicker compared to the conventional prosthetic alignment systems.

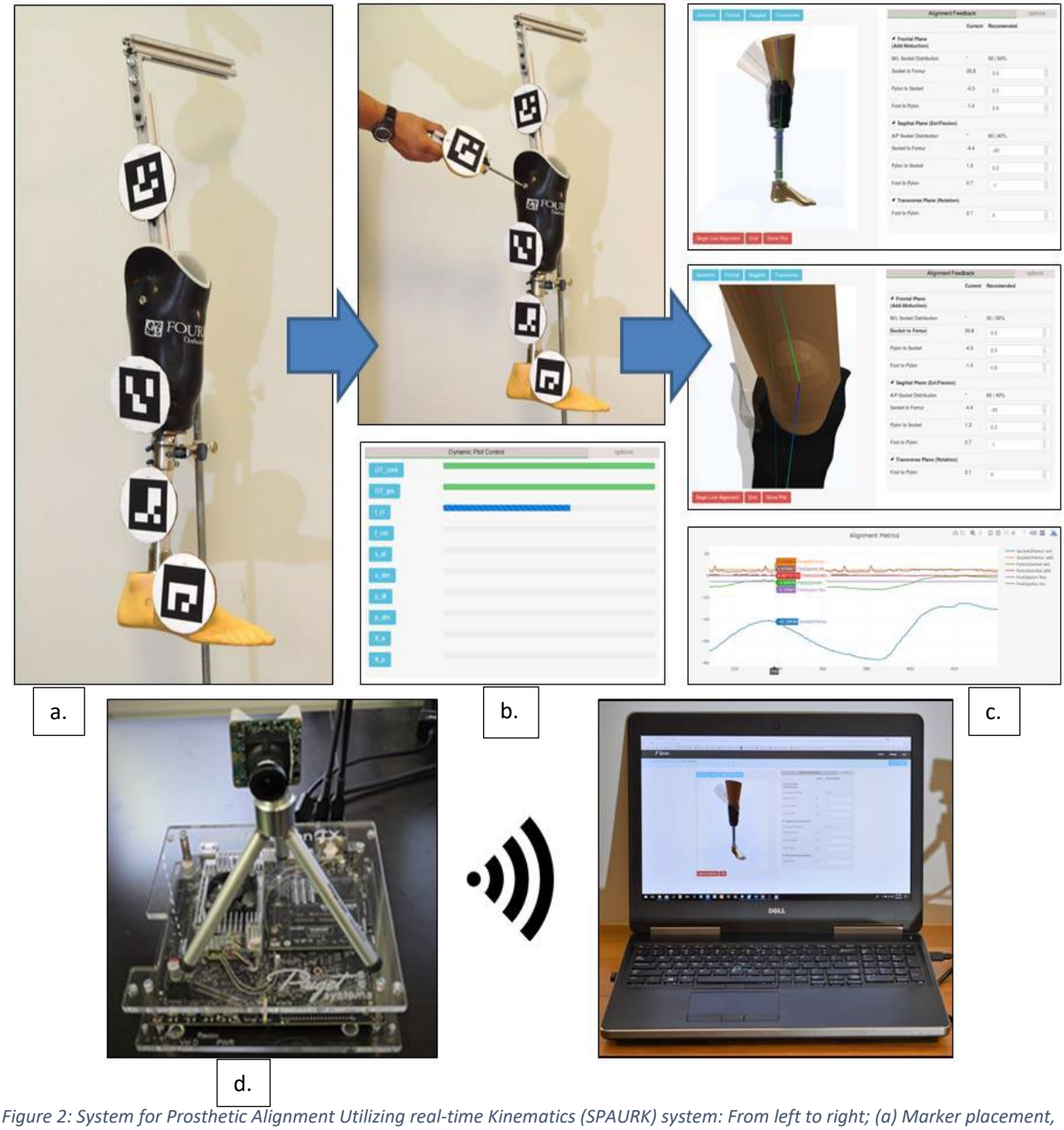

Figure 2: System for Prosthetic Alignment Utilizing real-time Kinematics (SPAURK) system: From left to right; (a) Marker placement, (b) Calibration (c) Web-based user Interface, (d) IDS UI3160 Camera

3.3 SPAURK SYSTEM SPECIFICATION AND INNOVATIONS

Some of the approaches and innovations done to accomplish this project's goals are listed as follows:

i. **The SPAURK system is built on a standardized biomechanical coordinate system and algorithms developed for a transtibial prosthesis -** The SPAURK system is built on a component-based coordinate system for transtibial prosthesis. The method and approach utilized to develop the coordinate system is explained in detail in chapter 4 of this thesis. The coordinate system is also utilized to develop the algorithms for the transtibial prosthesis alignment. This technique can be further adapted for a wide variety of prosthetic alignment requirements.

ii. **The SPAURK system is a very inexpensive system compared to conventional motion analysis systems -** In the beginning, the project started with the hardware worth $1000 which included a camera costing $400 and Jetson TX2 Module and development board costing $600. However, the systems available were not enough for processing speed required for data processing in real-time and for better tracking of the fiducial markers. Thus, having acquired hardware worth about $3600 which is still cheaper than the existing motion capture technologies. The hardware comprises of an IDS camera (UI3160 CPC with lens) and a quadcore workstation computer. The IDS camera costs under $2000 with the lens and a laptop costing approximately $1600.

iii. **The SPAURK is a portable system -** The system consists of a camera, computer system installed with software, a calibration wand, and paper printed fiducial markers each of which can fit in a small portable case and be setup in any location with ease. System setup only requires plugging in the camera and attaching the fiducial markers on the subject and calibrating the camera and biomechanical landmarks using the calibration wand with proper lighting in the area. All the setup process takes less than 30 minutes.

iv. **The simple and intuitive alignment process** – The alignment process in the SPAURK system is easy and simple and involves 3 steps:

1. Place fiducial markers on each component of the prosthesis and/or human body segment
2. Biomechanically register and calibrate the anatomical locations to the fiducial reference frames using the SPAURK Optical Coordinate Measurement Machine (OCMM), or the wand
3. Utilize the static and dynamic alignment tools on the User Interface (UI) to view, assess, and manipulate the alignment of the prosthetic limb in the real-time (Figure 2).

v. **The SPAURK system provides real-time alignment** – Optical registration of the anatomical locations of the rigid body provide the capability to track the alignment in real time. This capability also solves the problem of occlusion experienced by the other retroreflective marker-based motion tracking systems as this system only requires the fiducial markers to be seen by the camera which has registered all other anatomical landmarks that need to be tracked for dynamic alignment. Hence, not all the anatomical locations need to be tracked by unique marker placement on them.

vi. **The SPAURK system is designed to be modular and scalable -** The SPAURK system is a modular system. Parts or subcomponents can easily be upgraded with higher performance components without completely redesigning the system. For example, if a new camera enters the market with substantially higher resolution and frame rate, it can be integrated into the system with minimal cost and lead-time. Furthermore, because the two major components (computer/processor and camera) are commercially available, the

system is exceptionally easy to repair. Upgrading the accuracy and performance to meet additional future requirements can be as simple as replacing components with their higher performance counterparts.

vii. **The SPAURK user interface is intuitive, responsive, and simple** - A complete UI has been developed and coupled with the SPAURK prototype in order to guide the prosthetist through the alignment process and provide alignment feedback in a visual and understandable way. The user interface is an easy to use and simple design that provides the prosthetist with a multitude of visual tools including a 3D model that is updated in real-time to reflect the alignment of the limb under study. In addition to the model, charts and tables are also updated in real-time communicating the alignment metrics of the limb to the prosthetist.

3.3 VALIDATION OF THE SPAURK SYSTEM FOR APPLICATION IN PROSTHETIC ALIGNMENT

3.3.1 METHODS

A transtibial prosthetic leg was fixed to a mechanical jig which provided a simulated pelvis, thigh, and knee joint. A Vicon motion capture system was used as the traditional motion tracking system along with an Aruco/fiducial marker set (square model fiducial marker from the Aruco library [45].) The Vicon system included ten Vintage V5 Wide Optic cameras (framerate of 120 fps) and ten reflective markers (9 mm) placed on anatomically relevant landmarks of the prosthetic and test rig. These included the ipsilateral and contralateral greater trochanter, medial and lateral femoral epicondyles, medial and lateral proximal pylon screws, medial and lateral distal pylon screws, heel and second toe. The Aruco/fiducial marker system consisted of four markers total, with one placed on the jig, tibial socket, pylon, and foot as shown in Figure 2. The fiducial marker

system also included a calibration probe (the OCMM) and one IDS camera (UI-3241LE, USB 3.0 uEye LE, resolution of 1280x1024, framerate of 60 fps). Data collection consisted of the prosthetic leg placed in a static position, while the jig (pelvis and thigh) was flexed and extended about the mechanical knee joint. Eight replicates of this activity were recorded using both systems simultaneously.

Coordinates of the anatomical landmarks, at the location of the reflective markers, were loaded into the fiducial marker coordinate system of the corresponding segment with the calibration probe. Socket to femur flexion/extension was calculated in MATLAB based upon Euler angles between corresponding segment reference frames in a method similar to that described by Grood and Suntay [46]. Although, strict attempts were made to synchronize both systems during data collection, an approximate lag time of 1.37±0.07s for the fiducial system was realized. Therefore, the data from the fiducial system was adjusted accordingly to improve synchronicity between systems. As the framerate between both systems were inconsistent, the data obtained from the fiducial system was interpolated to match the total number of data points from the Vicon system. Part of the analysis included quantifying the kinematic offset between flexion/extension curves from both systems. In addition, in order to quantify differences between the curves not resulting from the offset, the offset was removed from the fiducial system results by adding the mean absolute difference between the curves for each trial.

Root mean square errors (RMSE) were calculated to analyze the accuracy of the fiducial marker system compared to the Vicon system. Paired sample t-tests with a confidence interval of 95% ($p<0.05$) were conducted to determine statistically significant differences in maximum flexion and extension angles provided by both systems. Finally, inter-system reliability was

determined for each trial using intraclass correlation coefficients (ICCs). IBM SPSS statistical analysis software was used to conduct the statistical analyses.

3.3.2 RESULTS

The maximum extension and flexion angle measured with the Vicon system was 58.8˚ and 100.6˚, respectively (fiducial system: 60.7˚ and 100.6˚, respectively). The mean kinematic offset between both systems was 0.94±0.28˚. After removal of the offset, the average RMSE of the flexion/extension angle throughout the trials measured by the fiducial marker system was found to be 3.3±0.91˚. All the results and calculation have been presented in Table 1. Paired sample t-tests

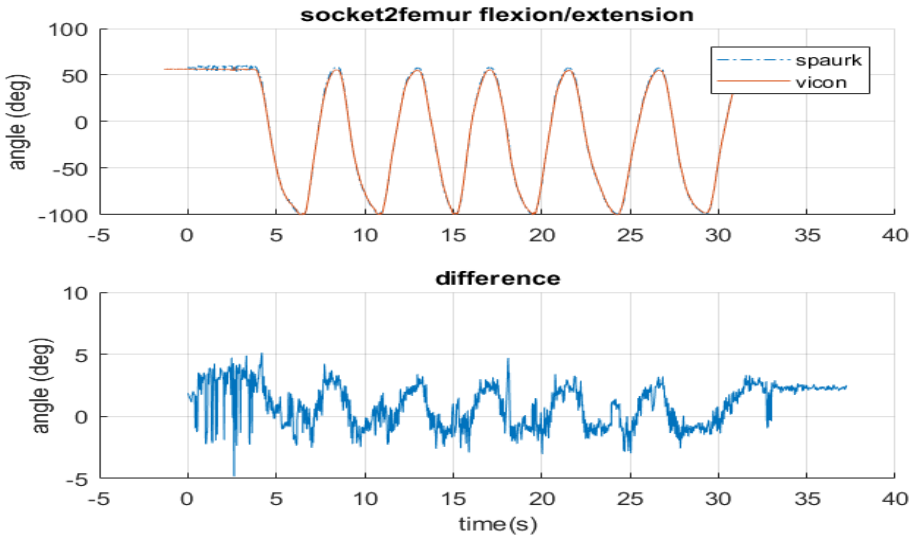

Figure 3: Upper graph showing socket to femur flexion/extension angle form Vicon and SPAURK system aligned and the difference in between both system in the bottom graph

indicated that there is a statistically significant effect of the systems on both maximum flexion angle ($p = 0.049$) and maximum extension angle ($p<0.01$), with average differences in maximum flexion and extension angles between the systems of 0.035˚±0.9 and 1.96˚±0.04, respectively. ICCs for the flexion/extension indicated a strong correlation between results obtained from both systems (average ICC = 0.99). The Figure 3 below shows the alignment of socket to femur flexion extension angles obtained from one of the trials for both systems and the differences between them.

	Max. Extension Angle(degree)			Max. Flex. Angle(degree)			
Trials	SPAURK	Vicon	Extension angle diff	SPAURK	Vicon	Flexion angle diff	RMSE (degree)
Trial 1	60.20	58.25	1.95	100.40	100.43	0.03	2.33
Trial 2	60.65	56.49	4.16	100.57	100.60	0.03	3.93
Trial 3	59.72	58.75	0.97	100.29	100.29	0.00	4.54
Trial 4	59.65	57.75	1.90	100.45	100.50	0.05	2.53
Trial 5	60.40	58.65	1.75	100.32	100.45	0.13	2.63
Trial 6	59.20	58.06	1.14	100.36	100.39	0.03	4.83
Trial 7	60.07	58.01	2.06	100.04	100.05	0.00	2.71
Trial 8	60.27	58.54	1.73	99.90	99.92	0.01	3.09
Mean	60.02	58.06	1.96	100.29	100.33	0.04	3.33
SD	0.44	0.68	0.91	0.20	0.22	0.04	0.91

Table 1: Maximum flexion and extension angles obtained from both system and their differences along with RMSE from each trials

3.3.3 DISCUSSION

Despite the significant effect of the system on the measured angles, the average RMSE of 3.3˚±0.91 occurred over a range of 58.8˚ extension to 100.6˚ flexion (measured with the Vicon system). It is likely that increased range of motion results in increased error [16]. As normal knee range of motion during gait is from 0˚ extension to 60˚ flexion [47], it is likely that RMSE would be reduced while analyzing human subject knee motion; however, this hypothesis remains to be tested.

A potential source of error in this study can be attributed to the size of the reflective markers used in the Vicon system. In the Vicon system, the centroid of the reflective markers was considered the location of the reflective marker in space [48] . However, the fiducial system determined the reflective marker location by capturing the average of 200 positions on the surface of the reflective markers touched by the probe. This error might be reduced by using reflective markers of smaller size (e.g. 3 mm).

This study has four limitations: 1) only one joint angle (knee flexion/extension) was analyzed due to the limitation in degrees of freedom of the prosthetic jig. 2) Only one camera was used to track the fiducial markers. This reduces the captured volume. Capture volume can be increased with better resolution, additional cameras and better lens. 3) Repeatability of the fiducial system was not tested. Accordingly, test-retest reliability of the fiducial system remains unknown. 4) True synchronicity was unachievable with the two independent motion capture systems.

In conclusion, the fiducial marker system has demonstrated the potential to be an alternative low cost, portable motion capture system for prosthetic alignment applications. Additional research is needed to further evaluate the system and broaden its capability of use in prosthetic alignment. Nevertheless, the study results suggest that the fiducial marker system may be useful for dynamic prosthetic alignment and tracking.

3.4 ACKNOWLEDGEMENTS

This project was supported by the US Army Medical Research and Materiel Command under Contract No. W81XWH-17-C-0101. This project was conducted in collaboration with Integrated Solutions for Systems (IS4S), a company working with government and military to provide solutions with innovative electronic systems design with sensor integration and navigation algorithms, vehicle dynamic analysis and modeling, and software design for variety of applications and programs. In this project, Auburn University Biomechanical Engineering (AUBE) lab was responsible for research and development of component based coordinate system for prosthesis and algorithms for prosthetic alignment and validation study of the accuracy of the SPAURK system while IS4S was responsible for developing the software and web based User Interface (UI) that utilizes the algorithms developed to display the results on a digital device for the end users (i.e. prosthetists).

CHAPTER 4
A COMPONENT-BASED COORDINATE SYSTEM FOR STANDARD TRANSTIBIAL PROSTHESES

4.1 ABSTRACT

INTRODUCTION: Lower limb loss is a disability that is currently estimated to affect more than one million Americans. Provision of a prosthetic lower limb oftentimes restores the ability of the individual to reengage in society by returning to work, sports, military service, or other activities requiring mobility. However, it is critical that these devices are properly aligned to avoid or reduce discomfort, pain, and even serious bone disorders such as osteoarthritis, osteopenia, and osteoporosis. Much work has been done on static prosthesis alignment measurement, and devices and tools currently exist to aid the prosthetist in this task. However, to the authors' knowledge, there is currently no standardized coordinate system for objectively calculating and expressing prosthesis alignment that can be used during both static and dynamic activities.

METHODS: The techniques presented here provide a method of creating component-specific coordinate systems for a standard transtibial prosthesis for the purpose of calculating objective measures of alignment while the prosthesis is being worn during both static and dynamic activities. This method is based upon a selection of anatomically-relevant points tracked on the residual limb and the prosthesis along with Euler angle decomposition techniques. A Case Study analysis was performed on one transtibial test subject to demonstrate the methods presented.

RESULTS: A method for tracking both static and dynamics transtibial prosthesis alignment was established. This method may be used with modern motion tracking technology that was not widely available when previous static alignment methods were established.

CONCLUSIONS: The potential benefits of this standardized method is improved understanding of the relationship between objective measures of prosthesis alignment and various measures of patient outcomes and success such as pain, discomfort, and daily steps walked. A standardized means of calculating and expressing prosthesis alignment will also benefit the design and development of future alignment tool technology.

4.2 INTRODUCTION

Lower limb loss is a permanent disability with numerous causes including trauma, cancer, congenital disorders, vascular disease, and diabetes[1–3]. In 2005, lower limb loss was estimated to affect over one million individuals in the United States, with over 600,000 of these classified as major amputations (excluding the toes)[1]. Unsurprisingly, loss of a lower limb has been shown to result in a significant decrease in measurable quality of life[3]. The negative effects of lower limb loss manifest as alterations in body image, changes in employment status/occupation and lifestyle, impairments in physical function, disruptions of valued activities, social discomfort, and pain[4,5].

The provision of a prosthetic limb to an individual affected by lower limb loss has been shown to significantly improve measurable quality of life scores[3]. A prosthesis often allows the individual to reengage in society by returning to work, sports, military service, or other activities that require mobility[49]. However, it is important that it is both properly fitted and aligned to achieve maximum benefit from the prosthesis and to prevent additional comorbidities[2,5,6]. Comfort, function, and appearance of the prosthesis in particular are strongly correlated with increased quality of life following amputation[6]. Improper fit or alignment of the prosthesis can lead to discomfort or pain in the lower limbs and back as well as a gait that may be undesirable to the patient;[2,6] moreover, serious bone diseases and disorders can follow such as osteoarthritis,

osteopenia and osteoporosis[2,6]. Optimal fit and alignment of a lower limb prosthesis is essential to maximizing the quality of life of an individual following limb loss.

Devices designed to aid in prosthesis alignment include a laser plumb line or various leveling tools. However, current alignment tools and techniques are incapable of providing detailed kinematic measurements of the device and all of its components to ensure that the most optimal alignment is achieved for the patient. Novel devices capable of a more detailed analysis of alignment are being designed and utilized in the field. As these novel devices are developed, a standardized coordinate system for kinematic analysis of each component of a lower limb prosthesis will be required. Previous work has been published which defines reference frames for the below-knee socket and a SACH foot (solid ankle, cushioned heel);[50–52] however, these methods provide no reference frame for the pylon and express all angles (except toe out) and offset differences in the ankle reference frame. Another alignment measurement technique was described by Sin et al.[53], however, this method requires use of a jig, therefore, cannot provide dynamic alignment during use of the device. Static alignment measurement (while the limb and/or the wearer remains still) is not new to the field of prosthetics; however, a robust coordinate system is lacking that accounts for all components of the prosthesis, defined independently, and established from a fixed reference frame so that both static and dynamic analysis (while the wearer is ambulating) of each component is achievable. This system must be based upon features common to lower limb prostheses as well as residual anatomical landmarks, similar to the anatomical joint coordinate systems put forth by Grood and Suntay in 1983[46,54]. A standardized coordinate system for lower limb prostheses such as this will allow for consistent analysis of various models of prostheses and the formulation of relationships between specific alignment parameters and function, comfort, and performance of the prosthesis. Below-knee amputations are one of the most

common forms of lower limb amputation[1]. Thus, the focus of this article is on transtibial prosthesis alignment. The purpose of this article is to provide an objective method for measuring alignment through the creation of component-based coordinate systems for standard transtibial prostheses. In the Appendix is a case example demonstrating the utility of these methods for measuring both static and dynamic prosthesis alignment on a single transtibial amputee.

4.3 COORDINATE SYSTEM FOR TRANSTIBIAL PROSTHESIS

Below is a proposed coordinate system to be used with standard transtibial prostheses comprised of three components: the tibial socket (including the pyramid), pylon, and foot/foot shell. This system utilizes points on the prosthesis as well as anatomical landmarks when available and accessible. As a reference, Figure 4 depicts a perfectly neutral alignment of a standard transtibial prosthesis, where the angle between each segment with respect to its proximal segment is zero based upon the definitions presented here.

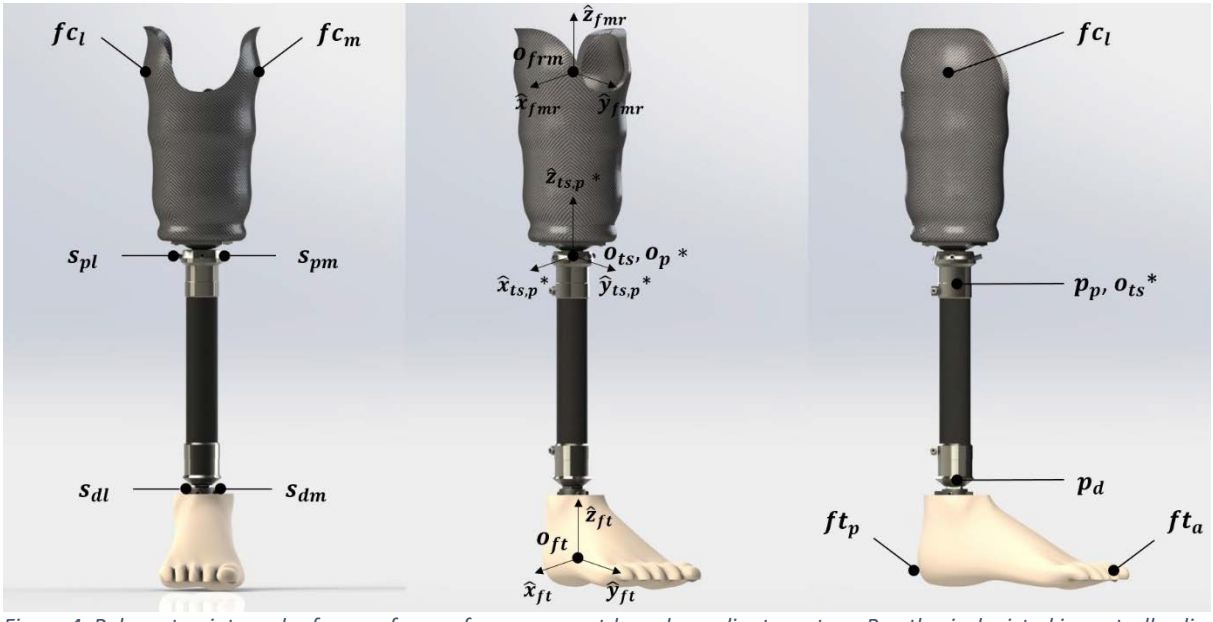

*Figure 4: Relevant points and reference frames for component-based coordinate system. Prosthesis depicted is neutrally aligned. *With neutral alignment, o_{ts} will be coincident with o_p and p_p, and the reference frames of the tibial socket and pylon will be aligned*

4.3.1 FEMUR/THIGH

As transtibial amputees have an intact femur on the affected side, it is possible to define the anatomical femoral reference frame, which has been previously described in the biomechanical literature[46,55]. The origin of the femoral coordinate system ($\boldsymbol{o_{frm}}$) is located at the midpoint of the points on the tibial socket adjacent to the most medial and lateral points of the femoral epicondyles ($\boldsymbol{fc_m}, \boldsymbol{fc_l}$), along the epicondylar axis[46]. Even with a transtibial prosthesis, direct access to the distal femur can be limited due to coverage by the tibial socket. However, as the tibial socket is made to conform to the residual limb of the amputee, the location of the femoral epicondyles are often visible and can still be utilized (Figure 5). The process of finding these two landmarks in particular is similar to the approach used extensively throughout the field of human subject marker-based motion capture[56–58]. If the femoral epicondyles are not visible, a reasonable estimation of their locations may be utilized instead by locating the center of the patella and the most medial and lateral points on the tibial socket at this height. The mechanical axis of the femur ($\hat{\boldsymbol{z}}_{\boldsymbol{fmr}}$) will point proximally with the distal end passing through the femoral coordinate system origin ($\boldsymbol{o_{frm}}$) and the proximal end passing through the center of the femoral head($\boldsymbol{h}$).[46,55] The location of the femoral head ($\boldsymbol{h}$) may be estimated as one-quarter of the distance from the ipsilateral to the contralateral greater trochanter ($\boldsymbol{gt_{ips}}$, $\boldsymbol{gt_{con}}$)[59]. The frontal plane may be defined as containing the femoral mechanical axis $(\hat{\boldsymbol{z}}_{\boldsymbol{fmr}})$ and the medial and lateral points $\boldsymbol{fc_m}$ and $\boldsymbol{fc_l}$ along the epicondylar axis. The normal to the frontal plane, or the femoral anterior-posterior axis $(\hat{\boldsymbol{y}}_{\boldsymbol{fmr}})$, will point anteriorly and is calculated as the cross product of the femoral mechanical axis $(\hat{\boldsymbol{z}}_{\boldsymbol{fmr}})$ and the line connecting the medial and lateral points of the femoral epicondyles along the epicondylar axis. The flexion axis of the femur $(\hat{\boldsymbol{x}}_{\boldsymbol{fmr}})$ will be

directed to the right and is calculated as the cross product of the femoral anterior-posterior axis $(\hat{\boldsymbol{y}}_{\boldsymbol{fmr}})$ and the femoral mechanical axis $(\hat{\boldsymbol{z}}_{\boldsymbol{fmr}})$. As the flexion axis points to the right, it will be directed laterally in the right femur and medially in the left femur[46].

$\boldsymbol{fc_m}$ – Point on the tibial socket adjacent to the most medial point of the femoral epicondyle along the epicondylar axis

(1)

$\boldsymbol{fc_l}$ – Point on the tibial socket adjacent to the most lateral point of the femoral epicondyle along the epicondylar axis

$$\boldsymbol{fc_l} = [fc_{l,x}\ fc_{l,y}\ fc_{l,z}] \tag{2}$$

$\boldsymbol{o_{fmr}}$ – Origin of the femoral coordinate system

$$\boldsymbol{o_{fmr}} = \frac{\boldsymbol{fc_m} + \boldsymbol{fc_l}}{2} \tag{3}$$

$\boldsymbol{gt_{ips}}$ – Ipsilateral greater trochanter

Figure 5: Dashed circle indicates location of femoral condyle contour that is often evident on a tibial socket.

$$\boldsymbol{gt_{ips}} = \left[gt_{ips,x}\ gt_{ips,y}\ gt_{ips,z}\right] \tag{4}$$

$\boldsymbol{gt_{con}}$ – Contralateral greater trochanter

$$\boldsymbol{gt_{con}} = \left[gt_{con,x}\ gt_{con,y}\ gt_{con,z}\right] \tag{5}$$

$\boldsymbol{h}$ – Center of the femoral head

$$\boldsymbol{h} = \boldsymbol{gt_{ips}} + \frac{\boldsymbol{gt_{con}} - \boldsymbol{gt_{ips}}}{\mathbf{4}} \tag{6}$$

$\hat{\boldsymbol{z}}_{\boldsymbol{fmr}}$ – Mechanical axis of the femur, directed proximally

$$\hat{\boldsymbol{z}}_{\boldsymbol{fmr}} = \frac{\boldsymbol{h} - \boldsymbol{o_{fmr}}}{\left\|\boldsymbol{h} - \boldsymbol{o_{fmr}}\right\|} \tag{7}$$

$\hat{\boldsymbol{y}}_{\boldsymbol{fmr}}$ – Anterior/Posterior axis of the femur, directed anteriorly, equation for right side

$$\hat{\boldsymbol{y}}_{\boldsymbol{fmr}} = \frac{\hat{\boldsymbol{z}}_{\boldsymbol{fmr}} \times \left\{\frac{\boldsymbol{fc_l} - \boldsymbol{fc_m}}{\left\|\boldsymbol{fc_l} - \boldsymbol{fc_m}\right\|}\right\}}{\left\|\hat{\boldsymbol{z}}_{\boldsymbol{fmr}} \times \left\{\frac{\boldsymbol{fc_l} - \boldsymbol{fc_m}}{\left\|\boldsymbol{fc_l} - \boldsymbol{fc_m}\right\|}\right\}\right\|} \tag{8}$$

Note: Medial-lateral vector used in calculation above $(\boldsymbol{fc_l} - \boldsymbol{fc_m})$ *will be reversed for left side calculations such that* $\hat{\boldsymbol{y}}_{\boldsymbol{fmr}}$ *always points anteriorly.*

$\hat{\boldsymbol{x}}_{\boldsymbol{fmr}}$ – Flexion axis of the femur, directed to the right

$$\hat{\boldsymbol{x}}_{\boldsymbol{fmr}} = \hat{\boldsymbol{y}}_{\boldsymbol{fmr}} \times \hat{\boldsymbol{z}}_{\boldsymbol{fmr}} \tag{9}$$

4.3.2 TIBIAL SOCKET

A portion of the proximal tibia may remain on the residual limb which is likely to be entirely covered by the tibial socket. Therefore, a description of the tibial coordinate system is often unnecessary and can be replaced by a coordinate system for the tibial socket instead. The tibial socket origin $(\boldsymbol{o_{ts}})$ is located at the center of the pyramid. The mechanical axis of the tibial socket $(\hat{\boldsymbol{z}}_{\boldsymbol{ts}})$ will point proximally with the distal end passing through the tibial socket origin $(\boldsymbol{o_{ts}})$

and the proximal end passing through the femoral origin($\boldsymbol{o_{frm}}$), which is rigidly fixed to the tibial socket. The frontal plane is defined as containing the tibial socket mechanical axis ($\hat{\boldsymbol{z}}_{\boldsymbol{ts}}$) and the medial and lateral points of the femoral epicondyles along the epicondylar axis($\boldsymbol{fc_m}, \boldsymbol{fc_l}$). The normal to the frontal plane, or the tibial socket anterior-posterior axis ($\hat{\boldsymbol{y}}_{\boldsymbol{ts}}$), is directed anteriorly and calculated as the cross product of the tibial socket mechanical axis ($\hat{\boldsymbol{z}}_{\boldsymbol{ts}}$) and vector containing $\boldsymbol{fc_m}$ and $\boldsymbol{fc_l}$ such that it is directed to the right. The medial-lateral or flexion axis of the tibial socket ($\hat{\boldsymbol{x}}_{\boldsymbol{ts}}$) is directed to the right and calculated as the cross product of the tibial socket anterior-posterior axis ($\hat{\boldsymbol{y}}_{\boldsymbol{ts}}$) and the tibial socket mechanical axis($\hat{\boldsymbol{z}}_{\boldsymbol{ts}}$). As the medial-lateral axis of the tibial socket ($\hat{\boldsymbol{x}}_{\boldsymbol{ts}}$) points to the right, it will be directed laterally in the right tibial socket and medially in the left[46].

$\boldsymbol{o_{ts}}$ – Origin of the tibial socket coordinate system, located at the center of the pyramid

$$\boldsymbol{o_{ts}} = \left[o_{ts,x}\ o_{ts,y}\ o_{ts,z}\right] \tag{10}$$

$\hat{\boldsymbol{z}}_{\boldsymbol{ts}}$ – Mechanical axis of the tibial socket, directed proximally

$$\hat{\boldsymbol{z}}_{\boldsymbol{ts}} = \frac{\boldsymbol{o_{fmr}} - \boldsymbol{o_{ts}}}{\left\|\boldsymbol{o_{fmr}} - \boldsymbol{o_{ts}}\right\|} \tag{11}$$

$\hat{\boldsymbol{y}}_{\boldsymbol{ts}}$ – Anterior/Posterior axis of the tibial socket, directed anteriorly

$$\hat{\boldsymbol{y}}_{\boldsymbol{ts}} = \hat{\boldsymbol{z}}_{\boldsymbol{ts}} \times \left\{\frac{\boldsymbol{fc_l} - \boldsymbol{fc_m}}{\left\|\boldsymbol{fc_l} - \boldsymbol{fc_m}\right\|}\right\} \tag{12}$$

Note: Medial-lateral vector used in calculation above ($\boldsymbol{fc_l} - \boldsymbol{fc_m}$) *will be reversed for left side calculations such that* $\hat{\boldsymbol{y}}_{\boldsymbol{ts}}$ *always points anteriorly.*

$\hat{\boldsymbol{x}}_{\boldsymbol{ts}}$ – Flexion axis of the tibial socket, directed to the right

$$\hat{\boldsymbol{x}}_{\boldsymbol{ts}} = \hat{\boldsymbol{y}}_{\boldsymbol{ts}} \times \hat{\boldsymbol{z}}_{\boldsymbol{ts}} \tag{13}$$

4.3.3 PYLON

The origin of the pylon coordinate system $(\boldsymbol{o_p})$ is located at the centroid of the cross section of the most proximal end of the pylon $(\boldsymbol{p_p})$. In the special case where the prosthesis does not allow translation between the tibial socket and the pylon, $\boldsymbol{p_p}$will be coincident with $\boldsymbol{o_{ts}}$. The mechanical axis of the pylon $(\hat{\boldsymbol{z}}_{\boldsymbol{p}})$ will be directed proximally with the proximal end passing through $\boldsymbol{p_p}$ and the distal end passing through the centroid of the cross section of the most distal end of the pylon($\boldsymbol{p_d}$). Oftentimes, four fixation screws, spaced 90˚ apart around the circumference of the pylon, will be located on a tube adapter at the proximal and distal ends of the pylon$(\boldsymbol{s_{pl}}, \boldsymbol{s_{pm}}, \boldsymbol{s_{dl}}, \boldsymbol{s_{dm}})$. The locations of two of these screws (Figure 4) may be used to construct two additional planes for the pylon, equivalent to the sagittal and frontal plane. These planes will not serve a truly anatomical purpose as the screw locations may be arbitrary, however, these two additional planes will allow for a calculation of rotational alignment between the pylon and adjacent components. It is recommended that two of the distal, instead of proximal, fixation screws be used for the temporary medial-lateral vector for the pylon (see the second argument of the cross product in Eq. (20)) as the proximal fixation screws are often stationary with the tibial socket while the pylon's rotational alignment is adjusted by loosening the set screw on the tube clamp adapter (Figure 6).

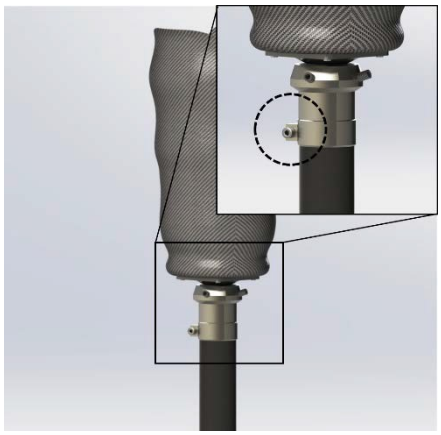

Figure 6: Proximal tube clamp adapter screw.

$\boldsymbol{p_p}$ – Centroid of the cross section of the most proximal end of the pylon

$$\boldsymbol{p_p} = [p_{p,x}\ p_{p,y}\ p_{p,z}] \tag{14}$$

$\boldsymbol{p_d}$ – Centroid of the cross section of the most distal end of the pylon

$$\boldsymbol{p_d} = [p_{d,x}\ p_{d,y}\ p_{d,z}] \tag{15}$$

$\boldsymbol{o_p}$ – Origin of the pylon coordinate system

$$\boldsymbol{o_p} = \boldsymbol{p_p} \tag{16}$$

$\hat{\boldsymbol{z}}_{\boldsymbol{p}}$ – Mechanical axis of the pylon, directed proximally

$$\hat{\boldsymbol{z}}_{\boldsymbol{p}} = \frac{\boldsymbol{p_p} - \boldsymbol{p_d}}{\|\boldsymbol{p_p} - \boldsymbol{p_d}\|} \tag{17}$$

$\boldsymbol{s_{dl}}$ – Distal lateral pylon fixation screw position

$$\boldsymbol{s_{dl}} = [s_{dl,x}\ s_{dl,y}\ s_{dl,z}] \tag{18}$$

$\boldsymbol{s_{dm}}$ – Distal medial pylon fixation screw position

$$\boldsymbol{s_{dm}} = [s_{dm,x}\ s_{dm,y}\ s_{dm,z}] \tag{19}$$

$\hat{\boldsymbol{y}}_{\boldsymbol{p}}$ – Anterior-posterior axis of the pylon, directed anteriorly

$$\hat{\boldsymbol{y}}_{\boldsymbol{p}} = \hat{\boldsymbol{z}}_{\boldsymbol{p}} \times \left\{ \frac{\boldsymbol{s_{dl}} - \boldsymbol{s_{dm}}}{\|\boldsymbol{s_{dl}} - \boldsymbol{s_{dm}}\|} \right\} \tag{20}$$

Note: Medial-lateral vector used in calculation above $(\boldsymbol{s_{dl} - s_{dm}})$ *will be reversed for left side calculations such that* $\hat{\boldsymbol{y}}_{\boldsymbol{p}}$ *always points anteriorly.*

$\hat{\boldsymbol{x}}_{\boldsymbol{p}}$ – Medial-lateral axis of the pylon, directed to the right

$$\hat{\boldsymbol{x}}_{\boldsymbol{p}} = \hat{\boldsymbol{y}}_{\boldsymbol{p}} \times \hat{\boldsymbol{z}}_{\boldsymbol{p}} \tag{21}$$

Note: An alternative approach is to first create the pylon x-axis by utilizing the proximal anterior and posterior pylon fixation screws to create and anterior-posterior vector crossed with the pylon z-axis. The final pylon y-axis can then be created by crossing the pylon z and x-axes.

4.3.4 FOOT/FOOT SHELL

Anatomic ankle joint motion has been traditionally quantified by measuring the kinematics of the foot with respect to the tibia/fibula with the origin of the foot set at the ankle joint center, defined as the midpoint of the medial and lateral malleoli[60]. However, the construction of a standard prosthetic foot is such that rotation in the sagittal plane does not occur at the pylon-foot junction (the analog of the ankle joint), but rather as a result of bending deformation of the foot itself. Therefore, a rigid body assumption for the prosthetic foot may not be as appropriate as with an anatomic foot. However, a rigid body assumption may be sufficient for a majority of the biomechanical research community due to substantially greater computational requirements for deformable body dynamic analysis. As the majority of prosthetic foot deformation is likely to occur in the sagittal plane between the plantar surface and the ankle, the foot mechanical axis $(\hat{\boldsymbol{y}}_{\boldsymbol{ft}})$ may be defined as along the plantar surface. The mechanical axis of the foot is directed distally with the proximal end passing through the most proximal point on the heel of the foot shell $(\boldsymbol{ft_p})$ and the distal end passing through the tip of the second toe of the foot shell$(\boldsymbol{ft_d})$. This is in keeping with the ISB recommendation for the anatomic foot axis that lies along the long axis of the second

metatarsal[60]. The origin of the foot $(\boldsymbol{o_{ft}})$ shall be located at the midpoint of $\boldsymbol{ft_p}$ and $\boldsymbol{ft_d}$. The sagittal plane may be defined as containing the foot mechanical axis $(\hat{\boldsymbol{y}}_{\boldsymbol{ft}})$ and the centroid of the cross section of the most distal end of the pylon $(\boldsymbol{p_d})$. The normal to the sagittal plane, or the foot medial-lateral/flexion axis $(\hat{\boldsymbol{x}}_{\boldsymbol{ft}})$, is directed to the right and is calculated as the cross product of the foot mechanical axis $(\hat{\boldsymbol{y}}_{\boldsymbol{ft}})$ and the vector directed from $\boldsymbol{ft_p}$ to $\boldsymbol{p_d}$. Finally, the rotational axis of the foot $(\hat{\boldsymbol{z}}_{\boldsymbol{ft}})$ is directed dorsally and calculated as the cross product of the foot medial-lateral/flexion axis $(\hat{\boldsymbol{x}}_{\boldsymbol{ft}})$ and the foot mechanical axis $(\hat{\boldsymbol{y}}_{\boldsymbol{ft}})$.

$\boldsymbol{ft_p}$ – The most proximal point on the heel of the foot shell

$$\boldsymbol{ft_p} = [ft_{p,x}\ ft_{p,y}\ ft_{p,z}] \tag{22}$$

$\boldsymbol{ft_d}$ – The tip of the second toe of the foot shell

$$\boldsymbol{ft_d} = [ft_{d,x}\ ft_{d,y}\ ft_{d,z}] \tag{23}$$

$\boldsymbol{o_{ft}}$ – Origin of foot coordinate system

$$\boldsymbol{o_{ft}} = \frac{\boldsymbol{ft_d} + \boldsymbol{ft_p}}{2} \tag{24}$$

$\hat{\boldsymbol{y}}_{\boldsymbol{ft}}$ – Mechanical axis of the foot, directed distally

$$\hat{\boldsymbol{y}}_{\boldsymbol{ft}} = \frac{\boldsymbol{ft_d} - \boldsymbol{ft_p}}{\|\boldsymbol{ft_d} - \boldsymbol{ft_p}\|} \tag{25}$$

$\hat{\boldsymbol{x}}_{\boldsymbol{ft}}$ – Medial-lateral/flexion axis of the foot, directed to the right

$$\hat{\boldsymbol{x}}_{\boldsymbol{ft}} = \frac{\hat{\boldsymbol{y}}_{\boldsymbol{ft}} \times \left\{\frac{\boldsymbol{p_d} - \boldsymbol{ft_p}}{\|\boldsymbol{p_d} - \boldsymbol{ft_p}\|}\right\}}{\left\|\hat{\boldsymbol{y}}_{\boldsymbol{ft}} \times \left\{\frac{\boldsymbol{p_d} - \boldsymbol{ft_p}}{\|\boldsymbol{p_d} - \boldsymbol{ft_p}\|}\right\}\right\|} \tag{26}$$

$\hat{\boldsymbol{z}}_{\boldsymbol{ft}}$– Rotational axis of the foot, directed dorsally

$$\hat{z}_{ft} = \hat{x}_{ft} \times \hat{y}_{ft} \quad (27)$$

PROSTHETIC ALIGNMENT CALCULATION

Once reference frames have been created for each component of the prosthesis, kinematic alignment can be calculated through use of transformation matrices, which provide a means of measuring differences in position and orientation between components. This will provide common prosthesis alignment parameters of interest including socket add/abduction, socket extension/flexion, and foot rotation. Details of how to perform these calculations using the points described above can be found in the Appendix B.

4.4 EXAMPLE CASE

In order to demonstrate the practical utility of the above-described methods, one transtibial amputee was tested in the Auburn University Biomechanical Engineering (AUBE) Lab. A ten (10) camera motion capture system (Vicon, Vantage V5 Wide Optics cameras, each with 22 high-powered IR LED strobe at 85 nm) was utilized in the study. The laboratory is also outfitted with two force plates (AMTI BP400600, 2000 lb. capacity) that were used to determine the timing of heel strike, thus the beginning and ending of a single gait cycle. The subject tested was a 39 year old male, 1.8 m tall, and weighed 92.5 kg. The subject had a right-sided transtibial amputation and wore a transtibial prosthesis (Ossur PRO-FLEX® LP with a Unity® Vacuum System). All study procedures were approved by the Auburn University Institutional Review Board.

A total of ten reflective markers were placed on the subject's prosthesis and both the ipsilateral and contralateral greater trochanter (Figure 7). After placement of the markers, a static reference trial was collected, followed by three walking trials at the subject's self-selected walking speed. Marker position data was collected at a rate of 120 Hz and filtered post-hoc with a low pass Butterworth filter with a cutoff frequency of 15 Hz.

Algorithms were created in MATLAB (R2017b) which utilized the previously-described alignment measurement methods. The filtered marker positions for the static trial as well as all three dynamic walking trials were used with the algorithms to calculate static alignment during quiet stance as well as dynamic alignment during walking. The alignment during quiet stance was taken as the mean value of the first 500 ms during static collection and is provided in Table 2.

Tibial Socket	Angle	Pylon	Angle	Foot	Angle
Extension (deg)	-14.4	Extension (deg)	7.1	Dorsiflexion (deg)	0.5
Adduction (deg)	22.9	Adduction (deg)	1.3	Inversion (deg)	0.6
Internal Rotation (deg)	-0.6	Anterior Translation (m)	0.0	*Internal Rotation (deg)	-5.3
		Lateral Translation (m)	0.0		

*Table 2: Static alignment values of the transtibial prosthesis during quiet stance. *Internal rotation of the foot measured with respect to the socket*

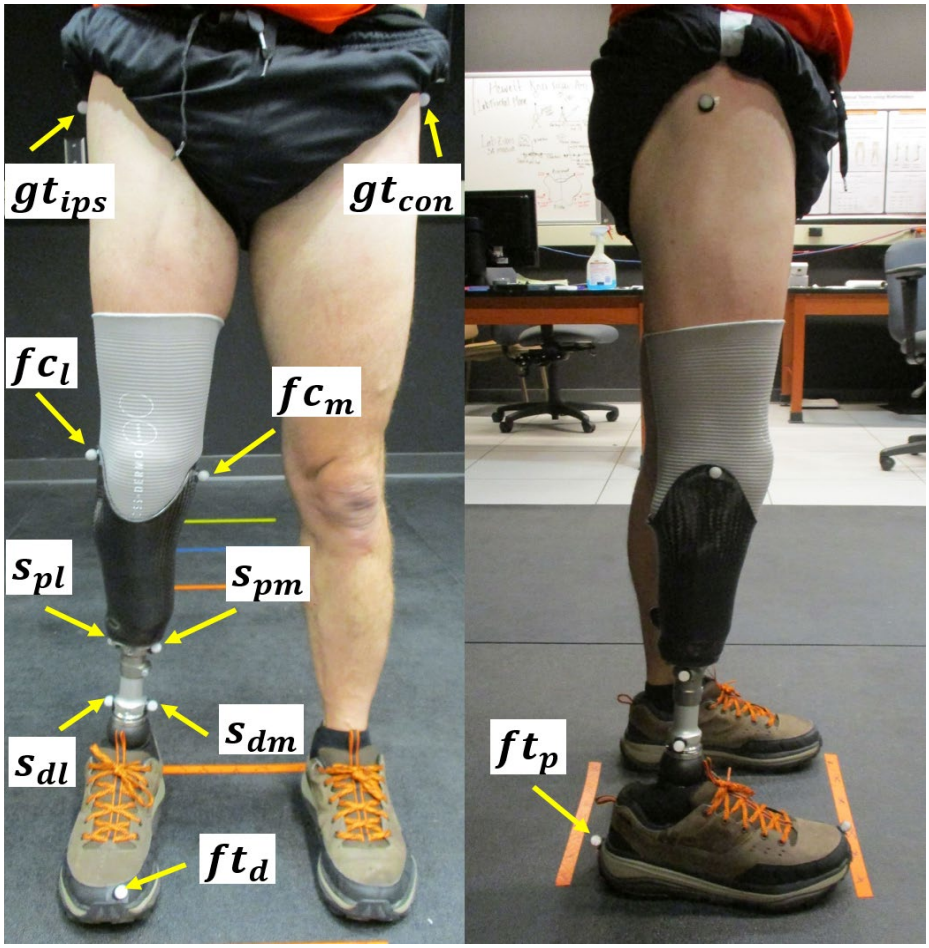

Figure 7: Reflective marker placement

Dynamic alignment was calculated for each of the three walking trials. Trial data was truncated at two consecutive heel strikes (> 20 N)[61] as to only include one gait cycle. Data was then resampled to 101 data points, and alignment data from all three trials were averaged together to provide one mean dynamic alignment curve per parameter of interest. These results are displayed in Figure 8-9.

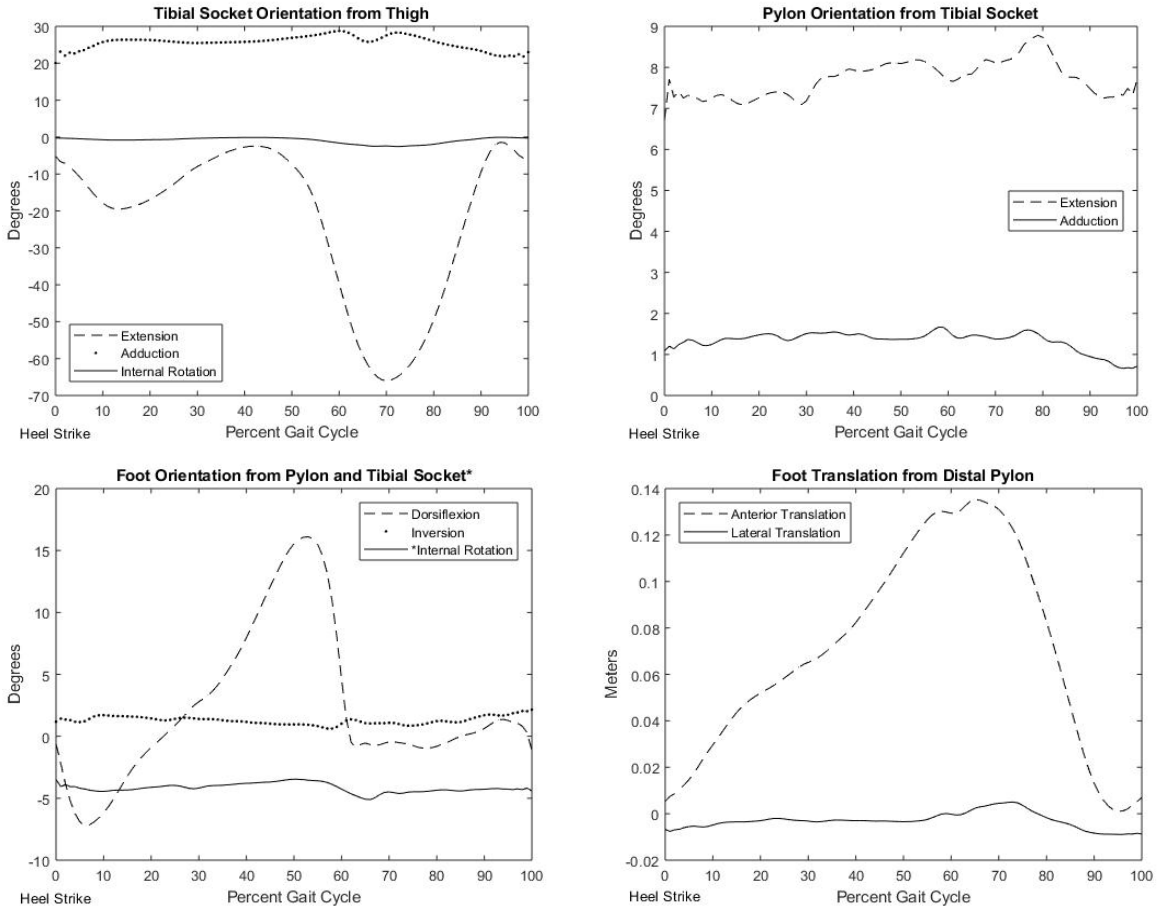

Figure 8: A. Tibial socket orientation measured from the ipsilateral thigh; B. Pylon orientation measured from the tibial socket; C. Foot dorsiflexion and inversion measured from the pylon and internal rotation measured from the tibial socket; D. Foot translation from the distal pylon. Note: although no movement is possible, mechanically, at the joint connecting the foot and the distal pylon, translation is non-zero because of the location of the origin of the foot combined with deformation of the foot during gait.

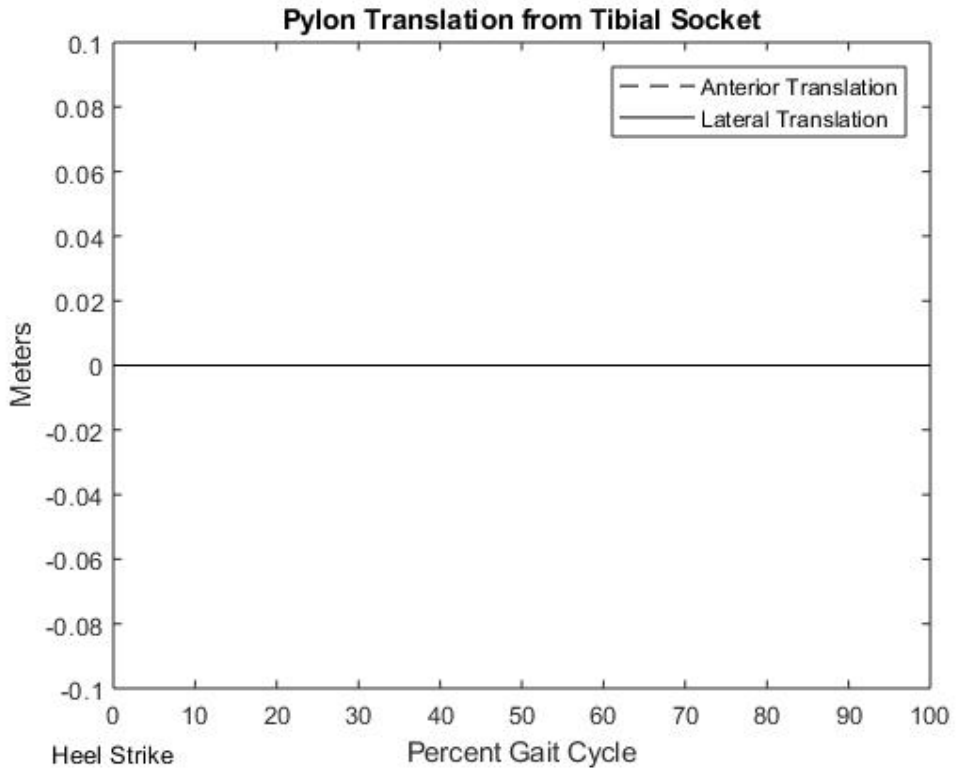

Figure 9: Pylon translation measured from the tibial socket. Zero translation, as expected, since the pylon and tibial socket share the same origin for this particular transtibial prosthesis (translation between these two components is not possible, mechanically)

4.5 DISCUSSION

The methods detailed in this article provide a standardized means of describing the three-dimensional alignment and relative motion of the components of a transtibial lower-limb prostheses. This technique utilizes points on both the residual limb and the prosthesis that are relevant to the patient-specific anatomy and the prosthesis itself. These points are utilized to create anatomically relevant reference frames for each component of interest beginning with the patient's thigh down to the prosthetic foot. Once the reference frames are established, relative rotations and displacements are calculated via transformation matrices between components. The construction of the reference frames and coordinate systems are such that the outputted rotations and displacements between components are anatomically relevant and meaningful, such as the tibial

socket flexion angle and proximal pylon translation. Access by the investigator or prosthetist to alignment parameters such as these can be valuable to the alignment process and potentially help to improve patient outcomes.

There are some limitations to the methods presented in this article. Primarily, this method requires knowledge of the three-dimensional spatial locations of each of the relevant anatomical points needed for the subsequent calculations. Static, bench-top alignment of the prosthesis can be accomplished by use of a device such as a digitizing arm to determine the coordinates of all the points. However, should the investigator or prosthetist want to measure alignment while the patient is wearing the device or moving, a more advanced means of motion capture will be required. Common systems for real-time 3-D motion capture include but are not limited to Vicon, Qualisys, and Motion Reality. Equipment such as these are costly, but can be found in many biomechanical analysis labs around the world, including the Human Performance Lab at Walter Reed National Military Center and the Motion Analysis Lab at the Center for the Intrepid, Brooke Army Medical Center. In addition, novel, substantially cheaper motion capture technology, such as the fiducial-based system, described by [43] which utilizes a GoPro camera and easily printable markers is and will continue to be developed. Technology such as this may very easily be incorporated into prosthetists' clinics in the near future. Should this occur, the establishment of a well-defined system for measuring alignment will be critical. Another limitation to the method presented is that there is large variation in the design and construction of lower-limb prostheses. For example, the standard pylon has a fixed length, while more advanced pylon systems may allow for shortening and lengthening of the distance between the socket and the ankle joints as a means of dampening the load transmitted from the ground to the body. This allows for translation between the proximal and distal end of the pylon that is not accounted for in this article. Nevertheless, whether additional

degrees of freedom are present or the construction of the device differs in other ways, it is possible that the methods and techniques presented here may be adjusted according to the characteristics and capabilities of the specific lower-limb prosthesis being evaluated, thus may still be useful to the investigator. For example, in the case where pylon length can change, displacement can be easily calculated between the distal pylon ($\boldsymbol{p_d}$) and proximal pylon ($\boldsymbol{p_p}$). Lastly, as the purpose and scope of this article is only to present the above-described methods for alignment determination, future work such as inter-day or inter-tester repeatability of anatomical point identification (such as the location of the epicondyles), thus alignment measures, is needed. However, anatomical point identification has been well established as the most frequently used technique for studying human motion [56] as this is required to place trackable markers on the surface of the skin prior to motion capture. As such, the authors believe that the methods described here can provide immediate benefit to the prosthetics and biomechanics research community.

The main benefit of the methods described in this article is the objective assessment of lower-limb prosthesis alignment as it may show to have a relationship with more practical patient outcomes such as comfort, fit, mobility, and long-term musculoskeletal health[2,5,6]. In addition to improved patient outcomes, an objective assessment of lower-limb prosthesis alignment allows for comparison across various prosthetic devices that are currently offered and available to patients. Along with a more objective device selection criteria for both patient and prosthetist, objective inter-device comparison may lead to improved device design, which will provide a direct benefit to the patient as well. Future technology aimed at aiding in the alignment process may also benefit from a means of objectively calculating device alignment.

Another benefit of the methods presented is that existing methods of natural limb alignment may be employed such that a kinematic comparison between the natural limb and the prosthetic

limb is possible. Previously referenced techniques for the calculation of three-dimensional motion of the natural limb include work by [46](Wu & Cavanagh, n.d.), and .[55] An inter-limb comparison for unilateral amputees may assist in providing baseline values for prosthesis alignment, as well as a measure of inter-limb symmetry which may further assist in patient comfort and improved outcomes. However, caution should be taken when performing inter-limb comparisons between natural and prosthetic limbs. Although the technique presented here for lower-limb prosthesis alignment calculation is modeled after previously described techniques for natural limbs, there are differences which may prevent a side-to-side comparison from being entirely appropriate. Nevertheless, parameters such as the natural limb knee flexion angle and the tibial socket flexion angle may be a worthy comparison and may benefit the patient through increased symmetry. Lastly, current understanding and theories of natural lower-limb function, such as the ground reaction force vector passing through the instantaneous axis of the knee or the relationship between alignment and energy expenditure,[62] can be studied for prosthetic limbs utilizing the system described herein.

4.6 CONCLUSION

The methods presented in this article provide a component-based coordinate system for lower limb prostheses. This allows for an objective means of quantifying lower-limb prosthesis alignment to ultimately serve the purpose of benefiting the patient. Proper device alignment may result in improved patient outcomes such as an improved body image, a reduction in pain, and a decrease in common comorbidities associated with malalignment including osteoarthritis, osteopenia and osteoporosis[2,5,6]. Furthermore, a more objective means of quantifying transtibial prosthesis alignment may lead to improved prosthetic device design and the development of future technology for aiding in the alignment process.

4.7 CONFLICT OF INTEREST STATEMENT

The authors are not in any conflict of interest with regards to the work presented in this paper.

4.8 ACKNOWLEDGMENTS

This work is supported by the US Army Medical Research and Materiel Command under Contract No.W81XWH-17-C-0101. The views, opinions and/or findings contained in this report are those of the author(s) and should not be construed as an official Department of the Army position, policy or decision unless so designated by other documentation. The authors would also like to acknowledge Ryan Hill and Leo Richard of Integrated Solutions for Systems (IS4S) for their technical input as well as Dr. JoEllen Sefton, Director of the Warrior Research Center, School of Kinesiology, Auburn University for her contextual oversight.

CHAPTER – 5
ACCURACY OF A FIDUCIAL MARKER-BASED TRACKING SYSTEM FOR HUMAN MOTION CAPTURE SYSTEM

5.1 ABSTRACT

Fiducial markers are widely used in the field of augmented reality (AR) and virtual reality (VR). The open source code along with a single action camera has the ability to calculate the position and orientation of the fiducial markers. However, having the ability to calculate the position and orientation of markers in 3D space serves the same purpose as that offered by more expensive, traditional retroreflective marker-based motion capture system. These fiducial markers however, have not been used much for the purpose of motion capture in the field of biomechanics. Thus, this study aims to validate the accuracy of tracking and calculating position and orientation of fiducial markers during the gait cycle in order to use this system for future applications in the field of biomechanics. The proposed study was performed on five physically fit participants using a traditional retroreflective marker-based motion capture system. This study design tested the effect of 3 different marker sizes placed on the thigh of participants walking at 3 different speeds from 0 to 3.5 m from the camera. Position and orientation of the fiducial markers were aligned using an established least square method-based auto alignment system called a “Dornaika” function in MATLAB software. The aligned data were then compared between measurement systems with RMSE and analyzed statistically by performing Multivariate Analysis of Variance (MANOVA) on the RMSE. The results showed an increase in RMSE for the position and orientation of the fiducial marker with increase in speed and decrease in fiducial marker size. The RMSE increased substantially beyond 3 m of distance from the camera. This study provides a reference data chart with information about the conditions when the system works for design of future work application of fiducial marker system in the field of biomechanics. The results were

comparable to previous studies performed during a static condition of fiducial markers for utilization in augmented reality. Thus, the fiducial marker system can be used for general motion capture and gait analysis, depending on the application and if cost and portability is considered.

5.2 INTRODUCTION

A fiducial marker system is an open source computer vision system that is commonly used in the field of augmented reality[32,34–36,40], endoscopic ultrasound guidance[14–16], and liver radiotherapy[18]. This system is comprised of a commercial camera and paper printed fiducial markers with a unique ID. Open source programs are used to detect the position and orientation of the markers in the 3D space. Since it uses only a commercial camera, which can be as cheap as $50, and open source software, this system can be setup for under $100. This makes it an extremely cost effective system to track the coordinates of a location and orientation of a body in 3D space[43].

Marker-based motion capture systems, such as Vicon, Qualisys, OptiTrack, etc., track the position of the reflective markers in the 3D space by using multiple infrared cameras costing tens of thousands each, reflective markers and a software. The software has the features to visualize the reflective markers in 3D space, export the position of the markers and perform kinematics and kinetics calculations [63–65]. This system is mostly used in the film industry, biomechanics, and research and development [63–65]. As this system is considered very robust and reliable, it is widely used to conduct research in the field of Biomechanics [43,44].

Fiducial marker tracking capability has been shown to be accurate and reliable in a static environment for applications in augmented reality[34–36,40]. It has also been found to be accurate by Nagymáté et. al. for tracking fiducial markers during dynamic motion[43]. Fiducial marker

tracking systems have several advantages over traditional marker based systems. For example, a fiducial marker system is low cost, requiring only paper printed markers and a regular camera. Traditional motion capture systems require special reflective markers along with multiple infrared cameras which cost tens of thousands of dollars. In addition, fiducial marker systems are easily portable as the camera(s) does not need to be fixed in a designated space. On the contrary, traditional motion capture systems typically require a highly controlled environment with multiple cameras at fixed locations [14,66]. However, fiducial marker systems have their own limitations. For example, the distance between the camera and the marker should be within 1-5 m, depending on the testing environment and camera specifications, to reduce any capture error [15,16]. Furthermore, accuracy of fiducial marker systems vary with respect to the environment due to the variability in lighting (i.e., indoor versus outdoor) [15,32].

Currently, fiducial markers are used for various applications including augmented reality [13], endoscopic ultra-sound guidance [13–17], and liver radiotherapy[18]. Several studies had been done to validate the fiducial system's accuracy and reliability for the utilization in these applications. Most of this research validates the fiducial marker system for a static application only. For example, Malbezin.et al. performed a study to track accuracy of the fiducial marker (ARToolKit) in a static condition and reported that the error increases with increase in distance and varies within the x and y-axis of fiducial marker plane[34]. Similarly, another study by Lopez-Cerone et. al. on the accuracy of the fiducial marker (AprilTag) in a static condition found that under 4 m, the distance error stayed below 5 cm. Also, further the marker from the camera, bigger will be the error in 3D estimations[36]. A third study performed by Abawi et. al. defined an error function based on intervals which differs between high and low systematic error and standard deviation of estimated camera distance and viewing angle again in static condition of the

marker[35,40]. Further, Pentenrieder et. al.[40] created a large data base to be used as a look-up table for accuracy queries for static condition. They created a model based on simulation of ground truth data and as improvement of previous work by Abawi et. al.[35], Malbezine et. al.[34] and Zhang et. al.[41].

However, according to our knowledge, little research has been done to examine the accuracy and reliability of fiducial markers for human motion tracking where the subjects are in dynamic motion. One example is a study by Nagymáté et. al[43] who looked into potential of fiducial marker to be used for motion capture while subjects were at fixed distance from camera on a treadmill. They designed a system to capture motion of human on a treadmill fixed at a distance of 1.5 meters form the camera utilizing fiducial (AprilTag) markers of a size 11 cm x 11 cm. They presented their result as accuracy of their system in comparison to traditional retroreflective motion capture system. However, this study does not provide information regarding the effect of marker size and the effect of distance from the camera on the accuracy of the marker position and orientation.

As a result, the aim of this study was to validate the position and orientation tracking ability of fiducial markers system with respect to a traditional retroreflective marker-based motion capture system. The effect of marker size and walking speed on the accuracy of position and orientation of markers over the distance of the markers from the camera in dynamic motion was evaluated. Position and orientation data obtained from a fiducial marker tracking system is compared to that provided by a traditional infrared (used as gold standard), retroreflective marker-based motion capture system. The hypotheses of this study were: (i) Slower walking speed will result in smaller position and orientation error (ii) Larger marker size will result in smaller RMSE for position and

orientation, and (iii) Greater distance from the camera will result in greater position and orientation error.

5.3 METHODS

5.3.1 Participants

Five participants (all male; mean age = 25.4±1.96 years old, mean height = 1.76±0.08 m, mean weight = 74.11±5.12 kg) were recruited through word of mouth for this study. All participants self-reported being free of any musculoskeletal disorders. Informed consent was given by the participants before participating in the data collection. Participants were provided with the data collection procedure beforehand in order to make an informed decision to participate in the study. The study was approved by the Auburn University Institutional Review Board (IRB) Committee (07/2018) (APPENDIX A).

5.3.2 Experimental Procedure

For the data collection, subjects were invited to the Auburn University Biomechanical Engineering (AUBE) Lab. After they signed the consent form, they were fitted with 79 retroreflective markers and a wide elastic band on right femur as shown in the Figure 10. These 79 markers were used to create the human model in Nexus 2.8.2 software using Andriacchi's point cluster method[56] to create a human model for Vicon system for further processing of the Vicon data. At first, the fiducial (Aruco) marker of size 10 cm x 10 cm was attached on the elastic band with the help of Velcro. The fiducial markers was attached on 3D printed flat boards of equal size in order to keep the markers flat throughout the data collection. Three reflective markers (size: 9.5mm each) were also attached on each of the fiducial markers in order to align both the fiducial and retroreflective marker-based coordinate systems. A static trial of the subjects was taken using a Vicon motion capture system. The subjects were then asked to sway their right leg 3 times in

order to align the data between the systems, immediately followed by walking at a self-selected speed starting from about 0.8 m in front of the GoPro camera (GoPro Hero 5 Black by GoPro Inc. USA) up to 3.5 m. This event was repeated for five times. The exact same procedure was then repeated with a self-selected slow pace and a self-selected fast pace walking speed. This entire process (all three speeds, five times each) was repeated by replacing the 10 cm x 10 cm fiducial marker with a 11 cm x 11 cm and a final time with a 12 cm x 12 cm sized fiducial marker. This resulted in a total of 45 dynamic trials were recorded per subject. The data were recorded using Nexus 2.8.2 software for Vicon motion capture system and the GoPro Hero 5 Black camera to capture the video for the Augmented Reality System. The video files from GoPro camera were

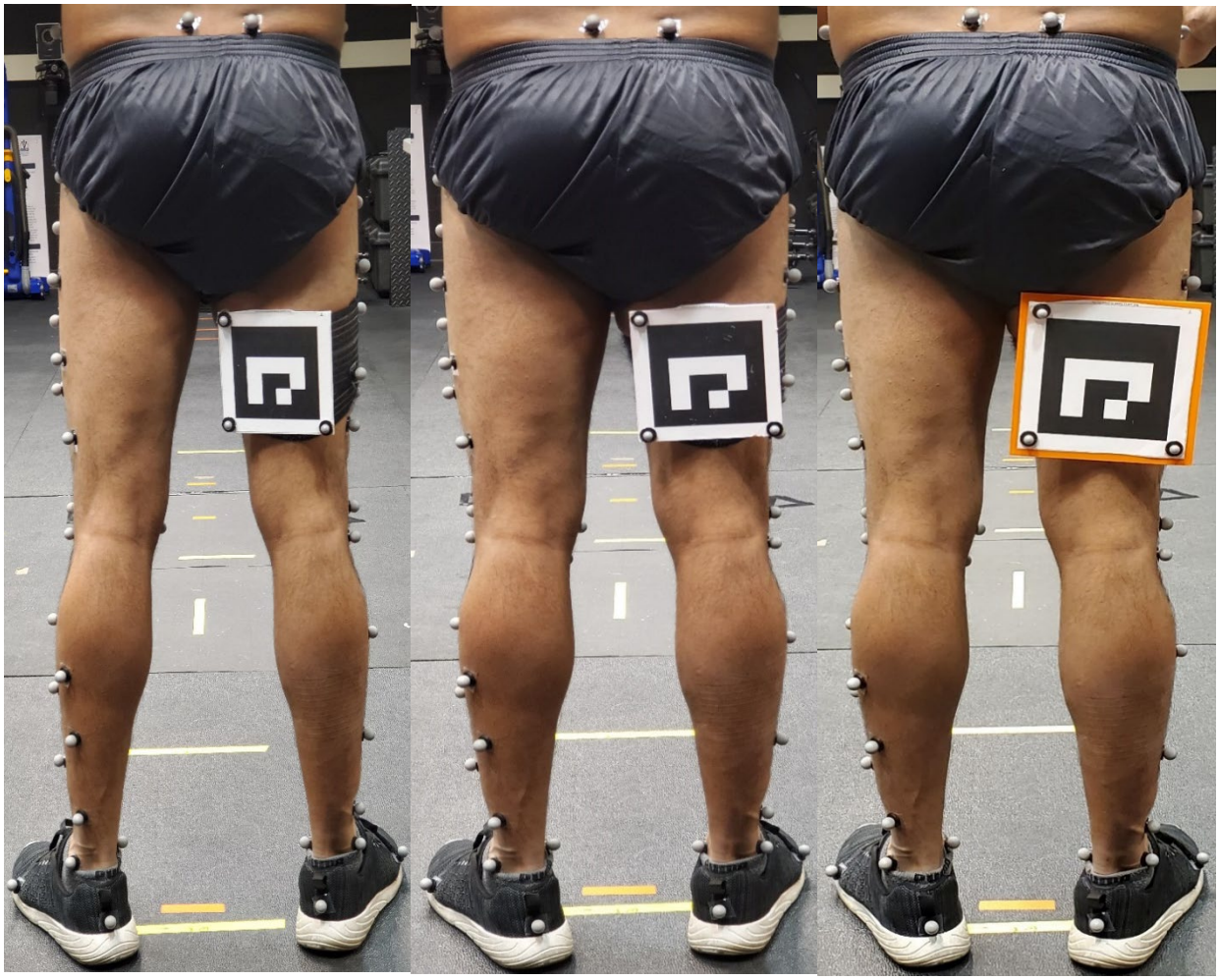

Figure 10: Test subject markered up with 79 retroreflective markers and a fiducial marker of size 10x10, 11x11, and 12x12 cm from left to right

then post-processed to obtain the fiducial markers' position and orientation as explained in image processing section below.

5.3.3 Instrumentation

A ten camera Vicon motion capture system (Vicon Motion System Ltd, UK) was used as the gold standard to simultaneously track the fiducial markers at the video sampling frequency of 120 Hz. The walking trial data captured by Vicon were then gap filled to eliminate gaps in continuous data caused due to occlusion of the reflective markers. The position of the markers data were then exported as a CSV file for further processing in MATLAB.

The fiducial system included a GoPro Hero 5 Black (GoPro, Inc. San Mateo, California, USA) camera, 3 paper printed unique fiducial marker (size 10 cm x 10 cm, 11 cm x 11 cm, and 12 cm x 12 cm) of aruco dictionary. The camera was mounted on selfie stick with a tripod. The camera was mounted at a height of 0.9 m from the ground and was tilted downward in order to ensure it would capture the fiducial markers in its frame. The GoPro was configured to 2.7k resolution at 50 fps with 1/100 shutter speed in linear mode as described in Nagymáté et. al. paper [43]. The linear mode of the camera has an inbuilt image undistortion function to avoid optical distortion while recording. The GoPro camera was calibrated once before capturing the trial using a 7x9 square checkerboard with square size of 20 mmx20 mm. The captured videos were then post-processed as described in the section below.

5.3.4 Image Processing

The video captured by the GoPro was exported to the PC and processed using Robotic Operating System (ROS). The command *ffmpeg* was used to convert the Gopro file to a ROS readable mp4 file. The video file was then run at $1/5^{th}$ of the frame rate (5fps) along with the

aruco_detect and *fiducial_pose rosnode* commands (see Appendix H). This was to detect the fiducial markers in the video file and record the fiducial markers position and orientation data as a .bag file. The video file image data were the recorded using the *rosbag* command while the video files were run through the *rosnodes*. The .bag files obtained for each trial was then stored and used for alignment with the Vicon data.

5.3.5 Fiducial System Accuracy

The data obtained from Vicon and the ROS fiducial marker system were then imported into a custom MATLAB code and were first resampled to fiducial system's camera frequency (50 Hz). The data from both systems were then synchronized to the same time using the side sway data of the right leg from the trials using an established auto-align function called "Dornaika" in the MATLAB software. Dornaika function is based on least square method to auto align data from two different systems as explained in Dornaika et. al. [67]. The aligned data were then plotted as x-axis, y-axis, and z-axis for both position and orientation. The MATLAB algorithm and script can be found in Appendix C and D.

The average error of the Aruco markers' position and orientation was calculated using the Root Mean Square Error (RMSE) equation shown below:

$$RMS = \sqrt{\frac{1}{n}\sum_{n}(\theta_{Vicon} - \theta_{ROS})^2}$$

The RMSE calculation was also performed in MATLAB software. The error values were calculated for four different distance intervals, namely 0-1 m, 1-2 m, 2-3 m, 3-3.5 m from the GoPro camera. The RMSE for both position and orientation were used for statistical analysis.

5.3.6 Statistical Analysis

The data analysis was performed using IBM SPSS statistical analysis software. A three-factor multivariate analysis of variance (MANOVA) was used to test the main and interactive effects of marker size, walking speed, and distance from the GoPro camera on RMSE of position and orientation or the fiducial markers. The RMSE in position of x-axis, y-axis, z-axis, and the magnitude data were used as dependent variables. The size of markers, walking speed and distance from the camera were coded as independent variables and subjects were coded as ID in the SPSS software. A similar procedure was followed for encoding the dependent and independent variables in SPSS for RMSE of orientation of the marker.

A Tukey HSD (Honestly Significant Difference) test was performed for all the three factors (speed, size, and distance). The descriptive statistics were outputted and bar charts of the marginal mean of RMSE were plotted with distance on x-axis, RMSE on y-axis, different speed RMSE stacked together, and separate charts for different marker sizes. The marginal mean bar charts were plotted for position and orientation results in the similar pattern described above for each dependent variables.

5.4 Results

5.4.1 RMSE in the Position

The histogram charts for the RMSE of the position of the center of the fiducial markers can be seen in the Figure 11. The histogram chart in the Figure 11 includes the RMSE for three walking speed (i.e. slow, self-selected and fast) over four distance intervals. The charts have been separated for size and shown in one column for each outcome (x-axis, y-axis, z-axis and magnitude (R)). The value of RMSE with their SD table can be found in Appendix G as Table 5. From the

histogram charts, it can be seen that the RMSE for position between the two systems increases as the walking speed increases, which can be seen if when reading the histogram stacks for each distance intervals from left to right. Similarly, the histograms also show that the RMSE for position decreases as the marker size increases, supporting our hypotheses about speed, size and distance.

Further, the MANOVA statistical analysis also supports our hypotheses as shown by the results in the Table 3. It was observed that the size and distance cause statistically significant ($p<0.01$) main effects on the RMSE of the position of fiducial marker. In addition, a univariate test (Tukey HSD) was performed on size and distance to further analyze the error in the sub-category of each of these factors (size, speed and distance). The results have been presented in Table 9 (included in the Appendix G) with multiple comparisons of each size and walking speed with each other. Their mean difference and significant value have been presented in the table. As expected, for x-axis and magnitude, the small to large size had significant differences at significance level of $p<0.05$ and $p<0.01$, respectively, with mean difference of 2.45 cm and 7.58 cm respectively. Thus, supporting the hypothesis that larger the size less will be the error, while for y and z-axes small to medium had a significant different with mean difference of 5.42 cm and 4.54 cm respectively rather than in between small and large marker size. There was also a significant difference in RMSE due to distance from the camera, supporting the hypothesis that the further the marker, the lower the accuracy of fiducial system.

Effect	Wilks' Lambda Value	Sig.	Partial Eta Squared
Size	0.658	0.000**	0.189
Speed	0.938	0.333	0.031
Distance	0.158	0.000**	0.459
Size*Speed	0.903	0.552	0.025
Size*Distance	0.727	0.000**	0.077
Speed*Distance	0.932	0.994	0.018
Size*Speed*Distance	0.914	1.000	0.022

*Table 3: MANOVA result for main effect and interaction effect on position RMSE. **Statistically-significant ($p<0.01$)*

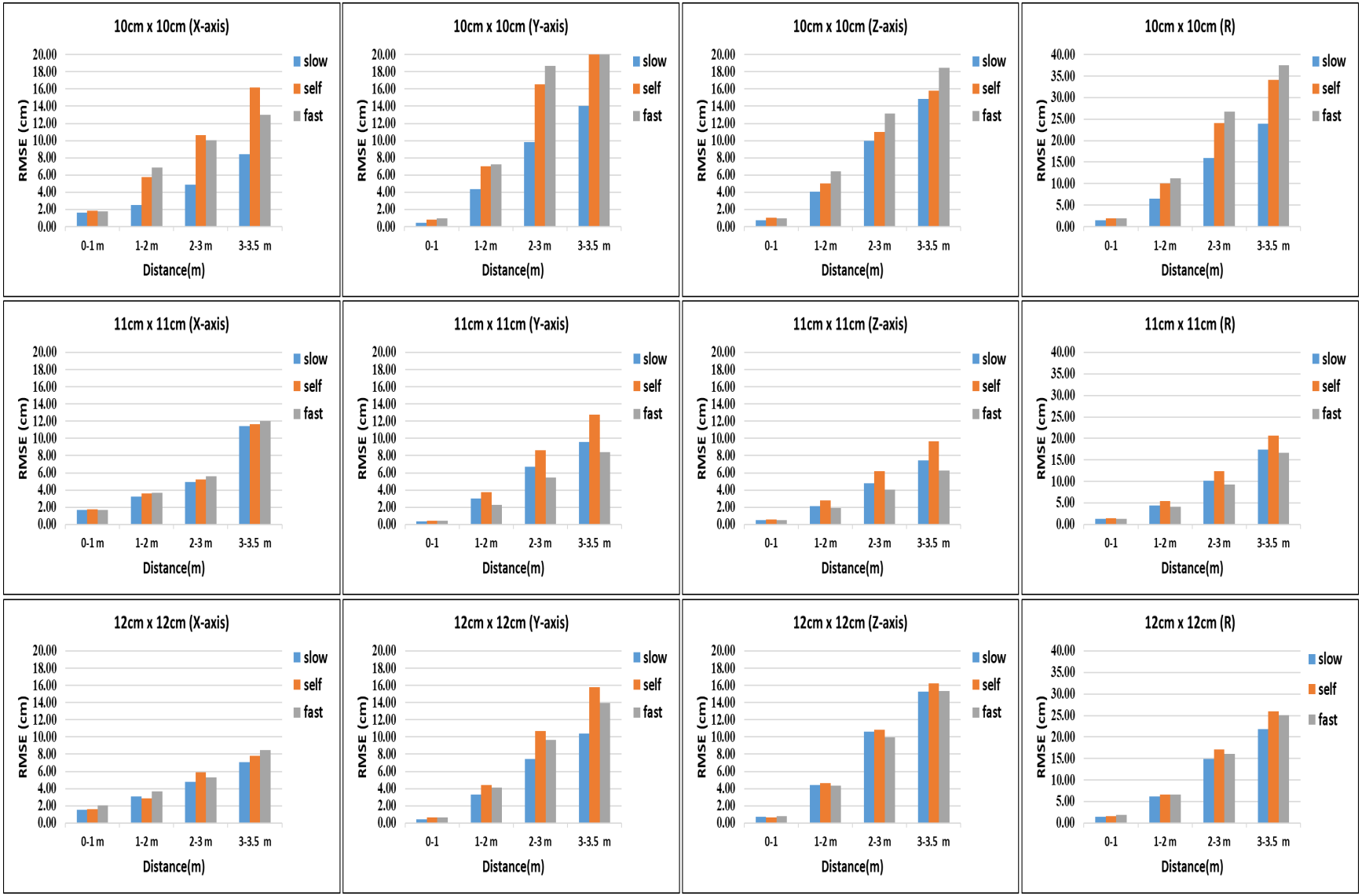

Figure 11: Histogram of RMS Error for the position of fiducial marker for all 3 size of markers, three walking speeds and in all axis Column1: RMSE in x-axis for all 3 sizes of marker from top to bottom, Column 2: RMSE in y-axis for all 3 sizes of marker from top to bottom, Column 3: RMSE in z-axis for all 3 sizes of marker from top to bottom, and Column 4: RMSE in magnitude of position (R) for all 3 sizes of marker from top to bottom

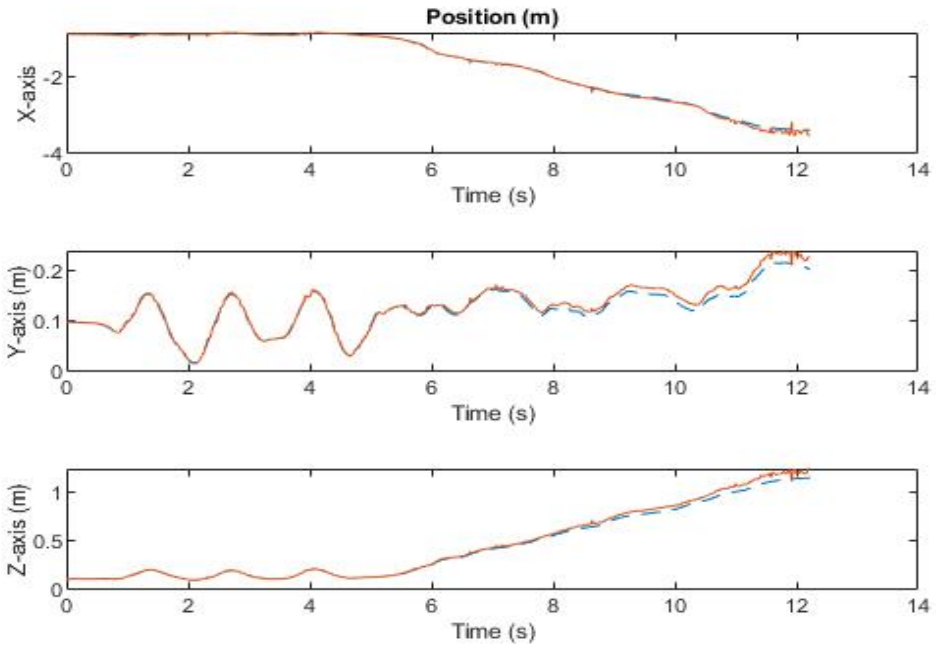

Figure 12: Time synchronized position data from both systems for the 11x11 cm marker size during slow speed.

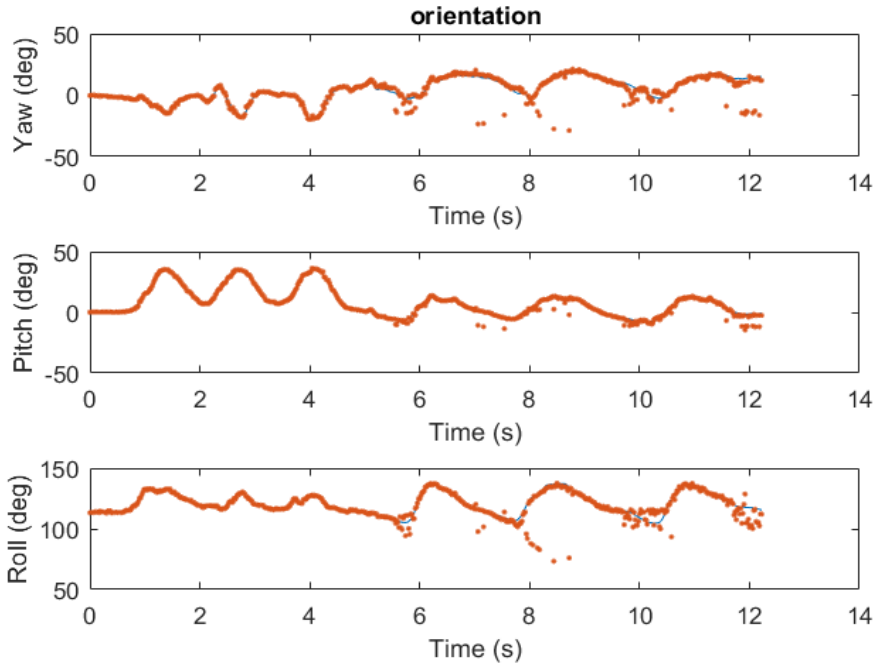

Figure 13: Time synchronized aligned orientation data from both system for 11x11 cm marker size and slow speed trial

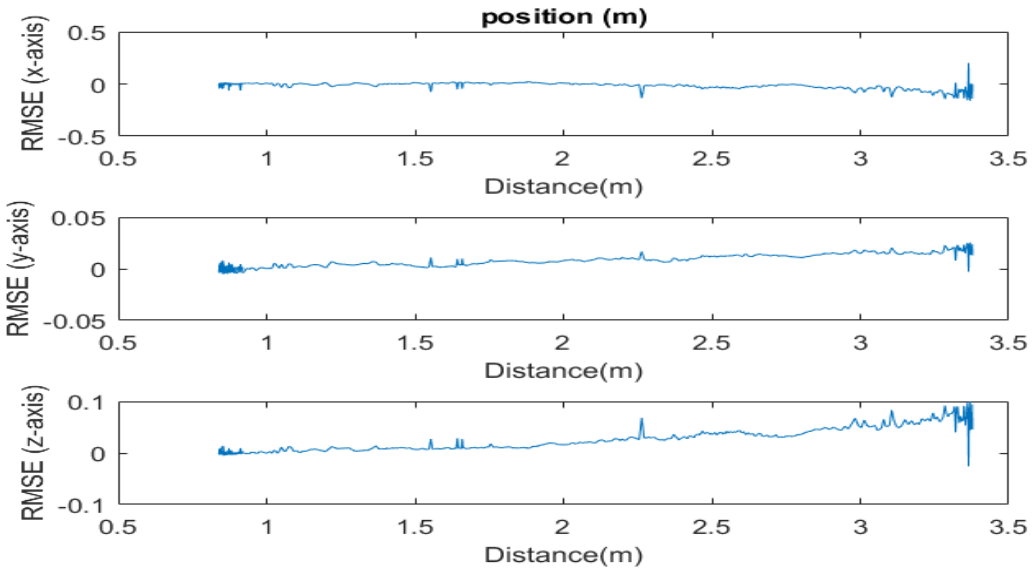

Figure 15: RMSE of position in x-axis, y-axis, and z-axis for 11x11 cm marker size during a slow speed trial

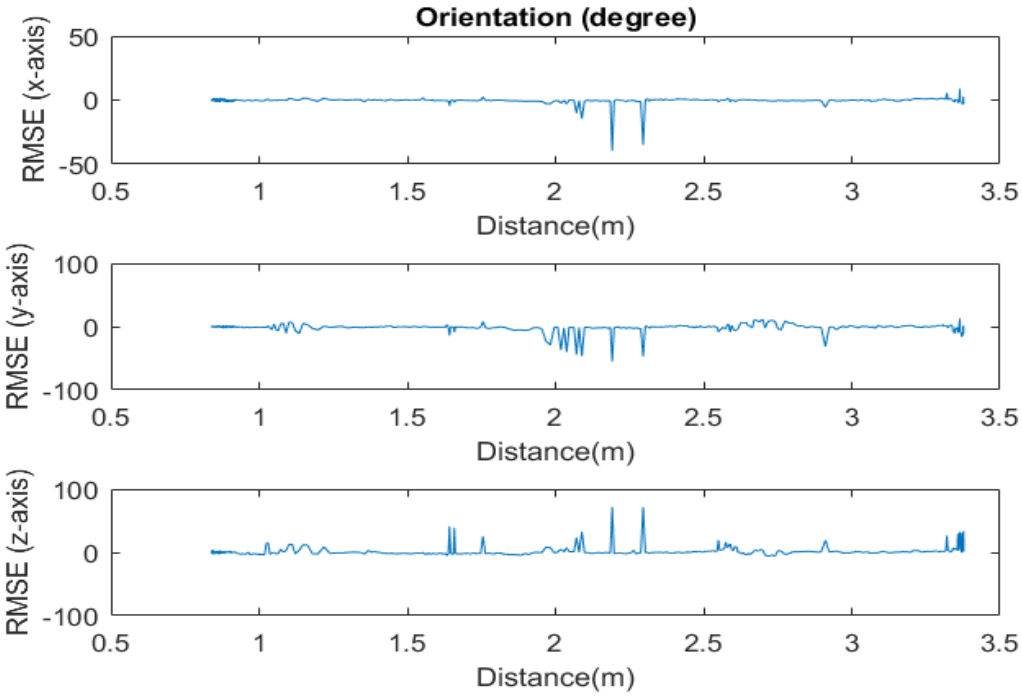

Figure 14: RMSE of orientation between both system data in x-axis, y-axis, and z-axis for 11x11 cm marker size and slow speed trial

5.4.2 RMSE of Orientation

The histogram charts for RMSE of orientation of the fiducial markers can be seen in the Figure 16. The histogram chart in Figure 16 includes the RMSE for three walking speed (slow, self-selected and fast) over four distance intervals from the camera position. The values of RMSE for orientation with standard deviation can be found in Appendix G as Table 6.

From the histogram charts, it can be seen that the RMSE for orientation between the two systems also increases as the walking speed increases which can be seen when reading the histogram stacks for each distance intervals from left to right. Similarly, the histograms also show that the RMSE for position decreases as the marker size increases supporting our hypotheses again for orientation similar to position error.

Further, the MANOVA statistical analysis also supports our hypotheses (Table 4). Unlike position error, it was observed that all three factors (size, speed, and distance) caused statistically significant ($p<0.01$) main effects on the RMSE of the orientation of the fiducial marker. It was also observed that the interaction of size and distance and the interaction of speed and distance also had a significant effect on the RMSE of orientation of the fiducial marker. Thus, a univariate test (Tukey HSD) was performed on size, speed, and distance and their interactions to further analyze the error in the sub-category of each of these factors. However, this study only focused on the effect of size, speed and distance and have included the interaction effect result in the appendix. The results have been presented in the Table 10 (included in Appendix G) with multiple comparison of each size, walking speed, and distance interval with each other. Their mean difference and significant value have been presented in the table. As expected, but in contrast to position results, all the comparisons for size had a significant effect ($p<0.05$) on all independent variables. However, the largest mean difference was between small and large except for y-axis

(which was between small and medium size) result. Thus, supporting the hypothesis that larger the size, less will be the error. There was also a significant difference in tracking orientation or fiducial marker between Vicon and fiducial system because of speed. However, the significant difference was only in x-axis of all speed and in y-axis for slow and fast speed. Finally, there was also a significant difference in tracking orientation between both systems because of distance of fiducial markers from the camera, which supports the hypothesis of further the marker less the accuracy in tracking of orientation by fiducial system.

Effect	Wilks' Lambda Value	Sig.	Partial Eta Squared
Size	0.621	0.000**	0.212
Speed	0.349	0.000**	0.186
Distance	0.215	0.000**	0.401
Size*Speed	0.858	0.144	0.038
Size*Distance	0.665	0.000**	0.097
Speed*Distance	0.711	0.002**	0.082
Size*Speed*Distance	0.831	0.993	0.045

*Table 4: MANOVA result for main effect and interaction effect on orientation RMSE. **Statistically-significant (p<0.01)*

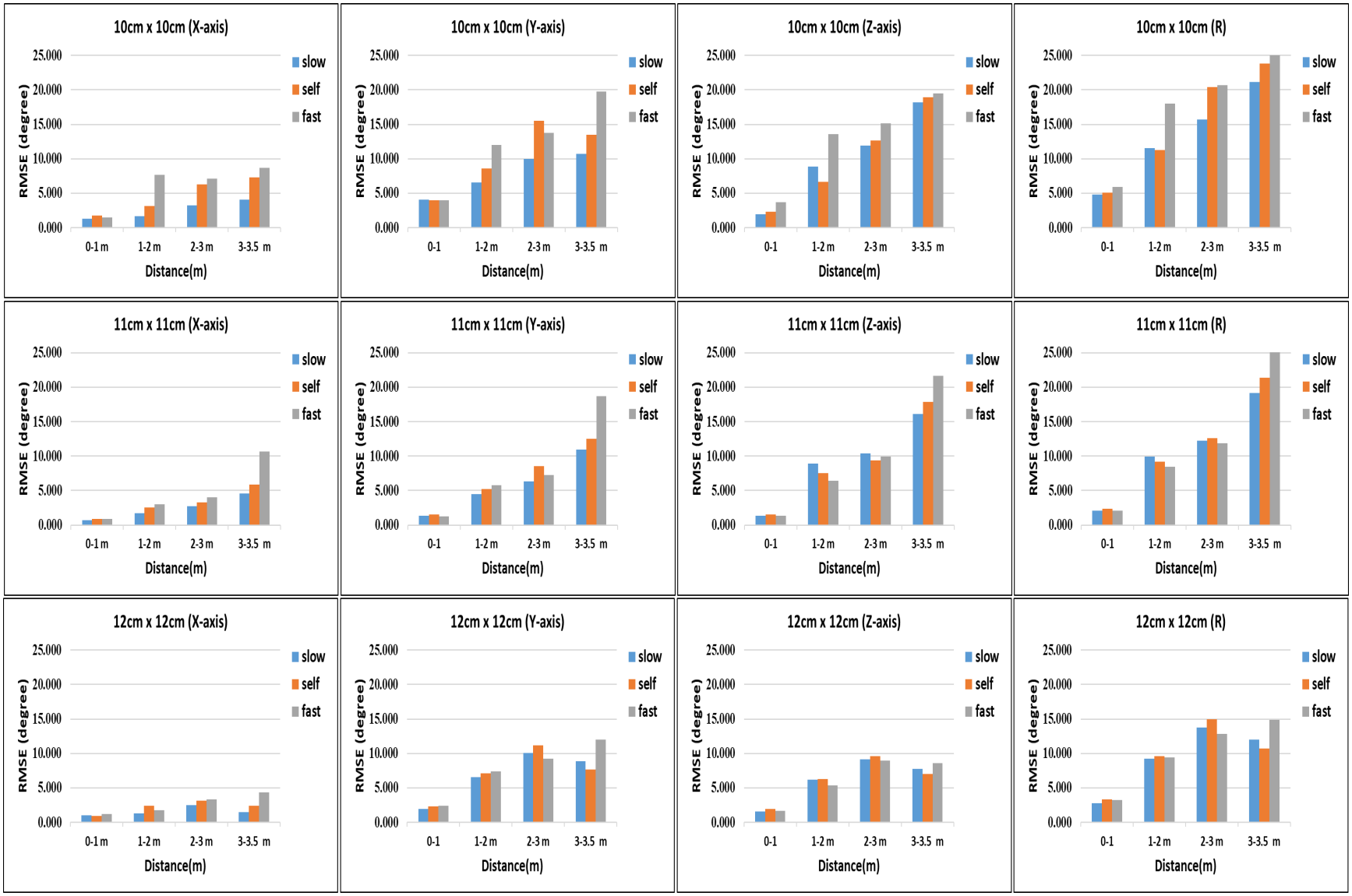

Figure 16: Histogram of RMSE for the orientation of fiducial marker for all 3 size of markers, three walking speeds and in all axis Column1: RMSE in x-axis for all 3 sizes of marker from top to bottom, Column 2: RMSE in y-axis for all 3 sizes of marker from top to bottom, Column 3: RMSE in z-axis for all 3 sizes of marker from top to bottom, and Column 4: RMSE in magnitude of position (R) for all 3 sizes of marker from top to bottom

5.5 Discussion

In general, the RMSE for both the position and orientation of the fiducial marker increased with an increase in walking speed, a decrease in marker size, and as the subject walked further away from the camera. However, the statistical analysis also showed that the y-axis and z-axis were always more accurate than x-axis for position. The results found in this study for slow speed and larger marker size are comparable to the previous work that assessed fiducial marker position accuracy for marker size of 20 cm x 20 cm in static condition at 1 m (1.4 cm error for magnitude of position)[34]. In the study conducted by Malbezin et. al. as well, the error in y-axis was smaller than that of in x-axis, similar to the results found in this study. Similarly, previous work that assessed a fiducial marker-based motion capture system (with marker size 11 cm x 11 cm) with subject walking on a treadmill fixed at 1.5 m from camera obtained an RMSE error of 2.3 cm in the measured step length of human subjects which is comparable to the RMSE error (4.36±1.94 cm for magnitude) obtained in this study for 11 cm x 11 cm marker, slow speed at 1-2 m from camera[43]. Another previous static study conducted by Abawi et. al. showed systematic error of 2 cm to 12 cm in the range of 20 cm to 100 cm distance of ARToolkit marker (size 5.5 cm x 5.5 cm) location from camera[35]. Compared to Abawi et. al.'s finding, the results obtained in this study have better accuracy even in dynamic condition.

In contrast, the accuracy was greater for the x-axis than the y-axis and the z-axis in context of error in orientation which is similar to the observation recorded by previous work done by Malbezine et. al.[34] Further, the RMSE for orientation of the 11 cm x 11 cm fiducial marker during slow speed at 1-2 m from camera were 0.69±0.15˚ along the x-axis, 1.33±0.50˚ along the y-axis, 1.37±0.21˚ along the z-axis resulting in 2.06±0.48˚ in magnitude RMSE. This is consistent

with the RMSE of 3.61˚ for the knee angle found in the previous work by Nagymáté et. al. under similar condition[43].

The consistent result for the comparable conditions of this study with previous work suggests that the results obtained by this study is promising. However, the results were expected to have a linear increase in error with increase in speed and decrease in size of marker, but it was observed that there is some inconsistency within the linear error increment pattern. For example, for increase in speed the error increased for the 10 cm x 10 cm marker as the subject walked further away from camera, while it decreased for 11 cm x11 cm and 12 cm x12 cm marker size. Such a trend can be attributed to better detection of the larger marker at distance, increasing the accuracy. Similarly, self-selected normal walking speed had higher error than the fast speed which was not expected. Thus, it need further exploration.

Although comparable result to previous studies was obtained from this study, several factors still likely affected the error. Some of the potential sources of error were: too low capture frame rate of the camera, inadequate lighting, too low resolution of the camera, uncontrolled walking speed, and calibration of the camera using a smaller square checker board. Thus, there is opportunity for future work for betterment and validation of this system because of its cost effectiveness and portability.

Some of the immediate future work based on this study that can be performed are use of multiple cameras with high resolution and high capture rate as one of the main reasons for the increase in error over distance is the resolution. As the marker moves away from the camera the pixel of the marker visible to the camera frame becomes smaller leading to added offset in the detection of position of center of the marker ultimately resulting in the error in tracking. Thus, a study on the effect of multiple cameras would be beneficial. Similarly, as camera resolution and

capture rate are crucial factors in tracking the fiducial markers in motion. Nagymáté et. al did a study to evaluate different cameras and found that GoPro Hero 5 Black was optimal to better track the fiducial markers in motion. However, a wide range of cameras with improved features and increased frame rates are available to be used in future testing. High resolution cameras with higher frame rates are still cheaper than infrared motion capture cameras used in retroreflective marker-based motion capture systems. Therefore, it would be valuable to use such higher resolution cameras in future studies in order to further decrease the tracking RMSE.

In this study, the GoPro camera was only calibrated once using a checker board with squares of size 2 cm x 2 cm before capturing the motion trial data on subjects. The proper calibration of the camera is important in the tracking of the fiducial markers. A camera's tracking accuracy increases if calibrated with a checkerboard with a larger square size. Thus, a better camera calibration might decrease the RMSE.

Also in this study, the speeds of the subjects were not controlled and were self-selected by individual subjects. Since effect of speed was seen on the orientation of the markers RMSE, the RMSE obtained might have been affected by the difference in actual speed of the subjects for each condition. Thus, to see the effect of controlled speed on the accuracy of fiducial marker tracking.

5.6 Conclusion

The overall goal of the study was to evaluate the capability of an fiducial marker-based system to be utilized in the field of biomechanics. In general, the fiducial marker- based system was most accurate in tracking the position and orientation of the fiducial marker in 3D space for slow speeds, thelarger marker size, and closer to camera. However, both position and orientation were negatively affected by faster speeds and smaller marker size. More importantly, both position

and orientations' RMSE increased substantially beyond 3 m from the camera. The results obtained indicates that the fiducial marker system can be used to track motion in a smaller capture area and with larger marker size at slow speed for the better accuracy. Further, the results can be utilized as a reference to design future applications or studies based on the requirement and importance of tracking accuracy. These results also tell what conditions the fiducial marker-based tracking system fails and what condition it works for the application such as motion tracking in the field of biomechanics.

CHAPTER – 6
CONCLUSIONS, STUDY LIMITATIONS, AND FUTURE WORKS

The use of fiducial marker-based tracking system research is expected to increase. The system is comparatively cost effective and has the capability to track landmarks in 3D space as does the existing and comparatively expensive retroreflective marker-based motion capture system. Capturing human motion and quantifying joint kinematics for various studies is one of the many applications of fiducial marker-based tracking systems in biomechanics. Tracking the lower body to calculate the joint kinematics of amputee for prosthetic alignment is one of the most promising applications of this system.

Overall, the findings from this thesis contribute to the biomechanics community in understanding of the current capability and limitations of the fiducial marker-based tracking system for general motion capture applications such as prosthetic alignment. This study suggests that although the accuracy of the system for tracking position and orientation of a location in 3D space is not as accurate as retroreflective marker-based motion capture system for a larger capture volume, the fiducial system is still accurate enough for the purpose of prosthesis alignment considering its cost effectiveness and portability. Also, this thesis contributes to the biomechanics community by providing a component-based coordinate system algorithm for lower limb prostheses which allows for an objective means of quantifying lower-limb prosthesis alignment to ultimately serve the purpose of benefiting the lower-limb amputee.

Further, the results obtained from the validation of fiducial marker accuracy suggests that the fiducial marker tracking system can be utilized for prosthetic alignment. However, this study had some limitations that need to be accounted in the future. This study did not look into the effect of lightning condition. Also, based on Nagyma´te´ et. al. study, GoPro Hero 5 Black camera was used for this study whereas we assume that even higher resolution camera with higher frame rate

may result in lower error. Additionally, the GoPro camera was calibrated once only using checkerboard with square size of 2 cm. It is likely that the accuracy will increase if the calibration is done with a larger square size checker board. Finally, the Vicon motion capture system also inherits errors based on the spacing between the retroreflective markers and the rigid body it is attached to compared to fiducial maker system. The retroreflective marker used in this research are 9.5mm diameter. The Vicon system tracks the location at the center of the retroreflective marker which is about 4.7 mm off the flat fiducial marker. This offset might have added to the comparative error as well.

A lot can to be done in further development of the fiducial tracking system for motion capture in near future. Joint angle tracking accuracy can be studied for prosthetic alignment. In addition, multiple cameras can be connected to increase the capture volume and further decrease the RMSE of the system. Similarly, the same study can be replicated on a treadmill placed at a fixed distance from the camera. Furthermore, as resolution of the camera and distance of the marker from the camera affects the accuracy, fusion of IMUs and fiducial markers might increase the accuracy of the system while still keeping it cost effective compared to traditional retroreflective marker-based motion capture systems.

REFERENCES

[1] Ziegler-Graham, K., MacKenzie, E. J., Ephraim, P. L., Travison, T. G., and Brookmeyer, R., 2008, "Estimating the Prevalence of Limb Loss in the United States: 2005 to 2050," Arch. Phys. Med. Rehabil., **89**(3), pp. 422–429.

[2] Gailey, R., 2008, "Review of Secondary Physical Conditions Associated with Lower-Limb Amputation and Long-Term Prosthesis Use," J. Rehabil. Res. Dev., **45**(1), pp. 15–30.

[3] Sinha, R., van den Heuvel, W. J., and Arokiasamy, P., 2011, "Factors Affecting Quality of Life in Lower Limb Amputees," Prosthet. Orthot. Int., **35**(1), pp. 90–96.

[4] Gallagher, P., Desmond, D., and Maclachlan, M., 2007, *Psychoprosthetics*, Springer Science & Business Media.

[5] Horgan, O., and MacLachlan, M., 2004, "Psychosocial Adjustment to Lower-Limb Amputation: A Review," Disabil. Rehabil., **26**(14–15), pp. 837–850.

[6] Matsen, S. L., 2000, "Correlations with Patients' Perspectives of the Result of Lower-Extremity Amputation," J. BONE Jt. Surg., **82**(8), p. 7.

[7] "Simplifying Alignment for Transtibial Prostheses | Lower Extremity Review Magazine."

[8] Pirouzi, G., Abu Osman, N. A., Ali, S., and Davoodi Makinejad, M., 2017, "A New Prosthetic Alignment Device to Read and Record Prosthesis Alignment Data," Proc. Inst. Mech. Eng. [H], **231**(12), pp. 1127–1132.

[9] "Dynamic Alignment of Artificial Legs with the Adjustable Coupling | O&P Virtual Library" [Online]. Available: http://oandplibrary.org/al/1963_01_031.asp. [Accessed: 28-Jan-2019].

[10] Boone, D. A., 2005, "Investigation of Socket Reactions from Transtibial Prosthesis Malalignment," Thesis, The Hong Kong Polytechnic University.

[11] Leydet, M. G., Harrington, R. H., Fedel, F. J., Link, M., and Street, J. J., 2012, "Prosthetic Sensing Systems and Methods."

[12] Fiedler, G., "Effects of Physical Exertion and Alignment Alterations on Trans-Tibial Amputee Gait, and Concurrent Validity of Prosthesis-Integrated Measurement of Gait Kinetics," p. 256.

[13] Garrido-Jurado, S., Muñoz-Salinas, R., Madrid-Cuevas, F. J., and Medina-Carnicer, R., 2016, "Generation of Fiducial Marker Dictionaries Using Mixed Integer Linear Programming," Pattern Recognit., **51**, pp. 481–491.

[14] Schmitz, A., Ye, M., Shapiro, R., Yang, R., and Noehren, B., 2014, "Accuracy and Repeatability of Joint Angles Measured Using a Single Camera Markerless Motion Capture System," J. Biomech., **47**(2), pp. 587–591.

[15] Raskar, R., and Barnwell, J., 2007, "Prakash: Lighting Aware Motion Capture Using Photosensing Markers and Multiplexed Illuminators," ACM Trans. Graph., **26**(99), p. 36.

[16] Babinec, A., Jurišica, L., Hubinský, P., and Duchoň, F., 2014, "Visual Localization of Mobile Robot Using Artificial Markers," Procedia Eng., **96**, pp. 1–9.

[17] Cheesman, A. R., and DiMaio, C. J., 2017, "Role and Technique of Endoscopic Ultrasound Placement of Fiducial Markers in Gastrointestinal Malignancies," Tech. Gastrointest. Endosc., **19**(4), pp. 213–218.

[18] Worm, E. S., Bertholet, J., Høyer, M., Fledelius, W., Hansen, A. T., Larsen, L. P., Nielsen, J. E., and Poulsen, P. R., 2016, "Fiducial Marker Guided Stereotactic Liver Radiotherapy: Is a Time Delay between Marker Implantation and Planning CT Needed?," Radiother. Oncol., **121**(1), pp. 75–78.

[19] Estévez-García, R., Martín-Gutiérrez, J., Mendoza, S. M., Marante, J. R., Chinea-Martín, P., Soto-Martín, O., and Lodeiro-Santiago, M., 2015, "Open Data Motion Capture: MOCAP-ULL Database," Procedia Comput. Sci., **75**, pp. 316–326.

[20] "The Fascination for Motion Capture," Xsens 3D Motion Track.

[21] Guerra-Filho, G. B., 2005, “Optical Motion Capture: Theory and Implementation,” p. 29.
[22] Zhou, H., and Hu, H., 2008, “Human Motion Tracking for Rehabilitation—A Survey,” Biomed. Signal Process. Control, **3**(1), pp. 1–18.
[23] Paley, D., 2002, “Normal Lower Limb Alignment and Joint Orientation,” *Principles of Deformity Correction*, D. Paley, ed., Springer Berlin Heidelberg, Berlin, Heidelberg, pp. 1–18.
[24] Cheung, G. K. M., Baker, S., and Kanade, T., 2003, “Visual Hull Alignment and Refinement across Time: A 3D Reconstruction Algorithm Combining Shape-from-Silhouette with Stereo,” IEEE Comput. Soc, pp. II-375–82.
[25] “DARI’s Markerless Motion Capture Process Acquires Data Quickly,” DARI.
[26] Chang, Y.-J., Chen, S.-F., and Huang, J.-D., 2011, “A Kinect-Based System for Physical Rehabilitation: A Pilot Study for Young Adults with Motor Disabilities,” Res. Dev. Disabil., **32**(6), pp. 2566–2570.
[27] Pfister, A., West, A. M., Bronner, S., and Noah, J. A., 2014, “Comparative Abilities of Microsoft Kinect and Vicon 3D Motion Capture for Gait Analysis,” J. Med. Eng. Technol., **38**(5), pp. 274–280.
[28] “The Cutting Edge of Motion Capture,” MCV.
[29] Cuesta-Vargas, A. I., Galán-Mercant, A., and Williams, J. M., 2010, “The Use of Inertial Sensors System for Human Motion Analysis,” Phys. Ther. Rev., **15**(6), pp. 462–473.
[30] “X2E Motion Capture – PhaseSpace Motion Capture.”
[31] Fiala, M., 2005, “ARTag, a Fiducial Marker System Using Digital Techniques,” *Computer Vision and Pattern Recognition, 2005. CVPR 2005. IEEE Computer Society Conference On*, IEEE, pp. 590–596.
[32] Garrido-Jurado, S., Muñoz-Salinas, R., Madrid-Cuevas, F. J., and Marín-Jiménez, M. J., 2014, “Automatic Generation and Detection of Highly Reliable Fiducial Markers under Occlusion,” Pattern Recognit., **47**(6), pp. 2280–2292.
[33] Fiala, M., 2010, “Designing Highly Reliable Fiducial Markers,” IEEE Trans. Pattern Anal. Mach. Intell., **32**(7), pp. 1317–1324.
[34] Malbezin, P., Piekarski, W., and Thomas, B. H., 2002, “Measuring ARTootKit Accuracy in Long Distance Tracking Experiments,” *The First IEEE International Workshop Agumented Reality Toolkit,* pp. 2 pp.-.
[35] Abawi, D. F., Bienwald, J., and Dorner, R., 2004, “Accuracy in Optical Tracking with Fiducial Markers: An Accuracy Function for ARToolKit,” *Proceedings of the 3rd IEEE/ACM International Symposium on Mixed and Augmented Reality*, IEEE Computer Society, pp. 260–261.
[36] Lopez-Ceron, A., Carlos, U. R. J., Canas, J. M., and Carlos, U. R. J., “Accuracy Analysis of Marker-Based 3D Visual Localization,” p. 8.
[37] Samarin, P., Kent, K. B., Herpers, R., and Saitov, T., 2013, “Fiducial Marker Detection Using FPGAs.”
[38] Tanaka, H., Sumi, Y., and Matsumoto, Y., 2012, “A High-Accuracy Visual Marker Based on a Microlens Array,” *2012 IEEE/RSJ International Conference on Intelligent Robots and Systems*, pp. 4192–4197.
[39] Freeman, R. M., Julier, S. J., and Steed, A. J., 2007, “A Method for Predicting Marker Tracking Error,” *2007 6th IEEE and ACM International Symposium on Mixed and Augmented Reality*, pp. 157–160.
[40] Pentenrieder, K., Meier, P., and Klinker, G., “Analysis of Tracking Accuracy for Single-Camera Square-Marker-Based Tracking,” p. 16.
[41] Zhang, X., Fronz, S., and Navab, N., 2002, “Visual Marker Detection and Decoding in AR Systems: A Comparative Study,” *Proceedings of the 1st International Symposium on Mixed and Augmented Reality*, IEEE Computer Society, Washington, DC, USA, pp. 97–.
[42] Leardini, A., Chiari, L., Croce, U. D., and Cappozzo, A., 2005, “Human Movement Analysis Using Stereophotogrammetry: Part 3. Soft Tissue Artifact Assessment and Compensation,” Gait Posture, **21**(2), pp. 212–225.

[43] Nagymáté, G., and Kiss, R. M., 2019, “Affordable Gait Analysis Using Augmented Reality Markers,” PLOS ONE, **14**(2), p. e0212319.
[44] Bejek, Z., Paróczai, R., Illyés, Á., and Kiss, R. M., 2006, “The Influence of Walking Speed on Gait Parameters in Healthy People and in Patients with Osteoarthritis,” Knee Surg. Sports Traumatol. Arthrosc., **14**(7), pp. 612–622.
[45] “ArUco,” SourceForge [Online]. Available: https://sourceforge.net/projects/aruco/. [Accessed: 20-Mar-2018].
[46] Grood, E. S., and Suntay, W. J., 1983, “A Joint Coordinate System for the Clinical Description of Three-Dimensional Motions: Application to the Knee,” J. Biomech. Eng., **105**(2), pp. 136–144.
[47] Kadaba, M. P., Ramakrishnan, H. K., and Wootten, M. E., 1990, “Measurement of Lower Extremity Kinematics during Level Walking,” J. Orthop. Res., **8**(3), pp. 383–392.
[48] 1995, “Motion Capture,” Gener., (10), p. 50.
[49] Stinner, D. J., Burns, T. C., Kirk, K. L., and Ficke, J. R., 2010, “Return to Duty Rate of Amputee Soldiers in the Current Conflicts in Afghanistan and Iraq:,” J. Trauma Inj. Infect. Crit. Care, **68**(6), pp. 1476–1479.
[50] Berme, N., Purdey, C. R., and Solomonidis, S. E., 1978, “Measurement of Prosthetic Alignment,” Prosthet. Orthot. Int., **2**(2), pp. 73–75.
[51] Zahedi, M. S., Spence, W. D., Solomonidis, S. E., and Paul, J. P., 1986, “Alignment of l Owe-Limb Prostheses,” J Rehabil Res Dev, **23**, pp. 2–19.
[52] Taylor, D. E. M., and Whamond, J., 1977, *Non-Invasive Clinical Measurement*, University Park Press.
[53] Sin, S. W., Chow, D. H. K., and Cheng, J. C. Y., 1999, “A New Alignment Jig for Quantification and Prescription of Three-Dimensional Alignment for the Patellar-Tendon-Bearing Trans-Tibial Prosthesis,” Prosthet. Orthot. Int., **23**(3), pp. 225–230.
[54] Wu, G., and Cavanagh, P., “ISB Recommendation for Standardization in the Reporting of Kinematic Data,” p. 5.
[55] Andriacchi, T. P., Johnson, T. S., Hurwitz, D. E., and Natarajan, R., “Musculoskeletal Dynamics Locomotion, and Clinical Applications,” p. 31.
[56] Andriacchi, T. P., Alexander, E. J., Toney, M. K., Dyrby, C., and Sum, J., 1998, “A Point Cluster Method for in Vivo Motion Analysis: Applied to a Study of Knee Kinematics,” J. Biomech. Eng., **120**(6), pp. 743–749.
[57] Benedetti, M., and Cappozzo, A., 1994, “Anatomical Landmark Definition and Identification in Computer Aided Movement Analysis in a Rehabilitation Context,” *Internal Report*, Universita Degli Studi La Sapienza.
[58] Hutton, R., 1976, *Physical Examination of the Spine and Extremities*, Prentice Hall.
[59] Weinhandl, J. T., and O’Connor, K. M., 2010, “Assessment of a Greater Trochanter-Based Method of Locating the Hip Joint Center,” J. Biomech., **43**(13), pp. 2633–2636.
[60] Wu, G., Siegler, S., Allard, P., Kirtley, C., Leardini, A., Rosenbaum, D., Whittle, M., D D’Lima, D., Cristofolini, L., and Witte, H., 2002, “ISB Recommendation on Definitions of Joint Coordinate System of Various Joints for the Reporting of Human Joint Motion—Part I: Ankle, Hip, and Spine,” J. Biomech., **35**(4), pp. 543–548.
[61] Zeni, J. A., Richards, J. G., and Higginson, J. S., 2008, “Two Simple Methods for Determining Gait Events during Treadmill and Overground Walking Using Kinematic Data,” Gait Posture, **27**(4), pp. 710–714.
[62] Kim, W., Veloso, A. P., Vleck, V. E., Andrade, C., and Kohles, S. S., 2013, “The Stationary Configuration of the Knee,” J. Am. Podiatr. Med. Assoc., **103**(2), pp. 126–135.
[63] VICON, “Nexus Motion Capture Software,” VICON [Online]. Available: http://www.vicon.com/products/software/nexus. [Accessed: 09-May-2019].
[64] “Applications | Qualisys.”

[65] “Motion Capture Applications,” OptiTrack [Online]. Available: http://optitrack.com/applications/index.html. [Accessed: 09-May-2019].
[66] Fern’ndez-Baena, A., Susín, A., and Lligadas, X., 2012, “Biomechanical Validation of Upper-Body and Lower-Body Joint Movements of Kinect Motion Capture Data for Rehabilitation Treatments,” *2012 Fourth International Conference on Intelligent Networking and Collaborative Systems*, pp. 656–661.
[67] Dornaika, F., and Horaud, R., 1998, “Simultaneous Robot-World and Hand-Eye Calibration,” IEEE Trans. Robot. Autom., **14**(4), pp. 617–622.

APPENDIX A (IRB)

AUBURN UNIVERSITY
DEPARTMENT OF MECHANICAL ENGINEERING

(NOTE: DO NOT SIGN THIS DOCUMENT UNLESS AN IRB APPROVAL STAMP WITH CURRENT DATES HAS BEEN APPLIED TO THIS DOCUMENT.)

INFORMED CONSENT
for a Research Study entitled
"System for Prosthetic Alignment Utilizing Real-Time Kinematics (SPAURK)"

You are invited to participate in a research study which aims at collecting data of walking, jogging, squatting, and seated leg extension from able subjects. These data will be used in development of a system for prosthetic alignment utilizing real time kinematics here at Auburn University. The study is being conducted under the supervision of Michael Zabala, Assistant Professor at Auburn University in the Department of Mechanical Engineering. Your participation is completely voluntary.

What will be involved if you participate?

If you decide to participate in this research study, you will be asked to fill out a form that will ask some basic information like your age, gender, height and weight which will be kept confidential using a 4 letter code and will not be accessible to anyone except key personnel involved in the study.

We will ask you to wear your own tennis or gym shoes and a pair of shorts that we will provide. We will then put little squares of double-sided tape on your lower and upper body. To the other side of the double-sided tape we will stick small balls with reflective material on the outside. We will also use double-sided tape to attach small cardboard circles with a QR-code-type image on it, to your lower body. We will have you stand on a force plate/pressure map sensor. We will then take location measurements at various points on your lower body and hips with a locator arm.

We will then take a number of still photographs of you from the chest down. We will ask you to walk and jog across the laboratory, squat and perform seated leg extensions 3 to 5 times. We expect the entire test to take no more than two hours. This testing will take place in the AUBE Lab at Auburn University, Wiggins Hall, Room 3401.

Only testing personnel will observe you during the experiment. Furthermore, we might ask you to follow up in future if we have any need to repeat the experiment for further validation of the study.

Are there any risks or discomforts?
The risks associated with participating in this study are:

1. Fatigue/Soreness: Discomfort that can reasonably be expected is the possibility that you will become tired from walking. In addition, you may experience sprains, strains, and/or soreness.
2. Reaction/Irritation from adhesive on markers: There will be a possible risk of reaction or irritation from the adhesive that will be used to attach the markers on the body.

To minimize any discomfort, we will:

1. Have you relax in between the walking tasks if needed by providing a chair for you to utilize.

Are there any benefits to yourself or others?
If you participate in this study, you can expect to receive no direct benefits. Your participation, however, provides the investigator with a greater amount of data that will be used by the investigator to learn about kinetics and kinematics of your limb and use those analyzed data for development of a system for prosthetic alignment utilizing real time kinematics.

1418 Wiggins Hall, Auburn, AL 36849-5341; Telephone: 334-844-4820; Fax: 334-844-3307
www.auburn.edu

Will you receive compensation for participating?
There is no compensation that will be offered to participate in this research but we will really appreciate your great help to participate in this study and we will always be grateful for your support.

Are there any costs?
If you decide to participate, you will not incur any costs.

We would like to contact you in the future for a follow up study.

May we contact you for the follow-up study? (Please circle) YES / NO _____
Initials

We would like to keep your data and use it in other research projects not specifically related to the current study.

May we use your data for other research studies? (Please circle) YES / NO _____
Initials

If you change your mind about participating, you can withdraw at any time during the study. Your participation is completely voluntary. If you choose to withdraw, your data can be withdrawn as long as it is identifiable. Your decision about whether or not to participate or to stop participating will not jeopardize your future relations with Auburn University, the Samuel Ginn College of Engineering, or AUBE Lab at Auburn University.

Your privacy will be protected. Any information obtained in connection with this study will remain confidential. At the end of the study all links to identifiable information will be destroyed. Information obtained through your participation may be published in a professional journal and/or presented at a professional meeting.

If you have questions about this study, *please ask them now or* contact Professor Michael Zabala at (334) 844-4916 (zabalame@auburn.edu) or Raju Gupta at (334) 333-9285 (rzg0050@tigermail.auburn.edu). A copy of this document will be given to you to keep.

If you have questions about your rights as a research participant, you may contact the Auburn University Office of Human Subjects Research or the Institutional Review Board by phone (334)-844-5966 or e-mail athsubjec@auburn.edu or IRBChair@auburn.edu.

HAVING READ THE INFORMATION PROVIDED, YOU MUST DECIDE WHETHER OR NOT YOU WISH TO PARTICIPATE IN THIS RESEARCH STUDY. YOUR SIGNATURE INDICATES YOUR WILLINGNESS TO PARTICIPATE.

_____		_____	
Participant's signature	Date	Investigator obtaining consent	Date
_____		_____	
Printed Name		Printed Name	

The Auburn University Institutional Review Board has approved this Document for use from 07/13/2018 to 07/18/2019
Protocol # 17-277 MR 1707

APPENDIX B (Prosthesis alignment Algorithm)

PROSTHESIS ALIGNMENT CALCULATION

Once reference frames have been created for each component of the prosthesis, kinematic alignment can be calculated through use of transformation matrices, which provide a means of measuring differences in position and orientation between components. This will provide common prosthesis alignment parameters of interest including socket add/abduction, socket extension/flexion, and foot rotation.

The transformation matrix for each component of the prosthesis must be established with respect to a fixed coordinate system (G). This matrix is composed of a 3×3 rotation matrix $[R]$, the displacement vector $\{\boldsymbol{d}\}$, and an additional row of three zeros and a 1 such that the result is a 4×4 square matrix.[14]

$$[T] = \begin{bmatrix} [R] & \{\boldsymbol{d}\} \\ 0\ 0\ 0 & 1 \end{bmatrix} \tag{28}$$

The rotation submatrix is populated with the unit vectors that describe the three orthogonal axes of the component reference frame in the fixed coordinate system.

$$R = [\hat{\boldsymbol{x}}' \quad \hat{\boldsymbol{y}}' \quad \hat{\boldsymbol{z}}'] = \begin{bmatrix} x_x & y_x & z_x \\ x_y & y_y & z_y \\ x_z & y_z & z_z \end{bmatrix} \tag{29}$$

The displacement vector is composed of the three coordinates describing the location of the component's origin in the fixed coordinate system.

$$\boldsymbol{d} = \begin{Bmatrix} o_x \\ o_y \\ o_z \end{Bmatrix} \tag{30}$$

The elements of the rotation matrix $[R]$ are nonlinear functions of the Euler angles that describe the orientation of the component with respect to the fixed coordinate system.

$$[R] = [R_z]\big[R_y\big][R_x] \tag{31}$$

$$where$$

$$[R_z] = \begin{bmatrix} \cos\theta_z & -\sin\theta_z & 0 \\ \sin\theta_z & \cos\theta_z & 0 \\ 0 & 0 & 1 \end{bmatrix} \tag{32}$$

$$\big[R_y\big] = \begin{bmatrix} \cos\theta_y & 0 & \sin\theta_y \\ 0 & 1 & 0 \\ -\sin\theta_y & 0 & \cos\theta_y \end{bmatrix} \tag{33}$$

$$[R_x] = \begin{bmatrix} 1 & 0 & 0 \\ 0 & \cos\theta_x & -\sin\theta_x \\ 0 & \sin\theta_x & \cos\theta_x \end{bmatrix} \tag{34}$$

$$thus$$

$$[R] = \begin{bmatrix} \cos\theta_y\cos\theta_z & \sin\theta_x\sin\theta_y\cos\theta_z - \sin\theta_z\cos\theta_x & \sin\theta_x\sin\theta_z + \sin\theta_y\cos\theta_x\cos\theta_z \\ \sin\theta_z\cos\theta_y & \cos\theta_x\cos\theta_z + \sin\theta_x\sin\theta_y\sin\theta_z & \sin\theta_y\sin\theta_z\cos\theta_x - \sin\theta_x\cos\theta_z \\ -\sin\theta_y & \sin\theta_x\cos\theta_y & \cos\theta_x\cos\theta_y \end{bmatrix} \tag{35}$$

The Euler angles $(\theta_x, \theta_y, \theta_z)$ of the rotation matrix can be extracted with the equations below.[14]

$$\theta_x = \arctan\left(\frac{[R]_{3,2}}{[R]_{3,3}}\right) \tag{36}$$

$$\theta_y = -\arcsin\big([R]_{3,1}\big) \tag{37}$$

$$\theta_z = \arctan\left(\frac{[R]_{2,1}}{[R]_{1,1}}\right) \tag{38}$$

Below are specific equations for determining various lower-limb prosthesis alignment parameters. It is recommended that all alignment parameters are expressed describing the distal segment position and orientation in the proximal segment coordinate system. Also, it is important to note that positive θ_x values correspond to extension (plantar flexion for the foot) for both right and left sides. However, due to the medial-lateral axis always pointing to the right for both limbs,

positive θ_y and θ_z values correspond to adduction (inversion for the foot) and internal rotation, respectively, for right legs only, while θ_y and θ_z values correspond to abduction (eversion for the foot) and external rotation, respectively, for left legs.

Tibial Socket Alignment with Respect to the Femur

Femur Transformation Matrix

$$\left[R_{f,G}\right] = \left[\hat{\boldsymbol{x}}_{\boldsymbol{f}}{}' \quad \hat{\boldsymbol{y}}_{\boldsymbol{f}}{}' \quad \hat{\boldsymbol{z}}_{\boldsymbol{f}}{}'\right] = \begin{bmatrix} x_{f,x} & y_{f,x} & z_{f,x} \\ x_{f,y} & y_{f,y} & z_{f,y} \\ x_{f,z} & y_{f,z} & z_{f,z} \end{bmatrix} \tag{39}$$

$$\left\{\boldsymbol{d}_{\boldsymbol{f},\boldsymbol{G}}\right\} = \begin{Bmatrix} o_{f,x} \\ o_{f,y} \\ o_{f,z} \end{Bmatrix} \tag{40}$$

$$\left[T_{f,G}\right] = \begin{bmatrix} \left[R_{f,G}\right] & \left\{\boldsymbol{d}_{\boldsymbol{f},\boldsymbol{G}}\right\} \\ 0\ 0\ 0 & 1 \end{bmatrix} \tag{41}$$

Tibial Socket Transformation Matrix

$$\left[R_{ts,G}\right] = \left[\hat{\boldsymbol{x}}_{\boldsymbol{ts}}{}' \quad \hat{\boldsymbol{y}}_{\boldsymbol{ts}}{}' \quad \hat{\boldsymbol{z}}_{\boldsymbol{ts}}{}'\right] = \begin{bmatrix} x_{ts,x} & y_{ts,x} & z_{ts,x} \\ x_{ts,y} & y_{ts,y} & z_{ts,y} \\ x_{ts,z} & y_{ts,z} & z_{ts,z} \end{bmatrix} \tag{42}$$

$$\left\{\boldsymbol{d}_{\boldsymbol{ts},\boldsymbol{G}}\right\} = \begin{Bmatrix} o_{ts,x} \\ o_{ts,y} \\ o_{ts,z} \end{Bmatrix} \tag{43}$$

$$\left[T_{ts,G}\right] = \begin{bmatrix} \left[R_{ts,G}\right] & \left\{\boldsymbol{d}_{\boldsymbol{ts},\boldsymbol{G}}\right\} \\ 0\ 0\ 0 & 1 \end{bmatrix} \tag{44}$$

Once a fixed coordinate system (G)-based transformation matrix has been established for two components of the prosthesis, a third transformation matrix can be formulated to relate the position and orientation of the two components. This is done by utilizing a forward transformation method where one transformation matrix is premultiplied by the inverse of the other. The equation

below, provides the position and orientation of the tibial socket (ts) with respect to the femur (f), thus can provide values including socket flexion, adduction, and rotation (A&H).

Tibial Socket-Femur Transformation Matrix

$$\left[T_{ts,f}\right] = [T]_{f,G}^{-1}[T]_{ts,G} \tag{45}$$

$$\left[T_{ts,f}\right] = \begin{bmatrix}\left[R_{ts,f}\right] & \{\boldsymbol{d_{ts,f}}\} \\ 0\ 0\ 0 & 1\end{bmatrix} \tag{46}$$

Utilizing the Euler angle equations above, the flexion, adduction, and rotation angles between of the tibial socket with respect to the femur can be extracted from the submatrix $\left[R_{ts,f}\right]$ where:

$$\theta_x = tibial\ socket\ extension/flexion$$

$$\theta_y = tibial\ socket\ adduction/abduction$$

$$\theta_z = tibial\ socket\ internal/external\ rotation$$

Finally, the translation of the tibial socket origin from the femoral origin, expressed in the femoral reference frame, is represented by the displacement submatrix $\boldsymbol{d_{ts,f}}$, where:

$$\{\boldsymbol{d_{ts,f}}\}_{\mathbf{1}} = displacement\ of\ tibial\ socket\ origin\ from\ femur\ origin\ along\ the\ femur\ x-axis$$

$$\{\boldsymbol{d_{ts,f}}\}_{\mathbf{2}} = displacement\ of\ tibial\ socket\ origin\ from\ femur\ origin\ along\ the\ femur\ y-axis$$

$$\{\boldsymbol{d_{ts,pf}}\}_{\mathbf{3}} = displacement\ of\ tibial\ socket\ origin\ from\ femur\ origin\ along\ the\ femur\ z-axis$$

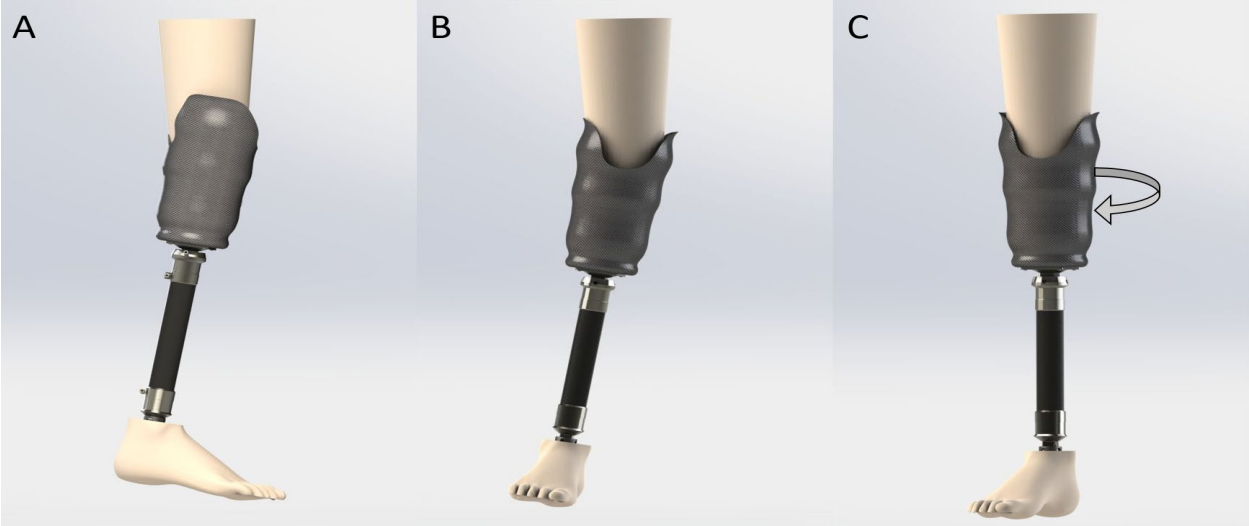

Figure 17: Tibial socket alignment. A. Flexion. B. Abduction. C. External Rotation.

Note that as the femoral origin is established utilizing points rigidly fixed to the tibial socket ($\boldsymbol{fc_m}, \boldsymbol{fc_l}$), the displacement values determined from this calculation will remain constant. The most relevant parameters associated with tibial socket alignment are depicted in Figure 17.

Pylon Alignment with Respect to the Tibial Socket

$$[T_{p,ts}] = [T]^{-1}_{ts,G}[T]_{p,G} \tag{47}$$

$$[T_{p,ts}] = \begin{bmatrix} [R_{p,ts}] & \{\boldsymbol{d_{p,ts}}\} \\ 0\ 0\ 0 & 1 \end{bmatrix} \tag{48}$$

The corresponding Euler angles will provide:

$$\theta_x = pylon\ extension/flexion$$

$$\theta_y = pylon\ adduction/abduction$$

$$\theta_z = pylon\ internal/external\ rotation$$

The corresponding displacement vector $\{\boldsymbol{d_{p,ts}}\}$ will provide:

$$\{\boldsymbol{d_{p,ts}}\}_{\boldsymbol{1}} = pylon\ origin\ displacement\ from\ tibial\ socket\ origin\ along\ the\ tibial\ socket\ x-axis$$

$$\{\boldsymbol{d_{p,ts}}\}_{\boldsymbol{2}} = pylon\ origin\ displacement\ from\ tibial\ socketorigin\ along\ the\ tibial\ socket\ y-axis$$

$\{\boldsymbol{d_{p,ts}}\}_{\mathbf{3}} = \ pylon\ origin\ displacement\ from\ tibial\ socket origin\ along\ the\ tibial\ socket\ z-axis$

Should the transtibial prosthesis not allow for translation between the pylon and the tibial socket, these displacement values will remain constant and even zero should the cross section of the proximal pylon ($\boldsymbol{p_p}$) be considered coincident with the tibial socket pyramid ($\boldsymbol{o_{ts}}$). The most relevant parameters associated with pylon alignment are depicted in Figure 18.

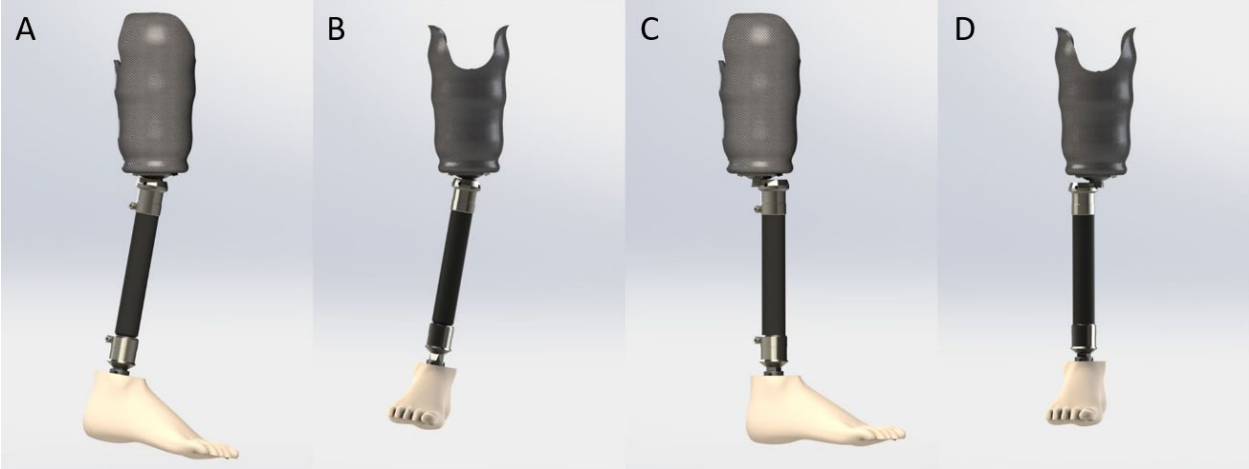

Figure 18: Pylon alignment. A. Flexion. B. Abduction. C. Anterior Translation. D. Lateral Translation.

Foot Alignment

It is recommended that foot displacement, dorsi/plantar flexion and inversion/eversion be measured with respect to the pylon, while foot rotation be measured with respect to the tibial socket as this is likely a more clinically meaningful measure of foot alignment.

Foot Dorsi/Plantar Flexion, Inversion/Eversion with Respect to the Pylon

$$[T_{ft,p}] = [T]_{p,G}^{-1}[T]_{ft,G} \tag{49}$$

$$[T_{ft,p}] = \begin{bmatrix} [R_{ft,p}] & \{\boldsymbol{d_{ft,p}}\} \\ 0\ 0\ 0 & 1 \end{bmatrix} \tag{50}$$

The corresponding Euler angles will provide:

$$\theta_x = foot\ dorsi/plantar\ flexion$$

$$\theta_y = foot\ inversion/eversion$$

$$\theta_z = foot\ internal/external\ rotation\ with\ respect\ to\ pylon - not\ suggested\ for\ use$$

The corresponding displacement vector $\{\boldsymbol{d_{ft,p}}\}$ will provide:

$$\{\boldsymbol{d_{ft,p}}\}_{\boldsymbol{1}} = foot\ origin\ displacement\ from\ pylon\ origin\ along\ the\ pylon\ x - axis$$

$$\{\boldsymbol{d_{ft,p}}\}_{\boldsymbol{2}} = foot\ origin\ displacement\ from\ pylon\ origin\ along\ the\ pylon\ y - axis$$

$$\{\boldsymbol{d_{ft,p}}\}_{\boldsymbol{3}} = foot\ origin\ displacement\ from\ pylon\ origin\ along\ the\ pylon\ z - axis$$

Foot Rotation with Respect to the Tibial Socket

$$[T_{ft,ts}] = [T]_{ts,G}^{-1}[T]_{ft,G} \tag{51}$$

$$[T_{ft,ts}] = \begin{bmatrix} [R_{ft,ts}] & \{\boldsymbol{d_{ft,ts}}\} \\ 0\ 0\ 0 & 1 \end{bmatrix} \tag{52}$$

The corresponding Euler angles will provide:

$$\theta_x = not\ suggested\ for\ use$$

$$\theta_y = not\ suggested\ for\ use$$

$$\theta_z = foot\ internal/external\ rotation\ with\ respect\ to\ the\ tibial\ socket$$

The displacement values above will be meaningless if the transtibial prosthesis does not allow for translational adjustment between the foot and the pylon (most do not). If translational adjustment between the foot and pylon is possible, the displacement values should only be considered for unloaded static alignment. This is because the location of the foot origin ($\boldsymbol{o_{ft}}$) will change in distance from the pylon origin during gait simply due to flexion of the foot, thus indicating spurious dynamic translation between both components.

The displacement of the foot with respect to the pylon $(\boldsymbol{d_{ft,p}})$ may be more meaningful if measured from the distal end of the pylon ($\boldsymbol{d_{ft,p_d}}$), the analog of the ankle joint, as opposed to the pylon origin which is located at its proximal end ($\boldsymbol{p_p}$). This adjustment can be made using the following equation.

$$\boldsymbol{d_{ft,p_d} = d_{ft,p} - (p_d - p_p)} \tag{53}$$

The most relevant parameters associated with foot alignment are depicted in Figure 19.

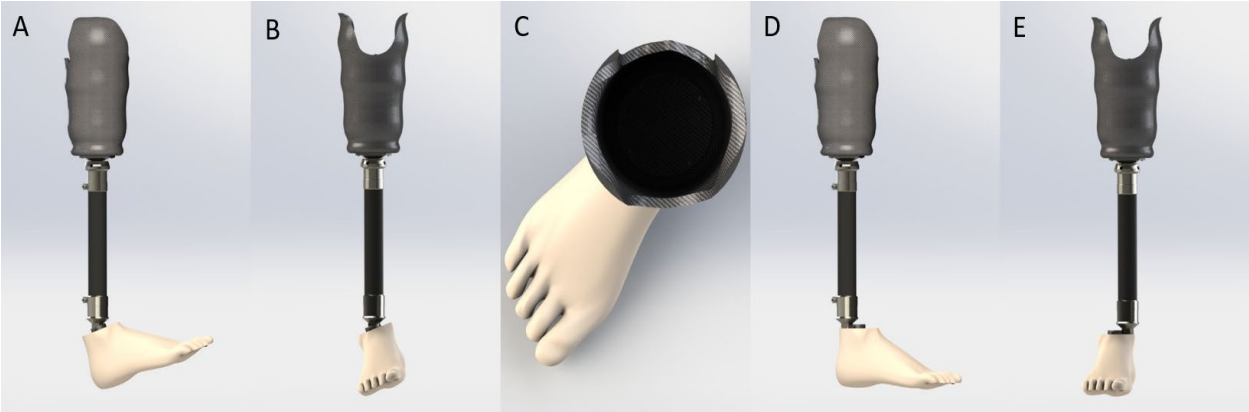

Figure 19: Foot alignment. A. Dorsiflexion. B. Inversion. C. External Rotation. D. Anterior Translation. E. Lateral Translation.

APPENDIX C (Populating data for alignment)

```
addpath('kinematics');
addpath('analysis');
addpath('aruco');
addpath('data_import');
addpath('alignment');
%% import ROS file
[aFileName,aPathName] = uigetfile('C:\D Drive\D Drive\D
Drive\Auburn University All\RA\Thesis work\aruco-
analysis\aruco_data\UKBF\*.bag','bag');
rosDataRaw = importJtPoseBag(aPathName,aFileName,'femur/pose');

% resample to 50 hz
rosTime=rosDataRaw(:,1)./10;
rosTime2=0:(1/50):floor(rosTime(end,1));
rosData=interp1(rosTime,rosDataRaw,rosTime2,'nearest');

posROS = rosData(:,2:4);
quatROS = quatNormalize(rosData(:,5:8));

%% plot ROS file
eulROS = quatToZXY(quatROS);
figure(1)
plot(eulROS(:,1),'.');
figure(2)
plot(eulROS(:,2),'.');
figure(3)
plot(eulROS(:,3),'.');

%% truncate ArUco for alignment
ros_align_st = 260;
ros_align_en = 480;

figure(2)
plot(rosTime2(ros_align_st:ros_align_en),eulROS(ros_align_st:ro
s_align_en,2),'.');


%% Import Vicon File
%col_order = [21,24,27];
%col_order =[240,243,246];
col_order =[243,240,246];
[bFileName,bPathName] = uigetfile('C:\D Drive\D Drive\D
Drive\Auburn University All\RA\Thesis work\aruco-
analysis\aruco_data\UKBF\*.csv','csv');
ptsRaw = importViconPos(bPathName,bFileName,col_order);
```

```
%resample to 50 Hz
pts = [];
pts(:,:,1) = resample(ptsRaw(:,:,1),50,120);
pts(:,:,2) = resample(ptsRaw(:,:,2),50,120);
pts(:,:,3) = resample(ptsRaw(:,:,3),50,120);
%
[quatOMCraw,posOMCraw] = ptsToQuat(pts);
%% plot data
eulOMCraw = quatToEuler(quatOMCraw);
figure(1)
plot(eulOMCraw(:,1));
figure(2)
plot(eulOMCraw(:,2));
figure(3)
plot(eulOMCraw(:,3));



%% Get vertical offset
off = .50;
i=1;
n = ros_align_en-ros_align_st+1;
time=1:n;
time=time./50;
plot(time,posOMCraw(i:i+n-
1,3),time,posROS(ros_align_st:ros_align_en,3)+off);


%% Get horizotal offset
i=i+5;
%posROS = rosData(:,2:4);
%eulROS=quatToEuler(rosData(:,5:8));

plot(time,posOMCraw(i:i+n-
1,3),time,posROS(ros_align_st:ros_align_en,3)+off);

%% Autoalign
% (make sure blue line is r of red line)
indices = 60; %number of indices to check
RMS = zeros;
tfROS2 =
zeros(4,4,size(quatROS(ros_align_st:ros_align_en,:),2));
%aligned
tfROS =
poseToTF(quatROS(ros_align_st:ros_align_en,:),posROS(ros_align_
st:ros_align_en,:));
```

```
%i=i-10;
for k=1:indices
    tfOMC = poseToTF(quatOMCraw(i+k:i+k+n-
1,:),posOMCraw(i+k:i+k+n-1,:));
    [X,Y]= dornaika(tfROS,tfOMC);

    %%apply transfer alignment
    for j=1:size(tfROS,3)
        tfROS2(:,:,j) = invT(Y)*tfROS(:,:,j)*X;
    end

    % convert back to pose
    [quatROS2,rosROS2] = tfToPose(tfROS2);

    %RMS(k) = quatRMS(quatOMCraw(i+k:i+k+n-1,:),quatROS2);
    eulROS = quatToEuler(quatROS2);
    RMS(k) = sqrt(mean((eulROS(:,2)-eulOMCraw(i+k:i+k+n-
1,2)).^2));
end
%plot([eulOMC(:,2),eulROS(:,2)]);
%get indice
ind = find(RMS==min(RMS))+i;

% apply alignment
tfROS2 = zeros(4,4,size(quatROS,1));
tfROS =
poseToTF(quatROS(ros_align_st:ros_align_en,:),posROS(ros_align_
st:ros_align_en,:));
tfOMC = poseToTF(quatOMCraw(ind:ind+n-1,:),posOMCraw(ind:ind+n-
1,:));
[X,Y]= dornaika(tfROS,tfOMC);

tfROS = poseToTF(quatROS,posROS);
for j=1:size(tfROS,3)
    tfROS2(:,:,j) = invT(Y)*tfROS(:,:,j)*X;
end

[quatROS_aligned,posROS_aligned] = tfToPose(tfROS2);
eulOMC = quatToEuler(quatOMCraw);
eulROS = quatToEuler(quatROS_aligned);

plot([eulOMC(ind:ind+n-
1,2),eulROS(ros_align_st:ros_align_en,2)]);
```

```
%% plot data
quatROS=quatROS_aligned(ros_align_st+1:end,:);
posROS=posROS_aligned(ros_align_st+1:end,:);

n = size(posROS,1);
quatOMC= quatOMCraw(ind:ind+n-8,:);
posOMC= posOMCraw(ind:ind+n-1,:);
eulROS = quatToEuler(quatROS);
eulOMC = quatToEuler(quatOMC);
figure(1)
time=0:length(quatOMC)-1;
time=time./50;

figure(1)
plot(time,radtodeg(eulOMC(:,1)),time,radtodeg(eulROS(:,1)),'.
');
figure(2)
plot(time,radtodeg(eulOMC(:,2)),time,radtodeg(eulROS(:,2)),'.
');
figure(3)
plot(time,radtodeg(eulOMC(:,3)),time,radtodeg(eulROS(:,3)),'.
');

%
figure(4)
plot(time,posOMC(:,1),time,(posROS(:,1)),'.');
figure(5)
plot(time,posOMC(:,2),time,(posROS(:,2)),'.');
figure(6)
plot(time,posOMC(:,3),time,(posROS(:,3)),'.');


%% export information
omc_align_st = ind;
omc_align_en = ind+(ros_align_en-ros_align_st);
out = [];
out{1} = aFileName;
out{2} = 'femur/pose';
out{3} = ros_align_st;
out{4} = ros_align_en;
out{5} = bFileName;
out{6} = col_order(1);
out{7} = col_order(2);
out{8} = col_order(3);
out{9} = omc_align_st;
out{10} = omc_align_en;
```

APPENDIX D (Alignment Algorithm)

```
clear all;
%%
addpath('kinematics');
addpath('analysis');
addpath('aruco');
addpath('data_import');
addpath('alignment');

%% get Info file
[aFileName,aPathName] = uigetfile('C:\D Drive\D Drive\D
Drive\Auburn University All\RA\Thesis work\aruco-
analysis\aruco_data\BHMQ\BHMQ_info.txt','txt');
[rosFile,rosTopic,rosInd,viconFile,col_order,omcInd] =
importValidationInfo(aPathName,aFileName);

%% get file based on index
%trial_ind = 6;

for trial_ind = 1 to 45
% Import ROS
rosDataRaw =
importJtPoseBag(aPathName,rosFile{trial_ind},rosTopic{tri
al_ind});

% resample to 50 hz
rosTime=rosDataRaw(:,1)./10;
rosTime2=0:(1/50):floor(rosTime(end,1));
rosData=interp1(rosTime,rosDataRaw,rosTime2,'nearest');
%rosData = rosDataRaw;
posROS = rosData(:,2:4);
quatROS = quatNormalize(rosData(:,5:8));
tfROS = poseToTF(quatROS,posROS);

% Import vicon
ptsRaw =
importViconPos(aPathName,viconFile{trial_ind},col_order(t
rial_ind,:));
pts = [];
pts(:,:,1) = resample(ptsRaw(:,:,1),50,120);
pts(:,:,2) = resample(ptsRaw(:,:,2),50,120);
pts(:,:,3) = resample(ptsRaw(:,:,3),50,120);
[quatOMCraw,posOMCraw] = ptsToQuat(pts);
```

```
tfOMC = poseToTF(quatOMCraw,posOMCraw);
plot(posOMCraw(:,2))

% align vicon to aruco

tfROSt =
poseToTF(quatROS(rosInd(trial_ind,1):rosInd(trial_ind,2),
:),posROS(rosInd(trial_ind,1):rosInd(trial_ind,2),:));
tfOMCt =
poseToTF(quatOMCraw(omcInd(trial_ind,1):omcInd(trial_ind,
2),:),posOMCraw(omcInd(trial_ind,1):omcInd(trial_ind,2),:
));
[X,Y]= dornaika(tfOMCt,tfROSt);


tfOMCa = zeros(4,4,size(tfOMC,3));
for j=1:size(tfOMC,3)
    tfOMCa(:,:,j) = invT(Y)*tfOMC(:,:,j)*X;
end
[quatOMC_aligned,posOMC_aligned] = tfToPose(tfOMCa);

% truncate data

quatROS_trunc = quatROS(rosInd(trial_ind,1):end,:);
posROS_trunc = posROS(rosInd(trial_ind,1):end,:);
quatOMC_trunc =
quatOMC_aligned(omcInd(trial_ind,1):end,:);
posOMC_trunc = posOMC_aligned(omcInd(trial_ind,1):end,:);

if length(quatROS_trunc) > length(quatOMC_trunc)
    quatROS_trunc =
quatROS_trunc(1:length(quatOMC_trunc),:);
    posROS_trunc =
posROS_trunc(1:length(quatOMC_trunc),:);
else
    quatOMC_trunc =
quatOMC_trunc(1:length(quatROS_trunc),:);
    posOMC_trunc =
posOMC_trunc(1:length(quatROS_trunc),:);
end
```

```
%plot data

eulOMC_final = radtodeg(quatToZXY(quatOMC_trunc));
eulROS_final = radtodeg(quatToZXY(quatROS_trunc));
time = 0:length(eulOMC_final)-1;
time=time./50;
figure(1);
subplot(3,1,1);
plot(time,eulOMC_final(:,1),time,eulROS_final(:,1),'.');
xlabel('Time (s)');
ylabel('Yaw (deg)');
title('orientation');
subplot(3,1,2);
plot(time,eulOMC_final(:,2),time,eulROS_final(:,2),'.');
xlabel('Time (s)');
ylabel('Pitch (deg)');

subplot(3,1,3);
plot(time,eulOMC_final(:,3),time,eulROS_final(:,3),'.');
xlabel('Time (s)');
ylabel('Roll (deg)');
%
figure(2);
subplot(3,1,1);
plot(time,posOMC_trunc(:,1),time,posROS_trunc(:,1),'.');
xlabel('Time (s)');
ylabel('X-axis');
title('Position (m)');
%
%
subplot(3,1,2);
plot(time,posOMC_trunc(:,2),time,posROS_trunc(:,2),'.');
xlabel('Time (s)');
ylabel('Y-axis (m)');

subplot(3,1,3);
plot(time,posOMC_trunc(:,3),time,posROS_trunc(:,3),'.');
xlabel('Time (s)');
ylabel('Z-axis (m)');
```

```
% Position Error Calculation
x_pos = -posOMC_trunc(:,1);

for i=1:3
RMS_tot(i) = sqrt(mean((posROS_trunc(:,i)-
posOMC_trunc(:,i)).^2));
mag_tot = mean(sqrt(((posROS_trunc(:,1)-
posOMC_trunc(:,1)).^2) + ((posROS_trunc(:,2)-
posOMC_trunc(:,2)).^2) + ((posROS_trunc(:,3)-
posOMC_trunc(:,3)).^2)));

indL1 = max(find(x_pos(:,1)<1.0));
RMS_L1(i) = sqrt(mean((posROS_trunc(1:indL1,i)-
posOMC_trunc(1:indL1,i)).^2));
mag_L1 = mean(sqrt(((posROS_trunc(1:indL1,1)-
posOMC_trunc(1:indL1,1)).^2) + ((posROS_trunc(1:indL1,2)-
posOMC_trunc(1:indL1,2)).^2) + ((posROS_trunc(1:indL1,3)-
posOMC_trunc(1:indL1,3)).^2)));

indL2 = max(find(x_pos(:,1)<=1));
indM2 = max(find(x_pos(:,1)<2));
RMS_L2(i) = sqrt(mean((posROS_trunc(indL2:indM2,i)-
posOMC_trunc(indL2:indM2,i)).^2));
mag_L2 = mean(sqrt(((posROS_trunc(indL2:indM2,1)-
posOMC_trunc(indL2:indM2,1)).^2) +
((posROS_trunc(indL2:indM2,2)-
posOMC_trunc(indL2:indM2,2)).^2) +
((posROS_trunc(indL2:indM2,3)-
posOMC_trunc(indL2:indM2,3)).^2)));

indL3 = max(find(x_pos(:,1)<=2));
indM3 = max(find(x_pos(:,1)<3));
RMS_L3(i) = sqrt(mean((posROS_trunc(indL3:indM3,i)-
posOMC_trunc(indL3:indM3,i)).^2));
mag_L3 = mean(sqrt(((posROS_trunc(indL3:indM3,1)-
posOMC_trunc(indL3:indM3,1)).^2) +
((posROS_trunc(indL3:indM3,2)-
posOMC_trunc(indL3:indM3,2)).^2) +
((posROS_trunc(indL3:indM3,3)-
posOMC_trunc(indL3:indM3,3)).^2)));

indL4 = max(find(x_pos(:,1)<=3));
indM4 = max(find(x_pos(:,1)<3.5));
```

```
RMS_L4(i) = sqrt(mean((posROS_trunc(indL4:indM4,i)-
posOMC_trunc(indL4:indM4,i)).^2));
mag_L4 = mean(sqrt(((posROS_trunc(indL4:indM4,1)-
posOMC_trunc(indL4:indM4,1)).^2) +
((posROS_trunc(indL4:indM4,2)-
posOMC_trunc(indL4:indM4,2)).^2) +
((posROS_trunc(indL4:indM4,3)-
posOMC_trunc(indL4:indM4,3)).^2)));
end

RMS_pos = [RMS_L1 mag_L1 RMS_L2 mag_L2 RMS_L3 mag_L3
RMS_L4 mag_L4 RMS_tot mag_tot];

% Orientation RMS Error

quatErr=
quatNormalize(quatMultiply(quatConj(quatOMC_trunc),quatROS
_trunc));

errTot= zeros(length(quatErr),1);
for i=1:length(quatErr)
    errTot(i) = radtodeg(2.*acos(quatErr(i,1)));
    if errTot(i) > 180
        errTot(i)= errTot(i)-360;
    end
end

err_ornt = [-posOMC_trunc(:,1),errTot,
radtodeg(quatToEuler(quatErr))];

for i=3:5
RMS_ornt_tot(i) = sqrt(mean(err_ornt(:,i).^2));
RMS_ornt_mag_tot = sqrt(mean(errTot.^2));

indL1 = max(find(err_ornt(:,1)<1.0));
RMS_ornt_L1(i) = sqrt(mean(err_ornt(1:indL1,i).^2));
RMS_ornt_mag_L1 = sqrt(mean(errTot(1:indL1).^2));

indL2 = max(find(err_ornt(:,1)<=1));
indM2 = max(find(err_ornt(:,1)<2));
RMS_ornt_L2(i) = sqrt(mean(err_ornt(indL2:indM2,i).^2));
RMS_ornt_mag_L2 = sqrt(mean(errTot(indL2:indM2).^2));
```

```
indL3 = max(find(err_ornt(:,1)<=2));
indM3 = max(find(err_ornt(:,1)<3));
RMS_ornt_L3(i) = sqrt(mean(err_ornt(indL3:indM3,i).^2));
RMS_ornt_mag_L3 = sqrt(mean(errTot(indL3:indM3).^2));


indL4 = max(find(err_ornt(:,1)<=3));
indM4 = max(find(err_ornt(:,1)<3.5));
RMS_ornt_L4(i) = sqrt(mean(err_ornt(indL4:indM4,i).^2));
%RMS_ornt_mag_L4 =
sqrt(mean(((err_ornt(indL4:indM4,2)).^2) +
((err_ornt(indL4:indM4,3)).^2) +
((err_ornt(indL4:indM4,4)).^2)));
RMS_ornt_mag_L4 = sqrt(mean(errTot(indL4:indM4).^2));
end

RMS_ornt = [RMS_ornt_L1(3:5) RMS_ornt_mag_L1
RMS_ornt_L2(3:5) RMS_ornt_mag_L2 RMS_ornt_L3(3:5)
RMS_ornt_mag_L3 RMS_ornt_L4(3:5) RMS_ornt_mag_L4
RMS_ornt_tot(3:5) RMS_ornt_mag_tot]


RMS(trial_ind,:) = [RMS_pos,RMS_ornt];

end
```

APPENDIX E (Test Protocol)

Things to be done once

1. Calibrate wand to obtain the tip coordinates

2. Put vicon markers on Aruco (21 reflective markers: 2 arUco markers of 3 sizes and a wand arUco marker; 3 on each)

1. Put a reflective marker of sie 9.5 mm on the right top corner of each arUco markers of all 3 sizes and the wand

2. Put a reflective marker of sie 9.5 mm on the left top corner of each arUco markers of all 3 sizes and the wand

3. Put a reflective marker of sie 9.5 mm on the right buttom corner of each arUco markers of all 3 sizes and the wand

/----------/

Steps to follow per subject

A. Calibrate Aruco camera per subject

1. goto your catkin workspace `cd ~/aruco_ws`

2. source your workspace `source devel/setup.bash`

3. launch the IDS Camera `roslaunch ueye_cam rgb8.launch`

4. Open a new terminal (ctrl+shift+t)

5. Launch calibration module `rosrun camera_calibration cameracalibrator.py --size 6x8 --square 0.02 image:=/camera/image_raw`

6. use your calibration checkerboard. place at various orientations. Keep on moving it around.

7. click 'calibrate' once the circle turns from gray to dark green

8. click save once the circle turns from gray to dark green

9. click upload. GUI should disappear.

note: the flags `--size 6x8 --square 0.02` is for a square checkerboard that has 6x8 internal corners with a length of 2 cm for each square. Change these parameters for other calibration boards

B. Calibrate Vicon motion Capture
1. Turn on the vicon system
2. Remove any reflective material from the capture area
3. Open Vicon Nexus software
4. Click on `Go live` button on the left top corner of the software
5. Click on `system preparation` button on top right corner of the Nexus software
6. Click on `start button` in the `Mask cameras` section followed by `stop` button after 5 sec
7. Click on `start button` in the `Calibrate camera` section to start calibration
8. Turn on the `T-wand` and wave around near the force plate area until the calibration is complete
9. Place the `T-wand` in between the 2 force plates
10. Click on the `start` button in `Set Volume origin` section and then click `stop` button to set the origin
11. Turn off and remove the T-wand from center and place 3 reflective markers near the center
12. On Nexus, click on `show advanced` button in `set volume origin` section and click `start` button of `set floor plane:` topic
13. select the 3 reflective markers in the 3D perspective view using mouse and click on `set` button of the `set floor plane:` topic
14. Well Done!! Vicon calibration is complete now

C. Capture alignment file
1. Check the marker size on fiducial_detect.launch file and change it to the size of marker you are using
2. In a new terminal (ctrl+shift+t), run `cd ~/aruco_ws` followed by `source devel/setup.bash`
3. run`roslaunch aruco_biomech uEye.launch`
4. In a new terminal (ctrl+shift+t), run `rqt_image_view)`
5. New terminal (ctrl+shift+t), run `roscore`
2. In a new terminal, cd to location where bag files will be stored and then start `rosbag record /camera/camera_info/ /camera/image/compressed` on ROS
3. Click on `capture` to capture dynamic data on Vicon at the same time as ROS
4. Move ID = 1 of size 10 cm around as close to ArUco camera for about 5 to 10 second
5. Close rosbag record (ctlr+c) & click `stop capture` on Nexus
6. rename bag file and vicon file if necessary
7. Repeat step 1 to 6 for ID 2 of size 10 cm
8. Repeat step 1 to 6 for ID 1 of size 11 cm
9. Repeat step 1 to 6 for ID 2 of size 11 cm
10. Repeat step 1 to 6 for ID 1 of size 12 cm
11. Repeat step 1 to 6 for ID 2 of size 12 cm

/ ----------/

For Aruco marker size 10 cm

D. Put Aruco Markers on subject

1. Put Marker ID=1 on Femur

2. Put Marker ID=2 on Tibia

3. Put Marker ID=3 on Wand

E. Mark anatomical locations with sharpie

1. Find the anatomical landmark using hand

2. double check your finding with someone else in the lab

3. Mark the anatomical points with sharpie

F. Register Anatomical Points from Aruco for ArUco of size 10 cm

1. Launch register_landmark.launch file (ADD LAUNCH FILE) `roslaunch aruco_biomech register_landmark.launch`

2. Make sure subject is as close to the camera as possible with visibility of all 3 markers

3. start rosbag recording `rosbag record /camera/camera_info`

4. point wand to `lateral malleolus` followed by `medial malleolus`

5. point wand to `lateral epicondyle` followed by `medial epicondyle` (tibia)

6. point wand to `lateral condyle` followed by `medial condyle` (femur)

7. point wand to `ipsilateral greater trochanter` followed by `contralateral greater trochanter`

7. stop rosbag (ctrl+c)

8. rename rosbag

9. play back with aruco

Note: Put the wand away as its not needed for rest of the data collection

G. Place reflective markers on subject (# of markers?)

H. Take a static trial for vicon

Take pictures with camera

I. Capture dynamic data

Capture dynamic data with Vicon

1. Create a new session in the Nexus `communication tab` in your project folder on the middle buttom section

2. Add a subject by clicking on the `subject tab` on the left side panel and clicking on `create a black subject` button

3. Select a model by clicking on `the button next to subject creator`

4. Click on the the `capture` button on the right top corner of the Nexus

5. Rename the trial name as required and click on `start` button on the buttom whenever ready

J. ROS capturing dynamic data

1. In the ROS system, run `roscore`

2. In a new tab (`ctrl+shift+t`), run `cd ~/aruco_ws` followed by `source devel/setup.bash`

3. Launch IDS camera: `roslaunch aruco_biomech uEye.launch`

4. In a new tab `ctrl+shift+t`, run `cd ~/aruco_ws/bagfile/folderName` followed by `rosbag record /camera/camera_info /camera/image/compressed` as soon as you start capturing the data on the Vicon Nexus

5. Kick twice on lateral side of the right leg

6. Walk at slow speed starting from 0.5m from ROS camera upto 3.5m

7. Click `stop` on the Nexus to stop capturing

8. Hit `ctrl+c` on the ROS to stop recording

9. Rename the ROS trial name

10. Repeat for step 6 to 11 for 4 more trials for each speed walking

11. `Repeat step I through J 10 for self selected speed`

12. `Repeat step I through J 10 for fast pace walking`

Replace 10 cm arUco markers with 11 cm arUco markers

Repeat from Section D to J for arUco markers of size 11 cm

Replace 11 cm aruco markers woth 12 cm arUco markers

Repeat from Section D to J for arUco markers of size 12 cm

APPENDIX F (FiducialSystem Installment and Operational Guide)

fiducial-based mocap system based on Aruco fiducial detection

This software package will output the position and orientation (pose) of a fiducial marker relative to the coordinate axis of the camera. It is tested with ROS Kinetic. The code is primarily based on the 'fiducials' package from ROS, which relies on the ArUco package for openCV. A node subsequently parses the transform array from the ros arUco node into a pose topic specified by the maker ID. When visualizing the coordinate frames in rViz, the x, y, and z-axis are red, green, and blue, respectively.

Installation

1. Make catkin workspace

1. Make a catkin workspace `mkdir -p ~/aruco_ws/src`

2. Install aruco_biomech

1. goto catkin `src` folder within your catkin workspace `cd ~/aruco_ws/src`
2. clone the repository `git clone git@gitlab.eng.auburn.edu:spaurk/aruco_biomech.git`
3. goto catkin workspace `cd ~/aruco_ws`
4. build workspace `catkin_make`

3. Install joint_pose

1. goto catkin `src` folder within your catkin workspace `cd ~/aruco_ws/src`
2. clone the repository `git clone git@gitlab.eng.auburn.edu:spaurk/fiducial_pose.git`
3. goto catkin workspace `cd ~/aruco_ws`
4. build workspace `catkin_make`

4. Install camera calibration tools.

5. goto catkin `src` folder within catkin_ws `cd ~/aruco_ws/src`
6. clone the camera calibration tools `git clone https://github.com/ros-perception/image_pipeline`
7. goto your catkin workspace `cd ~/aruco_ws`
8. compile camera calibration tools `catkin_make`

5. Install ArUco

1. goto catkin `src` folder within catkin_ws `cd ~/aruco_ws/src`

2. clone ArUco `git clone https://github.com/UbiquityRobotics/fiducials`

3. goto your catkin workspace `cd ~/aruco_ws`

4. compile camera driver `catkin_make`

6. Install pyCairo (necessary for marker generation)

1. Type the following in a terminal `sudo apt install python-cairosvg`

7. Install, test, and calibrate camera

Webcam

Installation

1. goto catkin `src` folder within catkin workspace `cd ~/aruco_ws/src`

2. clone camera driver `git clone https://github.com/OTL/cv_camera.git`

3. goto your catkin workspace `cd ~/aruco_ws`

4. compile camera driver `catkin_make`

Testing

1. goto your catkin workspace `cd ~/aruco_ws`

2. source your workspace `source devel/setup.bash`

3. launch the webcam `roslaunch aruco_biomech cv_camera.launch`

Don't worry if you see a 'warning, no calibration file' displayed

4. open another new terminal window (ctrl+shift+t)

5. check output: `rqt_image_view /cv_camera/image_raw` you should see video streaming from your webcam.

note: if using vmware workstation: make sure you select "usb3.0" from your devices and make sure your camera is enabled in your virtual machine.

Calibration

1. goto your catkin workspace `cd ~/aruco_ws`

2. source your workspace `source devel/setup.bash`

3. launch the webcam `roslaunch aruco_biomech cv_camera.launch`

4. Open a new terminal (ctrl+shift+t)

5. Launch calibration module `rosrun camera_calibration cameracalibrator.py --size 6x8 --square 0.02 image:=/cv_camera/image_raw`

6. use your calibration checkerboard. place at various orientations. Keep on moving it around.

7. click 'calibrate' once the circle turns from gray to dark green

8. click save once the circle turns from gray to dark green

9. click upload. GUI should disappear.

note: the flags `--size 6x8 --square 0.02` is for a square checkerboard that has 6x8 internal corners with a length of 2 cm for each square. Change these parameters for other calibration boards

IDS Camera

Installation

1. Goto https://en.ids-imaging.com/download-ueye-lin64.html

2. Download the 64 bit linux driver

3. Extract files

4. goto file location and type `sudo sh ./ueye_4.91.1.0_amd64.run`

5. Restart linux. IDS Camera should turn green.

6. goto catkin `src` folder within catkin workspace `cd ~/aruco_ws/src`

7. clone camera driver `git clone https://github.com/anqixu/ueye_cam.git`

8. goto your catkin workspace `cd ~/aruco_ws`

9. compile camera driver `catkin_make`

note: the filename may be slightly different depending on the version.

You may need to comment the second line of the `rgb8.launch` file.

Testing

1. goto your catkin workspace `cd ~/aruco_ws`
2. source your workspace `source devel/setup.bash`
3. launch the IDS Camera `roslaunch ueye_cam rgb8.launch`

Don't worry if you see a 'warning, no calibration file' displayed

4. open another new terminal window (ctrl+shift+t)
5. check output: `rqt_image_view /camera/image_raw` you should see video streaming from your webcam.

Calibration

1. goto your catkin workspace `cd ~/aruco_ws`
2. source your workspace `source devel/setup.bash`
3. launch the IDS Camera `roslaunch ueye_cam rgb8.launch`
4. Open a new terminal (ctrl+shift+t)
5. Launch calibration module `rosrun camera_calibration cameracalibrator.py --size 6x8 --square 0.02 image:=/camera/image_raw`
6. use your calibration checkerboard. place at various orientations. Keep on moving it around.
7. click 'calibrate' once the circle turns from gray to dark green
8. click save once the circle turns from gray to dark green
9. click upload. GUI should disappear.

##For gopro

3. run `ffmpeg -i file.mp4 -vcodec copy -acodec copy file_copied.mp4`
4. rename the video file in the video_file.launch file
5. launch `roslaunch video_stream_opencv video_file.launch`
6. Open a new terminal (ctrl+shift+t)
7. Launch calibration module `rosrun camera_calibration cameracalibrator.py --size 6x8 --square 0.02 image:=/camera/image`
8. click 'calibrate' once the circle turns from gray to dark green
9. click save once the circle turns from gray to dark green and as soon as the sample # reaches 40
10. click 'commit' before the video closes, GUI should disappear.

Note: the flags `--size 6x8 --square 0.02` is for a square checkerboard that has 6x8 internal corners with a length of 2 cm for each square. Change these parameters for other calibration boards

Usage

1. Print your markers

1. open a terminal window and start ros by typing `roscore`

2. open a new terminal window (ctrl+shift+t)

3. goto your catkin workspace `cd ~/aruco_ws`

4. source your workspace `source devel/setup.bash`

5. run `rosrun aruco_biomech make_markers.py 1 10 fiducials.pdf 0 76.2` to create your markers. Note 1

5. run `rosrun aruco_biomech make_markers.py 1 10 fiducials.docx 0 76.2` to create your markers and save as .docx as PDF has scaling issue but .docx does not.

6. retrieve your markers from your catkin workspace `aruco_ws/fiducials.pdf` and print them out. Note 2

note 1: this will generate markers 1 to 10 from dictionary 0 to fiducials.pdf. Each marker will have a length of 3 inches (76.2 mm). Change these arguments as required.

Note 2: You can print the markers in PDF however, PDF has scaling issue and it shrinks the image while .docx does not. SO, I suggest to save the fiducials file as .docx

2. Let Aruco know which markers you are using

1. goto your catkin workspace `cd aruco_ws`

2. source your workspace `source devel/setup.bash`

3. goto your launch file directory `roscd aruco_biomech/launch`

4. open `fiducial_detect.launch` in a text editor (i.e. atom, gedit)

4. specify the value for `dictionary` (default is 0)

5. specify the value for `fiducial_length` (default is 0.0762 meters, which is 3 inches)

6. save and close fiducial_detect.launch

7. open `joint_pose.launch` in a text editor (i.e. atom, gedit)

8. specify the fiducial id that you want to be tracked (default is 2)

9. Open `aruco_simple.launch/aruco_multiple.launch` in a text editor and comment out `cv_camera.launch` and uncomment or add the `uEye.launch` file to launch IDS camera

3. Stream your files

1. goto your catkin workspace `cd aruco_ws`

2. source your workspace `source devel/setup.bash`

3. launch your file `roslaunch aruco_biomech aruco_simple.launch`

4. If you get error regarding uEye-API, open uEye.launch file in a text editor and comment the node with name `check_ueyey_api` in the ueye_cam package

4. Record your files

1. goto your catkin workspace `cd aruco_ws`

2. source your workspace `source devel/setup.bash`

3. launch your file `roslaunch aruco_biomech aruco_simple.launch`

4. open a new terminal (ctrl+shift+t)

5. start logging your data by typing `rosbag record leg_pose/pose`

6. press ctrl+c in the terminal that you started `rosbag` when done recording

Add multiple make_markers

1. open `joint_pose_multiple.launch`

2. Add arguments for each of the fiducial markers with `default value =` marker id that you are using

3. Add an argument for each of the added marker's frame as `<arg name="femur_frame" default="femur"/>`

4. Add a node with an uniques node name for each of the markers added. Make sure to change its `fiducial id` name as defined in the argument and `child_frame_id` as the frame name defined in the arguments

Additional Information:

ArUco: https://docs.opencv.org/3.1.0/d5/dae/tutorial_aruco_detection.html

ROS ArUco node: http://wiki.ros.org/aruco_detect?distro=kinetic

ROS Fiducial package: http://wiki.ros.org/fiducials

ROS IDS Camera Node: http://wiki.ros.org/ueye_cam

ROS Camera Calibration Node: http://wiki.ros.org/camera_calibration

ROS Camera Calibration Instructions:
http://wiki.ros.org/camera_calibration/Tutorials/MonocularCalibration

ROS record bag files: http://wiki.ros.org/rosbag/Commandline

APPENDIX G (Statistics)

Size	Speed	Distance	Mean±SD (X-axis)	Mean±SD (Y-axis)	Mean±SD (Z-axis)	Mean±SD (R)
S	Slow	0-1 m	1.64 ± .72	.48 ± .30	.78 ± .36	1.43 ± .58
		1-2 m	2.54 ± .91	4.36 ± 3.55	4.09 ± 2.70	6.44 ± 3.71
		2-3 m	4.89 ± 2.51	9.79 ± 8.14	9.96 ± 6.76	15.89 ± 8.74
		3-3.5 m	8.46 ± 4.01	14.00 ± 11.68	14.85 ± 9.62	23.87 ± 12.51
	Self	0-1 m	1.82 ± 1.10	.83 ± .90	1.01 ± .95	1.88 ± 1.45
		1-2 m	5.75 ± 4.60	7.01 ± 7.66	5.04 ± 2.29	10.04 ± 8.51
		2-3 m	10.63 ± 11.16	16.54 ± 19.65	10.99 ± 3.39	24.08 ± 21.99
		3-3.5 m	16.16 ± 13.74	21.67 ± 23.60	15.77 ± 3.02	34.15 ± 26.07
	Fast	0-1 m	1.80 ± .75	.99 ± .80	.97 ± .50	1.95 ± .96
		1-2 m	6.86 ± 5.76	7.25 ± 5.81	6.44 ± 3.12	11.22 ± 7.52
		2-3 m	10.01 ± 8.39	18.65 ± 16.50	13.13 ± 7.49	26.69 ± 17.55
		3-3.5 m	13.03 ± 10.98	25.22 ± 20.90	18.43 ± 11.18	37.52 ± 22.27
M	Slow	0-1 m	1.72 ± .67	.37 ± .14	.53 ± .23	1.31 ± .60
		1-2 m	3.21 ± 1.25	3.00 ± 2.06	2.14 ± .80	4.36 ± 1.94
		2-3 m	4.94 ± 2.45	6.71 ± 4.33	4.77 ± 1.89	10.11 ± 3.88
		3-3.5 m	11.41 ± 4.27	9.61 ± 5.81	7.45 ± 3.04	17.33 ± 4.97
	Self	0-1 m	1.75 ± .81	.40 ± .09	.58 ± .16	1.38 ± .61
		1-2 m	3.59 ± 1.01	3.74 ± 1.40	2.79 ± .62	5.43 ± .87
		2-3 m	5.21 ± 3.07	8.62 ± 3.38	6.20 ± 1.52	12.37 ± 2.78
		3-3.5 m	11.66 ± 5.34	12.78 ± 5.27	9.69 ± 2.42	20.64 ± 4.90
	Fast	0-1 m	1.68 ± .55	.40 ± .10	.52 ± .12	1.29 ± .46
		1-2 m	3.68 ± .27	2.29 ± 1.70	1.90 ± .65	4.09 ± 1.00
		2-3 m	5.62 ± 2.19	5.46 ± 3.93	4.01 ± 1.40	9.23 ± 3.30
		3-3.5 m	12.00 ± 5.06	8.38 ± 5.91	6.26 ± 2.50	16.64 ± 4.95
L	Slow	0-1 m	1.57 ± .33	.45 ± .17	.73 ± .14	1.41 ± .21
		1-2 m	3.08 ± .97	3.30 ± 3.81	4.45 ± 2.00	6.12 ± 3.33
		2-3 m	4.78 ± 2.48	7.42 ± 8.70	10.59 ± 4.87	14.93 ± 7.79
		3-3.5 m	7.04 ± 3.35	10.38 ± 12.02	15.29 ± 6.73	21.82 ± 10.52
	Self	0-1 m	1.64 ± .30	.64 ± .55	.66 ± .13	1.56 ± .46
		1-2 m	2.84 ± 1.06	4.41 ± 3.47	4.63 ± 2.60	6.61 ± 3.61
		2-3 m	5.86 ± 2.49	10.72 ± 8.37	10.86 ± 5.50	17.09 ± 8.98
		3-3.5 m	7.79 ± 4.28	15.81 ± 12.40	16.25 ± 8.05	25.96 ± 13.02
	Fast	0-1 m	2.06 ± .82	.63 ± .35	.82 ± .33	1.83 ± .76
		1-2 m	3.69 ± .73	4.12 ± 4.26	4.38 ± 2.35	6.58 ± 4.08
		2-3 m	5.32 ± 3.19	9.65 ± 10.44	9.92 ± 4.58	16.12 ± 10.47
		3-3.5 m	8.46 ± 4.53	13.96 ± 15.35	15.32 ± 7.39	25.13 ± 15.26

Table 5: Marginal mean RMSE table for potion of Fiducial marker with standard deviation (SD) for all the testing conditions

Size	Speed	Distance	Mean±SD (X-axis)	Mean±SD (Y-axis)	Mean±SD (Z-axis)	Mean±SD (R)
S	Slow	0-1 m	1.30 ± 1.03	4.04 ± 3.41	1.90 ± .69	4.76 ± 3.45
		1-2 m	1.64 ± .72	6.59 ± 3.07	8.85 ± 2.76	11.54 ± 2.27
		2-3 m	3.26 ± .89	10.01 ± 3.82	11.91 ± 1.71	15.69 ± 2.13
		3-3.5 m	4.06 ± .61	10.74 ± 1.70	18.21 ± 5.81	21.18 ± 4.90
	Self	0-1 m	1.80 ± 1.93	3.99 ± 3.68	2.31 ± 1.52	5.05 ± 4.32
		1-2 m	3.17 ± 2.03	8.58 ± 3.75	6.66 ± 2.70	11.25 ± 4.76
		2-3 m	6.24 ± 2.65	15.53 ± 7.77	12.61 ± 2.11	20.39 ± 5.62
		3-3.5 m	7.32 ± 5.64	13.51 ± 2.90	18.96 ± 13.53	23.82 ± 10.62
	Fast	0-1 m	1.47 ± .87	4.00 ± 1.78	3.70 ± 2.33	5.94 ± 2.87
		1-2 m	7.63 ± 8.26	12.04 ± 7.24	13.53 ± 12.84	18.04 ± 13.17
		2-3 m	7.11 ± 5.39	13.74 ± 3.27	15.18 ± 10.19	20.68 ± 8.82
		3-3.5 m	8.71 ± 3.83	19.79 ± 5.08	19.44 ± 2.59	27.33 ± 4.29
M	Slow	0-1 m	.69 ± .15	1.33 ± .50	1.37 ± .21	2.06 ± .48
		1-2 m	1.67 ± .77	4.52 ± .73	8.91 ± 1.94	9.93 ± 1.85
		2-3 m	2.70 ± .57	6.32 ± .56	10.38 ± 4.27	12.19 ± 3.59
		3-3.5 m	4.54 ± 2.29	10.92 ± 3.12	16.12 ± 5.26	19.19 ± 5.67
	Self	0-1 m	.86 ± .13	1.53 ± .55	1.54 ± .18	2.38 ± .44
		1-2 m	2.56 ± 1.13	5.18 ± 1.34	7.57 ± 5.18	9.19 ± 4.74
		2-3 m	3.30 ± .70	8.57 ± 2.12	9.35 ± 3.21	12.61 ± 3.23
		3-3.5 m	5.89 ± 3.72	12.51 ± 1.98	17.84 ± 7.91	21.38 ± 6.87
	Fast	0-1 m	.85 ± .20	1.27 ± .34	1.32 ± .13	2.05 ± .29
		1-2 m	3.01 ± 2.53	5.79 ± 1.76	6.46 ± 3.78	8.48 ± 3.00
		2-3 m	4.01 ± 1.64	7.26 ± 1.47	9.96 ± 3.01	11.85 ± 2.99
		3-3.5 m	10.70 ± 3.76	18.74 ± 4.49	21.64 ± 8.57	26.96 ± 7.71
L	Slow	0-1 m	1.00 ± .26	1.94 ± 1.08	1.61 ± .39	2.76 ± 1.07
		1-2 m	1.29 ± .54	6.56 ± 2.15	6.18 ± 1.45	9.25 ± 1.93
		2-3 m	2.55 ± .65	10.07 ± 1.35	9.18 ± 2.71	13.72 ± 1.36
		3-3.5 m	1.50 ± .23	8.89 ± 1.73	7.80 ± 2.30	12.02 ± 2.34
	Self	0-1 m	.95 ± .30	2.34 ± .94	1.98 ± 1.14	3.34 ± 1.33
		1-2 m	2.38 ± 1.10	7.11 ± 2.47	6.24 ± 2.82	9.63 ± 3.40
		2-3 m	3.12 ± 1.21	11.13 ± 2.62	9.59 ± 1.98	14.94 ± 2.25
		3-3.5 m	2.40 ± 1.21	7.70 ± 1.94	6.99 ± 2.93	10.68 ± 2.61
	Fast	0-1 m	1.25 ± .59	2.38 ± 1.36	1.66 ± .68	3.22 ± 1.56
		1-2 m	1.77 ± 1.04	7.38 ± 3.77	5.35 ± 1.16	9.44 ± 3.68
		2-3 m	3.30 ± 1.37	9.24 ± 2.48	8.95 ± 2.76	12.86 ± 3.30
		3-3.5 m	4.37 ± 2.22	11.98 ± 7.85	8.63 ± 2.73	14.85 ± 7.30

Table 6: Marginal mean RMSE table for orientation of Fiducial marker with standard deviation (SD) for all the testing conditions

Ivs	DVs	Sig	Partial Eta squared
Size	x	0.000**	0.155
	y	0.000**	0.2
	z	0.000**	0.185
	R	0.000**	0.237
Speed	x	0.000**	0.156
	y	0.000**	0.119
	z	0.318	0.016
	R	0.035	0.046
Distance	x	0.000**	0.343
	y	0.000**	0.629
	z	0.000**	0.556
	R	0.000**	0.657
Size*Speed	x	0.215	0.039
	y	0.173	0.043
	z	0.642	0.017
	R	0.409	0.027
Size*Distance	x	0.007**	0.114
	y	0.001**	0.146
	z	0.000**	0.174
	R	0.000**	0.188
Speed*Distance	x	0.057	0.08
	y	0.000**	0.157
	z	0.968	0.009
	R	0.291	0.049

*Table 8: Result of statistical analysis between subject effects for RMSE of orientation of fiducial marker. *Statistically significant at p<0.05, **Statistically-significant at p<0.01*

Ivs	DV	Sig	Partial Eta squared
Size	x	0.015*	0.057
	y	0.004**	0.073
	z	0.000**	0.219
	R	0.000**	0.117
Speed	x	0.092	0.033
	y	0.206	0.022
	z	0.618	0.007
	R	0.160	0.025
Distance	x	0.000**	0.395
	y	0.000**	0.309
	z	0.000**	0.611
	R	0.000**	0.523
Size*Speed	x	0.269	0.035
	y	0.596	0.019
	z	0.435	0.026
	R	0.431	0.026
Size*Distance	x	0.331	0.046
	y	0.465	0.038
	z	0.004	0.125
	R	0.160	0.061
Speed*Distance	x	0.918	0.014
	y	0.938	0.012
	z	0.999	0.003
	R	0.926	0.013

*Table 7: Result of statistical analysis between subject effects for RMSE of position of fiducial marker. *Statistically significant at p<0.05, **Statistically-significant at p<0.01*

Dependent Variables	IVs(I)	IVs(J)	Mean Diff. (I-J)	Sig.
x	S	M	1.4273	0.207
	S	L	2.4542*	0.011
	M	L	1.0268	0.440
y	S	M	5.422**	0.004
	S	L	3.776	0.061
	M	L	-1.646	0.580
Z	S	M	4.5497**	0.000
	S	L	0.6297	0.697
	M	L	-3.9200**	0.000
R	S	M	7.5805**	0.000
	S	L	4.1652*	0.047
	M	L	-3.4153	0.125
x	Fast	Slow	1.5757	0.148
	Fast	Self	-0.0422	0.999
	Self	Slow	1.6178	0.133
y	Fast	Slow	2.2608	0.360
	Fast	Self	-0.5138	0.948
	Self	Slow	2.7747	0.216
z	Fast	Slow	0.5395	0.767
	Fast	Self	-0.1977	0.965
	Self	Slow	0.7372	0.610
R	Fast	Slow	2.7725	0.113
	Fast	Self	-0.2403	0.890
	Self	Slow	3.0128	0.085
x	3-3.5 m	0-1 m	8.9258**	0.000
	3-3.5 m	1-2 m	6.7538**	0.000
	3-3.5 m	2-3 m	4.3062**	0.000
	2-3 m	0-1 m	4.6196**	0.000
	2-3 m	1-2 m	2.4476	0.059
	1-2 m	0-1 m	2.172	0.116
y	3-3.5 m	0-1 m	14.0709**	0.000
	3-3.5 m	1-2 m	10.2591**	0.000
	3-3.5 m	2-3 m	4.2518	0.120
	2-3 m	0-1 m	9.8191**	0.000
	2-3 m	1-2 m	6.0073*	0.011
	1-2 m	0-1 m	3.8118	0.193
z	3-3.5 m	0-1 m	12.5231**	0.000
	3-3.5 m	1-2 m	9.2731**	0.000
	3-3.5 m	2-3 m	4.3209**	0.000
	2-3 m	0-1 m	8.2022**	0.000
	2-3 m	1-2 m	4.9522**	0.000
	1-2 m	0-1 m	3.2500**	0.002
R	3-3.5 m	0-1 m	23.2233**	0.000
	3-3.5 m	1-2 m	18.0202**	0.000
	3-3.5 m	2-3 m	8.5064**	0.000
	2-3 m	0-1 m	14.7169**	0.000
	2-3 m	1-2 m	9.5138**	0.000
	1-2 m	0-1 m	5.2031	0.051

*Table 9: Univariate analysis of variance (UNIANOVA) multiple comparison (Tukey HSD) test results of position between independent variables (IVs) with mean differences and their significance values. *The mean difference is statistically-significant at the 0.05 level. **the mean difference is statistically-significant at the 0.01 level.*

Dependent Variables	IVs(I)	IVs(J)	Mean Diff. (I-J)	Sig.
x	S	M	1.0783*	0.048
	S	L	2.3193**	0.000
	M	L	1.241*	0.048
y	S	M	3.2178**	0.000
	S	L	2.986**	0.000
	M	L	-0.2318**	0.000
Z	S	M	1.7335	0.119
	S	L	4.9257**	0.000
	M	L	3.1922**	0.001
R	S	M	3.9482**	0.000
	S	L	5.7463**	0.000
	M	L	1.7982	0.105
x	Fast	Slow	2.3300**	0.000
	Fast	Self	1.1812*	0.027
	Self	Slow	1.1488*	0.032
y	Fast	Slow	2.6408**	0.000
	Fast	Self	1.3295	0.070
	Self	Slow	1.3113	0.076
z	Fast	Slow	1.1143	0.411
	Fast	Self	1.1813	0.368
	Self	Slow	-0.067	0.997
R	Fast	Slow	2.2832*	0.028
	Fast	Self	1.4183	0.243
	Self	Slow	0.8648	0.588
x	3-3.5 m	0-1 m	4.3693	0.019
	3-3.5 m	1-2 m	2.7067	0.000
	3-3.5 m	2-3 m	1.5438	0.000
	2-3 m	0-1 m	2.8256	0.120
	2-3 m	1-2 m	1.1629**	0.000
	1-2 m	0-1 m	1.6627**	0.009
y	3-3.5 m	0-1 m	10.2173**	0.000
	3-3.5 m	1-2 m	5.6676*	0.000
	3-3.5 m	2-3 m	2.5447**	0.002
	2-3 m	0-1 m	7.6727**	0.000
	2-3 m	1-2 m	3.1229**	0.000
	1-2 m	0-1 m	4.5498**	0.000
z	3-3.5 m	0-1 m	13.1391**	0.000
	3-3.5 m	1-2 m	7.3193**	0.000
	3-3.5 m	2-3 m	4.2798**	0.000
	2-3 m	0-1 m	8.8593**	0.000
	2-3 m	1-2 m	3.0396*	0.016
	1-2 m	0-1 m	5.8198**	0.000
R	3-3.5 m	0-1 m	16.2062**	0.000
	3-3.5 m	1-2 m	8.9624**	0.000
	3-3.5 m	2-3 m	4.7204**	0.000
	2-3 m	0-1 m	11.4858**	0.000
	2-3 m	1-2 m	4.242**	0.000
	1-2 m	0-1 m	7.2438**	0.000

*Table 10: variate analysis of variance (UNIANOVA) multiple comparison (Tukey HSD) test results of orientation between independent variables (IVs) with mean differences and their significance values for orientation RMSE. *The mean difference is statistically-significant at the 0.05 level. **the mean difference is statistically-significant at the 0.01 level.*

APPENDIX H (ROS files)

This file is named as aruco_mulpitple_10x10.launch. This launch file contains the codes that is used to run the AR based detection system in ROS system. The name of the video file to be run also needs to be changed in the arg name “video_stream_provider”.

```
<!-- Top-level launch file  -->
<launch>
        <!-- using a webcam -->
        <!-- <include file="$(find aruco_biomech)/launch/cv_camera.launch"/> -->

        <!-- using IDS camera -->
        <!-- <include file="$(find aruco_biomech)/launch/uEye.launch"/> -->

        <include file="$(find video_stream_opencv)/launch/camera.launch" >
                        <arg name="video_stream_provider"
value="/home/rajugupta/aruco_ws/bagfile/PJXA/PJXA_slow_10x10_06_copied.MP4" />
                        <arg name="frame_id" value="cam_1" />
                        <arg name="fps" value="5" />
                        <arg name="camera_info_url" value="" />
                        <arg name="flip_horizontal" value="false" />
                        <arg name="flip_vertical" value="false" />
                        <arg name="visualize" value="false" />
        </include>

        <!-- launched fiducial detection node -->
        <include file="$(find aruco_biomech)/launch/fiducial_detect_10cm.launch"/>

        <!-- launches joint_pose -->
        <include file="$(find aruco_biomech)/launch/joint_pose_multiple.launch"/>

        <!-- launches rViz or visualization node -->
         <node type="rviz" name="rviz" pkg="rviz" args="-d $(find
aruco_biomech)/rviz/rviz_simple.rviz" />
</launch>
```

This file is named as joint_pose_multiple.launch. This launch file contains the codes that transform aruco msgs to pose messages and is launched by aruco_mulpitple_10x10.launch file in FIDUCIAL based detection system in ROS system.

```
<!-- transform aruco msgs to pose msgs -->
<launch>
        <arg name="femur_id" default="1"/>
        <arg name="tibia_id" default="2"/>
        <!-- <arg name="foot_id" default="3"/> -->
        <arg name="camera" default="/camera"/>
        <arg name="parent_frame" default="cam_1"/>
        <arg name="femur_frame" default="femur"/>
        <arg name="tibia_frame" default="tibia"/>
        <!-- <arg name="foot_frame" default="foot"/> -->

<!-- Femur Tracking Frame -->
        <node pkg="fiducial_pose" name="femur"
  type="fiducial_pose_node" output="screen" respawn="false">
        <param name="fiducial_transforms" value="/$(arg camera)/fiducial_transforms"/>
        <param name="fiducial_id" value="$(arg femur_id)"/>
        <param name="parent_frame_id" value="$(arg parent_frame)"/>
        <param name="child_frame_id" value="$(arg femur_frame)"/>
        </node>

<!-- Tibia Tracking Frame -->
                <node pkg="fiducial_pose" name="tibia"
           type="fiducial_pose_node" output="screen" respawn="false">
                <param name="fiducial_transforms" value="/$(arg
camera)/fiducial_transforms"/>
                <param name="fiducial_id" value="$(arg tibia_id)"/>
                <param name="parent_frame_id" value="$(arg parent_frame)"/>
                <param name="child_frame_id" value="$(arg tibia_frame)"/>
                </node>
</launch>
```

This file is named as fiducial_detect_10cm.launch. This launch file contains the codes that is used to detect the aruco by using camera message and is launched by aruco_multiple_10x10.launch in ROS system.

```
<!-- namespace for camera input -->
<launch>
  <arg name="dictionary" default="0"/>
  <arg name="fiducial_len" default="0.10"/>
  <arg name="camera" default="/camera"/>

  <node pkg="aruco_detect" name="aruco_detect"
    type="aruco_detect" output="screen" respawn="false">
  <!-- <node pkg="ml_detector" name="ml_detector" -->
    <!-- type="ml_detector_node" output="screen" clear_params="true" respawn="false"> -->
    <param name="image_transport" value="compressed"/>
    <param name="publish_images" value="true" />
    <!-- <param name="adaptiveThreshConstant" value="7"/> -->
    <param name="fiducial_len" value="$(arg fiducial_len)"/>
    <param name="minMarkerPerimeterRate" value="0.05"/> <!--0.075 -->
    <param name="maxMarkerPerimeterRate" value="2.0"/>  <!--4.0 -->
    <param name="polygonalApproxAccuracyRate" value="0.02"/> <!--0.02 -->
    <param name="minCornerDistanceRate" value="0.01"/>  <!--0.01 -->
    <param name="minMarkerDistanceRate" value="0.01"/>
    <param name="cornerRefinementMinAccuracy" value="0.005"/> <!--0.005 -->
    <param name="minOtsuStdDev" value="0.5"/>
    <param name="dictionary" value="$(arg dictionary)"/>
    <param name="do_pose_estimation" value="true"/>
    <param name="ignore_fiducials" value=""/>
    <param name="fiducial_len_override" value=""/>
    <remap from="/camera/compressed" to="$(arg camera)/image/compressed"/>
    <remap from="/camera_info" to="$(arg camera)/camera_info"/>
    <remap from="/fiducial_transforms" to="$(arg camera)/fiducial_transforms"/>
  </node>
</launch>
```